Preparation and Characterization of Molecular Assemblies with New Morphologies Composed of Amphiphilic Helical Peptides(Dissertation_全文)

AUTHOR(S):

Ueda, Motoki

Preparation and Characterization of Molecular Assemblies with New Morphologies Composed of Amphiphilic Helical Peptides

Motoki Ueda

2011

CONTENTS

Contents ····· iii

List of Abbreviations ····· iv

List of the Measurement Instruments Used in the Present Thesis ····· v

General Introduction ····· 1

Chapter 1 Transformation of Peptide Nanotubes to Vesicle via Fusion Driven by Stereo-Complex Formation ····· 19

Chapter 2 Temperature Triggered Fusion of Vesicles Composed of Right-Handed and Left-Handed Amphiphilic Helical Peptides ····· 35

Chapter 3 Rational Design of Peptide Nanotubes for Varying Diameters and Lengths ····· 49

Chapter 4 Patchwork Self-Assembling with Using Chiral Amphiphilic Helical Peptides Generates Nano-Size Round-Bottom Flask ····· 65

Chapter 5 Morphology Collage with Using Phase-Separation of Peptide Membranes; “Patchwork Self-Assembling” ····· 79

Concluding Remark ····· 95

List of Publications ····· 98

Acknowledgement ····· 100

List of Abbreviations

^{1}H HMR	proton nuclear magnetic resonance spectroscopy
Boc	*tert*-butyloxycarbonyl
CD	circular dichroism
Cryo-TEM	cryogenic transmission electron microscopy
DCC	dicyclohexylcarbodiimide
DIEA	*N*,*N*-diisopropylethylamine
DLS	dynamic light scattering
DMF	*N*,*N*-dimethylformamide
DPPC	dipalmitoylphosphatidylcholine
DSC	differential scanning calorimetry
ED	electron diffraction
EtOH	ethanol
FITC	fluorescein isothiocyanate
FT-IR/ATR	Fourier transform infrared spectroscopy/attenuated total reflection
GA	glucosamino acid
HATU	*O*-(7-azabenzotriazol-1-yl)-1,1,3,3-tetramethyluronium haxafluorophosphate
HOBt	1-hydroxybenzotriazole
MALDI-TOF	matrix-assisted laser desorption ionization time of flight
MeOH	methanol
MS	mass spectroscopy
NBD-PE	1,2-dipalmitoyl-*sn*-glycero-3-phosphoethanolamine-*N*-(7-nitro-2-1,3--benzoxadiazol-4-yl)
Rho-PE	1,2-dipalmitoyl-*sn*-glycero-3-phosphoethanolamine-*N*-(lissamine rhodamine B sulfonyl)
TEM	transmission electron microscopy
TFA	trifluoroacetic acid
TLC	thin layer chromatography

List of the Measurement Instruments Used in the Present Thesis

^{1}H NMR	Bruker DPX-400 spectrometer
CD	JASCO J-600 CD spectropolarimeter
DLS	Photal DLS-8000
DSC	Seiko SSC5200 DSC120
FAB MS	JEOL HA110 spectrometer
Fluorometer	JASCO FP-6600 spectro fluorometer
FT-IR/ATR	Nicolet 6700 FT-IR spectrometer
MALDI-TOF MS	JEOL JMS-ELITE spectrometer
	Bruker ultraflex III mass spectrometer
Optical and fluorescence microscope	
	Olympus IX70
	Keyence VHX-1000
TEM	JEOL JEM-2000EXII instrument
UV	Hitachi U-2001 spectrophotometer

General Introduction

General Introduction

Molecular assembly

Molecular self-assembly is based on the spontaneous association of molecules via noncovalent bonds under equilibrium conditions to generate stable, structurally well-defined aggregates. These self-assemblies are constructed by a great number of molecules and their assembling mechanism is often very complex because a number of parameters play important roles in cooperative and dynamic ways. Further, the self-assembling process is mediated through weak intermolecular forces, such as van der Waals forces, electrostatic interactions, hydrogen bonds, and π-π stacking interactions. Therefore, it is still difficult to predict the morphologies and dynamics of the assemblies from their constituent molecular structures.

On the other hand, in nature, complex multicomponent three-dimensional structures are formed through the spontaneous association of molecules.[1] Membrane proteins show various biological functions, and their localization in lipid bilayer with constructing complex morphologies allows amplification of the protein functions. For example, a localization of G-protein-coupled inwardly-rectifying potassium channels, which is specifically located at the postsynaptic membrane on the dendrites of dopaminergic neurons, enables an efficient cell signalling.[2–4] This fact obviously indicates that morphology of the molecular assembly is deeply related with function of living cells. In addition, it was reported on the internalization into HeLa cells of specifically designed, monodisperse hydrogel particles as a function of their sizes, shapes, and surface charges.[5] This observation is also a good example stressing the importance of the relationship of the shape of biomaterials with their bioprocesses.

The morphology control has been considered to be one of the most important challenges in the field of molecular assembling. Understanding about the mechanism on molecular self-assembling is directly related to the structural study about biological self-assemblies. For the accomplishment of the morphology control on molecular assembling,

there have been many reports on clarification of requirements for the constituent molecules to self-assemble into a specified morphology under proper preparative conditions.

Amphiphiles

The most important force to prepare molecular assembly is intermolecular hydrophobic interaction between amphiphilic molecules. Bangham and Horne found out that the bilayer vesicles were prepared from the egg yolk lecithin in 1964.[6] Since then, lipid amphiphiles have been extensively examined, and molecular assembly having various unique morphologies such as micelles,[7,8] worm-like micelles,[9,10] and vesicles[11,12] were prepared. Morphologies of molecular assemblies from lipid amphiphiles are revealed to be dependent on the critical packing parameter (CPP), which describes a balance of hydrophilic surface area and hydrophobic length of amphiphiles (Figure 1).[13] However, the molecular assembly is so soft, fluid, flexible, and imbalance due to low molecular weights of the lipids. Therefore, the assembly has a tendency to form thermodynamically stable and symmetrical shapes of

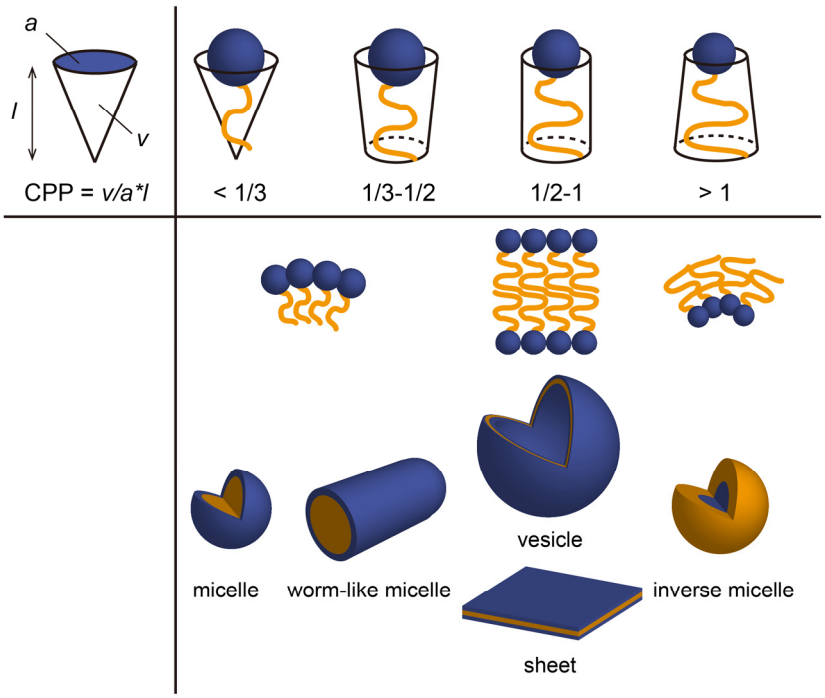

Figure 1. Relationship between the critical packing parameters (CPP) of lipids and their assembly morphologies.

vesicles etc. as described above. More complex morphologies found in nature are thus considered to be difficult to be prepared from lipid amphiphiles via self-assembling.

In addition to lipid amphiphiles, various types of amphiphilic compounds,[14–17] including synthetic polymers[18–20] and poly (oligo)peptides, have been studied from 1990s. These molecular assemblies are mostly more robust than those prepared from lipid amphiphiles, because high molecular weight hydrophobic moieties strongly associate with each other.[21] Further, these amphiphiles can be arbitrarily designed and modified by functional groups. Therefore, various forces such as aromatic interaction, dipole moment, and hydrogen bond can be utilized for control of the molecular assembling. Hydrophilic-lipophilic (hydrophilic-hydrophobic) balance (HLB)[22–24] of the amphiphiles is also an important factor for amphiphiles to take a specified morphology. To establish the principles of molecular design for amphiphiles to take a specified morphology, it is necessary to clarify the relationship between constituent molecular structures and assembly morphologies. Especially, amphiphilic polypeptides are suitable for the clarification because they are molecularly designed to take a specified conformation. Further, polypeptides are applicable to biomaterials due to their biocompatibility. For example, peptide-derived specific interactions can be utilized for bio-sensing and molecular recognition. Therefore, the author focuses his attention on preparation of molecular assemblies from peptides and/or their derivatives.

Peptide Vesicle

Vesicular assembly formation from peptide amphiphiles has been actively investigated from mid 1990s.[25–29] Bergeron et al. found out microcapsule formation from tetrapeptides derived from L-aspartic acid diketopiperazine.[25] On the other hand, Kimura et al. prepared vesicle assemblies from amphiphilic polypeptides, one having a gramicidin A unit and polyethylene glycol (PEG)[27] and the other with 8-mer peptide forming α-helix.[28] Since the hydrophobic layer in the peptide membrane was constituted of secondary structure of helix, the peptide vesicles (named peptosomes) show membrane fluidity. Polypeptide can be

also utilized as a hydrophilic segment.[30–35] For example, the ability of poly(butadiene)-*b*-poly(L-glutamic acid) block copolymers to form micelles and vesicular assemblies was confirmed.[36,37] These reports suggest that the vesicle size is well-defined by control of the length of poly(butadiene) and poly(L-glutamic acid). Amphiphilic peptides, which were constituted by hydrophilic and hydrophobic peptide moieties such as surfactant-like oligopeptide[38,39] and diblock copolypeptide,[40–47] also self-assembled to vesicular assemblies.

Recently, various kinds of peptide-based vesicles were prepared. Kataoka et al. prepared a novel polymer vesicle by a simple mixing of a pair of oppositely charged block copolymers composed of PEG and poly(amino acid)s in an aqueous medium and named it as polyion complex (PICsome).[48] Electric charges were cancelled by the ion-complex formation and worked as a constituent of hydrophobic core. Hadjichristidis et al. and Nolte et al. used triblock polypeptides for vesicle formation (Table 1).[49,50]

Table 1. Vesicle forming amphiphiles with polypeptide block.

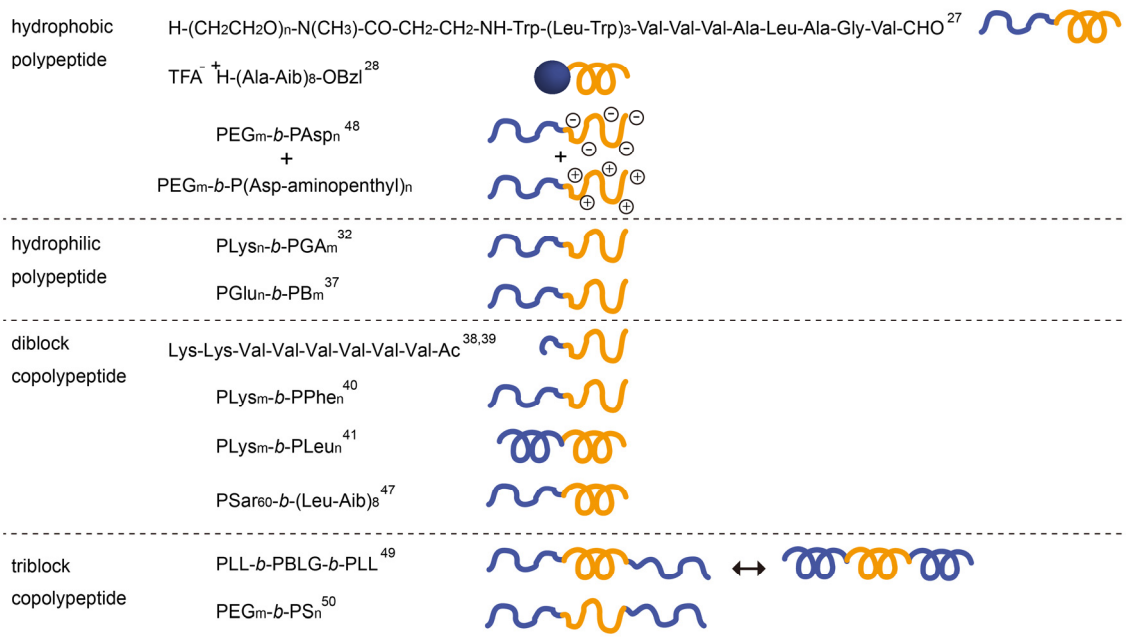

About nonpeptide polymer amphiphiles, Würthner et al. reported that the size control of vesicular assembly by co-self-assembly of wedge- and dumbbell-shaped amphiphilic perylene bisimides.[51] These examples suggest that the CPP is one of the most important factors for the formation of vesicle assembly. In the case of polymer amphiphiles, the assembly formation manner was also regulated by CPP, but was not so simple. This is because the hydrophilic segment of the amphiphilic polypeptides is a polymer with a defined molecular length, whereas that of lipid amphiphiles is considered as a dot.

Peptide Nanotube

Preparation of molecular assembly having tubular shapes also has made rapid progress in these ten years. At 2001, Matsui et al. demonstrated that bola-amphiphilic peptides, GG-heptane-GG containing both peptidic and non-peptidic segments, formed nanotubes whose diameter (50 nm–1 μm) was controllable by co-assembling with polycarbonate.[52,53] Various peptide surfactants, which are consisted of a hydrophilic head group with one or two charged amino acids and a hydrophobic tail with four or more consecutive segments such as A_6D, V_6D, G_8DD, KV_6 were synthesized.[38,54–56] Upon dissolution in water, these peptides formed the mixture of network of open-ended nanotubes, and numerous three-way junctions that may act as links between the nanotubes were observed. These molecules also formed a bilayer in the same way with conventional surfactants.

On the other hand, unlike conventional surfactants, peptide surfactants formed typical *β*-sheet structure implying a fairly extended backbone. The *β*-sheet peptides tend to be regularly packed with a tilt angle and to form a fibril or tubular assembly. Preparation of nanotube from a *β*-sheet peptide segment contained amphiphiles was reported by some research groups as follows. Mihara's group showed that the biotinylated peptides, BiXX-PKFKIIEFEP, having different linkers between biotin and *β*-sheet peptide segment, self-assembled to form a tubular structure in an aqueous solution with external diameter of *ca*. 60 nm and inner diameter of *ca*. 30 nm.[57] Lynn et al. prepared nanotube from a biological

peptide derived from the amphiphilic core Aβ(16–22).[58,59] Liskamp's group used modified Amylin(20–29). Amylin is known to form fibril structure. By controlling strength of intermolecular hydrogen bond by chemical modification, nanotubular assembly could be constructed.[60] On the other hand, Gazit et al. demonstrated nanotube formation from planar sheets using aromatic stacking inducement.[61–63] They used simple dipeptide, Phe-Phe, of the diphenylalanine motif in the Alzheimer's *β*-amyloid peptide. These nanotubes prepared from the amphiphilic peptides were robust, straight and so long, and their diameters showed a narrow distribution. This is because long helical ribbon generally fused the edges together to grow into nanotubes (Figure 2, top).[58,59] In 2008, Kimura's group showed the short nanotube with 70 nm in diameter and 200 nm in length.[64] In this case, nanotube formation mechanism is different from that of conventional peptide nanotube. They explained the mechanism of nanotube formation that the block polypeptide initially formed a curved square sheet assembly, and transformed the morphology quantitatively into nanotube upon heating. The transformation mechanism from the curved sheet into the nanotube is just to stick two opposing hydrophobic sides of the square sheet (Figure 2, bottom). Therefore, the size of the nanotube is determined by the initial size of the curved square sheet, which has an advantage of a very narrow size distribution of the produced nanotubes.

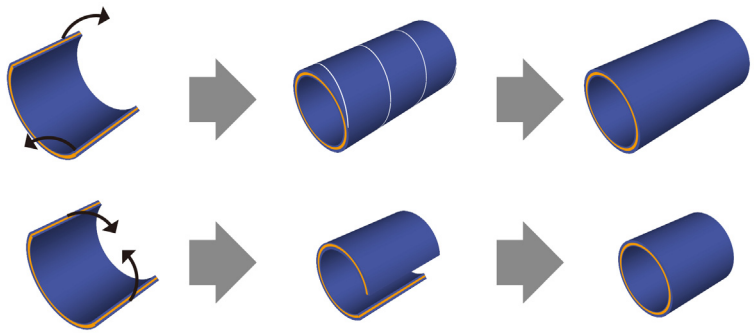

Figure 2. Transformation mechanism from nanosheet into nanotube assembly.

In the self-assembling fields with using lipid surfactants and aromatic amphiphiles, chirality of amphiphiles is reported to be important to form nanotube (Figure 3).[65–74] In peptidic amphiphiles, however, it is so difficult to clarify the relation between chirality and

nanotube formation, because peptides have chiral points of constituent residues and chirality derived from the secondary structure.

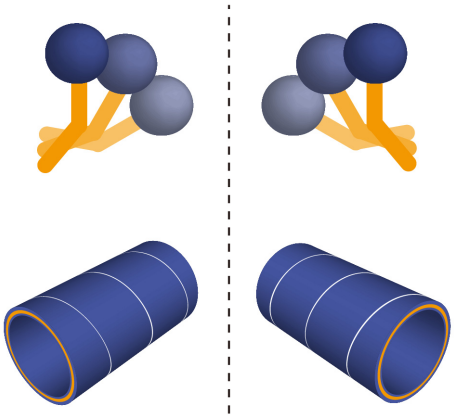

Figure 3. Schematic illustration of the relation between chirality of amphiphiles and their nanotube formation.

Complex Assembly

In recent years, some reports on Janus materials have been published in lipid assemblies,[75–77] protein derivate,[78–80] polymer particles,[81–91] and inorganic materials.[92–94] Janus materials have two or more faces of different chemical or physical characters within themselves (Figure 4). For example, Janus structures are classified into three categories according to their architecture: spherical micelles and particles (3D),[81–85,93] two types of cylinders (1D),[86] and sheets or discs (2D).[87] These structures are attractive in nanoscience due to their interesting properties in terms of an academic point of view as well as technological reasons.[88,95,89,83] Inorganic and polymeric Janus materials have been developed but their structures are particles different from membranes of self-assembling. On the other hand, examples of Janus assemblies from amphiphiles are hardly reported because they are difficult to be prepared. Some phase-separated lipid membrane formed Janus vesicle morphology and its phase-separated assembly may have a complex morphology.[75] The preparation of these Janus assemblies is an important challenge for control of the novel complex morphology and for development of the molecular assembly field.

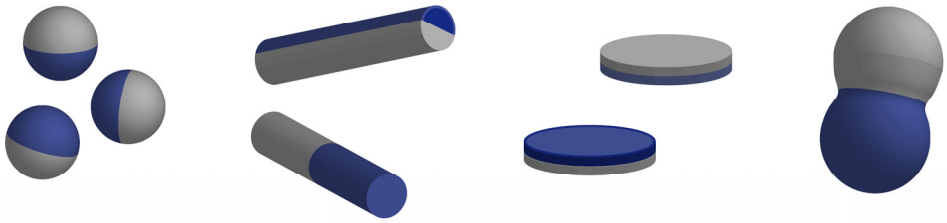

Figure 4. Schematic illustration of Janus materials.

Aim

Peptide amphiphilies can be molecularly designed in terms of dipole moment, secondary structure, functionalization, and precisely controllable hydrophilic-hydrophobic balance. The peptide amphiphiles therefore have advantages for elucidation of the assembling mechanism into a specific morphology. As described before, various molecular assemblies have been prepared with using peptide-based molecules, and these reports help us understand the relationship between assembly morphologies and constituents. However, several factors of peptide amphiphiles remain to be evaluated. Especially, the author focuses his attention on examination of amphiphilic polypeptides having a hydrophobic helical block. Helical peptides have a good ability to be regularly packed in the molecular assembly as frequently observed helix bundles in nature.[96,97] With using these amphiphilic peptides, stable assemblies can be prepared and the effects of helicity in hydrophobic core of molecular assemblies on morphology can be elucidated. In addition, the author tries to prepare the molecular assemblies having more complex morphology composed of patchwork patterns, where different peptide membranes are combined like the Janus assembly by using a phase-separation strategy in the membrane.

With the background described above, the control and the preparation of molecular assemblies having vesicular, tubular and more complex structures from peptide amphiphiles are investigated in the present thesis.

Outline

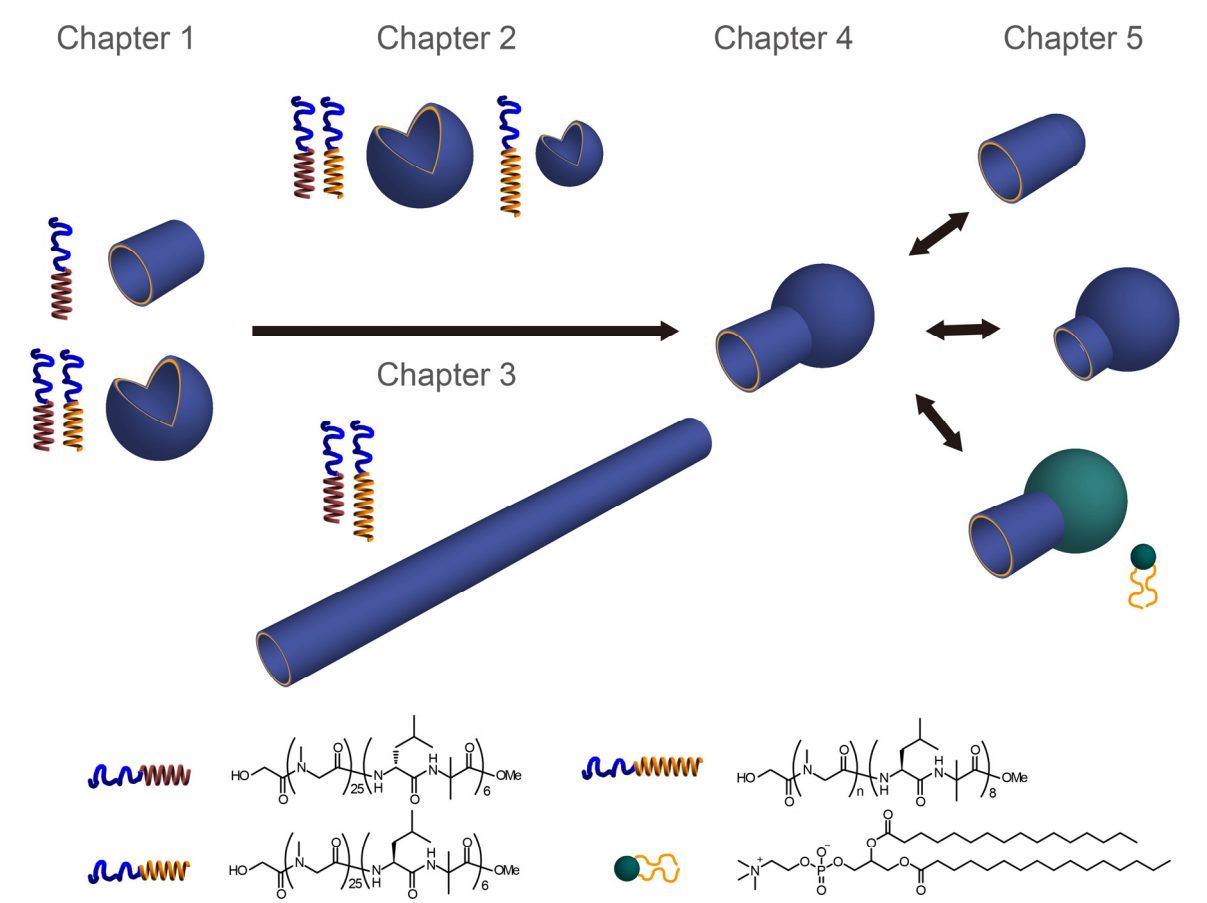

Figure 5. Schematic illustration of amphiphiles and assembly morphologies dealt in each chapters of this present thesis.

In Chapter 1, the morphology of peptide assembly is evaluated in the viewpoint of the helicity of constituent peptides. A right-handed helix and a left-handed helix may form a stereo-complex, which should lead to morphology different from a right-handed helix or a left-handed helix alone. Here, two different amphiphilic polypeptides, $(Sar)_{25}$-*b*-(L-Leu-Aib)$_6$ and $(Sar)_{25}$-*b*-(D-Leu-Aib)$_6$, are designed and synthesized. The hydrophobic blocks of the former and the latter peptides form a right-handed and a left-handed helix, respectively. The size and shape of molecular assemblies prepared from a single component and from an equimolar mixture of these peptides are compared by TEM observation. Further, a difference

of thermodynamic stability between these two assemblies is also studied by occurrence of membrane fusion.

In Chapter 2, a membrane fusion ability of vesicles composed of an equimolar mixture of $(Sar)_{25}$-*b*-(L-Leu-Aib)$_6$ and $(Sar)_{25}$-*b*-(D-Leu-Aib)$_6$ is studied. A stereo-complex membrane in this vesicle becomes more flexible upon heating. The flexibility may cause the vesicle fusion to become a more stable morphology. This point is precisely investigated by using a stereo-complex between these peptides.

In Chapter 3, a series of stereo-complexes between $(Sar)_{25}$-*b*-(D-Leu-Aib)$_6$ and $(Sar)_{24}$-*b*-(L-Leu-Aib)$_n$ (n = 7, 8, 10) are examined on their self-assemblies. The right-handed helix and the left-handed helix favor to associate together, but in these stereo-complexes there are misfits about the helix lengths between them. The effects of these misfits in helix length on self-assembling are examined and discussed.

Chapter 4 deals with the preparation of molecular assembly having novel morphology. It is expected that morphology is able to be controlled by a combination of a nanotube forming membrane from a single component and a vesicle forming membrane from a stereo-complex of $(Sar)_{25}$-*b*-(L-Leu-Aib)$_6$ and $(Sar)_{25}$-*b*-(D-Leu-Aib)$_6$. In addition, distribution of one component in the assembly is evaluated by labeling the component with a gold nano particle.

Chapter 5 describes preparation of new morphologies with extension of the results obtained in Chapter 4. The author examines self-assembling with combinations of two different membranes, which form vesicle and nanotube. As vesicle forming molecules, $(Sar)_{25}$-*b*-(L-Leu-Aib)$_6$ and a dipalmitoylphosphatidylcholine (DPPC) are examined. As nanotube forming membrane, $(Sar)_{24}$-*b*-(L-Leu-Aib)$_7$ and a mixture of $(Sar)_{24}$-*b*-(L-Leu-Aib)$_7$ and $(Sar)_{25}$-*b*-(D-Leu-Aib)$_6$ are examined.

These patchwork assemblies are characteristic from others because the membranes

are phase-separated into two phases, which take their own morphologies. The size of each morphology is also controllable. In this sense, the principles which are shown in this thesis are quite new and are expected to be applied to various materials fields. The details are described in the following chapters.

References

(1) Whitesides, G. M.; Mathias, J. P.; Seto, C. T. *Science* **1991**, *254*, 1312–1319.

(2) Shimada, A.; Niwa, H.; Tsujita, K.; Suetsugu, S.; Nitta, K.; Hanawa-Suetsugu, K.; Akasaka, R.; Nishino, Y.; Toyama, M.; Chen, L.; Liu, Z.; Wang, B.; Yamamoto, M.; Terada, T.; Miyazawa, A.; Tanaka, A.; Sugano, S.; Shirouzu, M.; Nagayama, K.; Takenawa, T.; Yokoyama, S. *Cell* **2007**, *129*, 761–772.

(3) Wang, H.; Kunkel, D.; Schwartzkroin, P.; Tempel, B. *J. Neurosci.* **1994**, *14*, 4588–4599.

(4) Yellen, G. *Nature* **2002**, *419*, 35–42.

(5) Gratton, S. E. A.; Ropp, P. A.; Pohlhaus, P. D.; Luft, J. C.; Madden, V. J.; Napier, M. E.; DeSimone, J. M. *Proceedings of the National Academy of Sciences* **2008**, *105*, 11613–11618.

(6) Bangham, A.; Horne, R. *Journal of Molecular Biology* **1964**, *8*, 660–668, IN2-IN10.

(7) Turro, N. J.; Yekta, A. *Journal of the American Chemical Society* **1978**, *100*, 5951–5952.

(8) Streletzky, K.; Phillies, G. D. J. *Langmuir* **1995**, *11*, 42–47.

(9) Lin, Z.; Cai, J. J.; Scriven, L. E.; Davis, H. T. *The Journal of Physical Chemistry* **1994**, *98*, 5984–5993.

(10) Rodrigues, R. K.; da Silva, M. A.; Sabadini, E. *Langmuir* **2008**, *24*, 13875–13879.

(11) Huang, C. *Biochemistry* **1969**, *8*, 344–352.

(12) Mui, B. L.; Döbereiner, H. G.; Madden, T. D.; Cullis, P. R. *Biophysical Journal* **1995**, *69*, 930–941.

(13) Israelachvili, J. N. *Intermolecular and Surface Forces, Third Edition*; 3日 ed.; Academic Press, 2010.

(14) Tanaka, Y.; Miyachi, M.; Kobuke, Y. *Angew. Chem. Int. Ed.* **1999**, *38*, 504–506.

(15) Lee, M.; Lee, S.; Jiang, L. *Journal of the American Chemical Society* **2004**, *126*, 12724–12725.

(16) Houmadi, S.; Coquière, D.; Legrand, L.; Fauré, M. C.; Goldmann, M.; Reinaud, O.; Rémita, S. *Langmuir* **2007**, *23*, 4849–4855.

(17) Jeon, Y. J.; Bharadwaj, P. K.; Choi, S.; Lee, J. W.; Kim, K. *Angew. Chem. Int. Ed.* **2002**, *41*, 4474–4476.

(18) Ayres, L.; Deming, T. J.; Hest, J. C. M. V.; Klok, H.; Schlaad, H. *Peptide Hybrid Polymers*; Advances in Polymer Science; 1日 ed.; Springer-Verlag, 2006.

(19) Luo, L.; Eisenberg, A. *Journal of the American Chemical Society* **2001**, *123*, 1012–1013.

(20) Schrage, S.; Sigel, R.; Schlaad, H. *Macromolecules* **2003**, *36*, 1417–1420.

(21) Ahmed, F.; Photos, P. J.; Discher, D. E. *Drug Dev. Res.* **2006**, *67*, 4–14.

(22) Griffin, W. C. *Journal of the Society of Cosmetic Chemists* **1949**, *1*, 311–326.

(23) Griffin, W. C. *Journal of the Society of Cosmetic Chemists* **1954**, 259–.

(24) Devies, J. T. *A Quantitative Kinetic Theory of Emulsion Type. I Physical Chemistry of the Emulsifying Agent.*
In Gas/Liquid and Liquid/Liquid Interfaces.; Proceedings of 2nd International Congress Surface Activity; Butterworths, London, 1957.

(25) Bergeron, R. J.; Phanstiel, O.; Yao, G. W.; Milstein, S.; Weimar, W. R. *Journal of the American Chemical Society* **1994**, *116*, 8479–8484.

(26) Chornelissen, J. J. L. M.; Fischer, M.; Sommerdijk, N. A. J. M.; Nolte, R. J. M. *Science* **1998**, *280*, 1427–1430.

(27) Kimura, S.; Kim, D.; Sugiyama, J.; Imanishi, Y. *Langmuir* **1999**, *15*, 4461–4463.

(28) Fujita, K.; Kimura, S.; Imanishi, Y. *Langmuir* **1999**, *15*, 4377–4379.

(29) Harada, A.; Kataoka, K. *Science* **1999**, *283*, 65–67.

(30) Ayres, L.; Hans, P.; Adams, J.; Löwik, D. W. P. M.; van Hest, J. C. M. *J. Polym. Sci. A Polym. Chem.* **2005**, *43*, 6355–6366.

(31) Al-Jamal, K. T.; Sakthivel, T.; Florence, A. T. *International Journal of Pharmaceutics* **2003**, *254*, 33–36.

(32) Rodríguez-Hernández, J.; Lecommandoux, S. *Journal of the American Chemical Society* **2005**, *127*, 2026–2027.

(33) Chécot, F.; Brûlet, A.; Oberdisse, J.; Gnanou, Y.; Mondain-Monval, O.; Lecommandoux, S. *Langmuir* **2005**, *21*, 4308–4315.

(34) Carlsen, A.; Lecommandoux, S. *Current Opinion in Colloid & Interface Science* **2009**, *14*, 329–339.

(35) Kim, W.; Thévenot, J.; Ibarboure, E.; Lecommandoux, S.; Chaikof, E. *Angewandte Chemie International Edition* **2010**, *49*, 4257–4260.

(36) Chécot, F.; Lecommandoux, S.; Gnanou, Y.; Klok, H. *Angewandte Chemie International Edition* **2002**, *41*, 1339–1343.

(37) Kukula, H.; Schlaad, H.; Antonietti, M.; Förster, S. *Journal of the American Chemical Society* **2002**, *124*, 1658–1663.

(38) Vauthey, S.; Santoso, S.; Gong, H.; Watson, N.; Zhang, S. *Proceedings of the National Academy of Sciences of the United States of America* **2002**, *99*, 5355–5360.

(39) von Maltzahn, G.; Vauthey, S.; Santoso, S.; Zhang, S. *Langmuir* **2003**, *19*, 4332–4337.

(40) Jan, J.; Lee, S.; Carr, C. S.; Shantz, D. F. *Chemistry of Materials* **2005**, *17*, 4310–4317.

(41) Bellomo, E. G.; Wyrsta, M. D.; Pakstis, L.; Pochan, D. J.; Deming, T. J. *Nat Mater* **2004**, *3*, 244–248.

(42) Holowka, E. P.; Sun, V. Z.; Kamei, D. T.; Deming, T. J. *Nat Mater* **2007**, *6*, 52–57.

(43) Kimura, S.; Muraji, Y.; Sugiyama, J.; Fujita, K.; Imanishi, Y. *Journal of Colloid and Interface Science* **2000**, *222*, 265–267.

(44) Kimura, S.; Sugiyama, J.; Muraji, Y.; Kim, D.; Imanishi, Y. *Pept Sci* **2001**, *2000*, 397–400.

(45) Nishikawa, H.; Morita, T.; Sugiyama, J.; Kimura, S. *Journal of Colloid and Interface Science* **2004**, *280*, 506–510.

(46) Tanisaka, H.; Kizaka-Kondoh, S.; Makino, A.; Tanaka, S.; Hiraoka, M.; Kimura, S. *Bioconjugate Chemistry* **2008**, *19*, 109–117.

(47) Makino, A.; Kizaka-Kondoh, S.; Yamahara, R.; Hara, I.; Kanzaki, T.; Ozeki, E.; Hiraoka, M.; Kimura, S. *Biomaterials* **2009**, *30*, 5156–5160.

(48) Koide, A.; Kishimura, A.; Osada, K.; Jang, W.; Yamasaki, Y.; Kataoka, K. *Journal of the American Chemical Society* **2006**, *128*, 5988–5989.

(49) Iatrou, H.; Frielinghaus, H.; Hanski, S.; Ferderigos, N.; Ruokolainen, J.; Ikkala, O.; Richter, D.; Mays, J.; Hadjichristidis, N. *Biomacromolecules* **2007**, *8*, 2173–2181.

(50) Reynhout, I. C.; Cornelissen, J. J. L. M.; Nolte, R. J. M. *Journal of the American Chemical Society* **2007**, *129*, 2327–2332.

(51) Zhang, X.; Chen, Z.; Würthner, F. *Journal of the American Chemical Society* **2007**, *129*, 4886–4887.

(52) Matsui, H.; Douberly, G. E. *Langmuir* **2001**, *17*, 7918–7922.

(53) Porrata, P.; Goun, E.; Matsui, H. *Chemistry of Materials* **2002**, *14*, 4378–4381.

(54) Zhang, S.; Zhao, X. *J. Mater. Chem.* **2004**, *14*, 2082.

(55) Zhao, X. J.; Zhang, S. *Polymers for Regenerative Medicine*; Advances in Polymer Science; 2006.

(56) Zhang, S. *Nat Biotech* **2003**, *21*, 1171–1178.

(57) Matsumura, S.; Uemura, S.; Mihara, H. *Mol. BioSyst.* **2005**, *1*, 146.

(58) Lu, K.; Jacob, J.; Thiyagarajan, P.; Conticello, V. P.; Lynn, D. G. *Journal of the American Chemical Society* **2003**, *125*, 6391–6393.

(59) Lu, K.; Guo, L.; Mehta, A. K.; Childers, W. S.; Dublin, S. N.; Skanthakumar, S.; Conticello, V. P.; Thiyagarajan, P.; Apkarian, R. P.; Lynn, D. G. *Chem. Commun.*

2007, 2729.

(60) Elgersma, R. C.; Meijneke, T.; Posthuma, G.; Rijkers, D. T. S.; Liskamp, R. M. J. *Chem. Eur. J.* **2006**, *12*, 3714–3725.

(61) Adler-Abramovich, L.; Reches, M.; Sedman, V. L.; Allen, S.; Tendler, S. J. B.; Gazit, E. *Langmuir* **2006**, *22*, 1313–1320.

(62) Reches, M.; Gazit, E. *Phys. Biol.* **2006**, *3*, S10–S19.

(63) Yemini, M.; Reches, M.; Rishpon, J.; Gazit, E. *Nano Letters* **2005**, *5*, 183–186.

(64) Kanzaki, T.; Horikawa, Y.; Makino, A.; Sugiyama, J.; Kimura, S. *Mcromolecular Bioscience* **2008**, *8*, 1026–1033.

(65) Cornelissen, J. J. L. M.; Rowan, A. E.; Nolte, R. J. M.; Sommerdijk, N. A. J. M. *Chemical Reviews* **2001**, *101*, 4039–4070.

(66) Yamamoto, T.; Fukushima, T.; Kosaka, A.; Jin, W.; Yamamoto, Y.; Ishii, N.; Aida, T. *Angewandte Chemie International Edition* **2008**, *47*, 1672–1675.

(67) Brizard, A.; Ahmad, R. K.; Oda, R. *Chemical Communications* **2007**, 2275–2277.

(68) Fukushima, K.; Chang, Y.; Kimura, Y. *Macromolecular Bioscience* **2007**, *7*, 829–835.

(69) Oda, R.; Huc, I.; Candau, S. J. *Angewandte Chemie International Edition* **1998**, *37*, 2689–2691.

(70) Brizard, A.; Aime, C.; Labrot, T.; Huc, I.; Berthier, D.; Artzner, F.; Desbat, B.; Oda, R. *Journal of the American Chemical Society* **2007**, *129*, 3754–3762.

(71) Selinger, J. V.; MacKintosh, F. C.; Schnur, J. M. *Physical Review E* **1996**, *53*, 3804–3818.

(72) Zhong-can, O. *Physical Review A* **1991**, *43*, 6826–6836.

(73) Selinger, J. V.; Spector, M. S.; Schnur, J. M. *The Journal of Physical Chemistry B* **2001**, *105*, 7157–7169.

(74) Oda, R.; Huc, I.; Schmutz, M.; Candau, S. J.; MacKintosh, F. C. *Nature* **1999**, *399*, 566–569.

(75) Semrau, S.; Schmidt, T. *Soft Matter* **2009**, *5*, 3174.

(76) Loew, M.; Springer, R.; Scolari, S.; Altenbrunn, F.; Seitz, O.; Liebscher, J.; Huster, D.; Herrmann, A.; Arbuzova, A. *Journal of the American Chemical Society* **2010**, *132*, 16066–16072.

(77) Christian, D. A.; Tian, A.; Ellenbroek, W. G.; Levental, I.; Rajagopal, K.; Janmey, P. A.; Liu, A. J.; Baumgart, T.; Discher, D. E. *Nat Mater* **2009**, *8*, 843–849.

(78) Uchida, M.; Kang, S.; Reichhardt, C.; Harlen, K.; Douglas, T. *Biochimica et Biophysica Acta (BBA) - General Subjects* **2010**, *1800*, 834–845.

(79) Suci, P. A.; Kang, S.; Young, M.; Douglas, T. *Journal of the American Chemical Society* **2009**, *131*, 9164–9165.

(80) Kang, S.; Suci, P. A.; Broomell, C. C.; Iwahori, K.; Kobayashi, M.; Yamashita, I.; Young, M.; Douglas, T. *Nano Letters* **2009**, *9*, 2360–2366.

(81) Erhardt, R.; Böker, A.; Zettl, H.; Kaya, H.; Pyckhout-Hintzen, W.; Krausch, G.; Abetz, V.; Müller, A. H. E. *Macromolecules* **2001**, *34*, 1069–1075.

(82) Erhardt, R.; Zhang, M.; Böker, A.; Zettl, H.; Abetz, C.; Frederik, P.; Krausch, G.; Abetz, V.; Müller, A. H. E. *Journal of the American Chemical Society* **2003**, *125*, 3260–3267.

(83) Walther, A.; Hoffmann, M.; Müller, A. *Angew. Chem. Int. Ed.* **2008**, *47*, 711–714.

(84) Yan, L.; Popp, N.; Ghosh, S.; Böker, A. *ACS Nano* **2010**, *4*, 913–920.

(85) Wurm, F.; Kilbinger, A. F. M. *Angewandte Chemie International Edition* **2009**, *48*, 8412–8421.

(86) Liu; Abetz, V.; Müller, A. H. E. *Macromolecules* **2003**, *36*, 7894–7898.

(87) Walther, A.; André, X.; Drechsler, M.; Abetz, V.; Müller, A. H. E. *Journal of the American Chemical Society* **2007**, *129*, 6187–6198.

(88) Roh, K.; Martin, D. C.; Lahann, J. *Nat Mater* **2005**, *4*, 759–763.

(89) Li, X.; Yang, H.; Xu, L.; Fu, X.; Guo, H.; Zhang, X. *Macromol. Chem. Phys.* **2010**, *211*, 297–302.

(90) Walther, A.; Drechsler, M.; Rosenfeldt, S.; Harnau, L.; Ballauff, M.; Abetz, V.; Müller, A. H. E. *Journal of the American Chemical Society* **2009**, *131*, 4720–4728.

(91) Tang, C.; Zhang, C.; Liu, J.; Qu, X.; Li, J.; Yang, Z. *Macromolecules* **2010**, *43*, 5114–5120.

(92) Lin, C.; Liao, C.; Chao, Y.; Kuo, C. *ACS Applied Materials & Interfaces* **2010**, *2*, 3185–3191.

(93) Jonas, U.; Vamvakaki, M. *Angewandte Chemie International Edition* **2010**, *49*, 4542–4543.

(94) Berger, S.; Synytska, A.; Ionov, L.; Eichhorn, K.; Stamm, M. *Macromolecules* **2008**, *41*, 9669–9676.

(95) Nonomura, Y.; Komura, S.; Tsujii, K. *Langmuir* **2004**, *20*, 11821–11823.

(96) Milburn, M. V.; Prive, G. G.; Milligan, D. L.; Scott, W. G.; Yeh, J.; Jancarik, J.; Koshland, D. E.; Kim, S. H. *Science* **1991**, *254*, 1342–1347.

(97) Parker, M. W.; Pattus, F.; Tucker, A. D.; Tsernoglou, D. *Nature* **1989**, *337*, 93–96.

Chapter 1

Transformation of Peptide Nanotubes to Vesicle via Fusion Driven by Stereo-Complex Formation

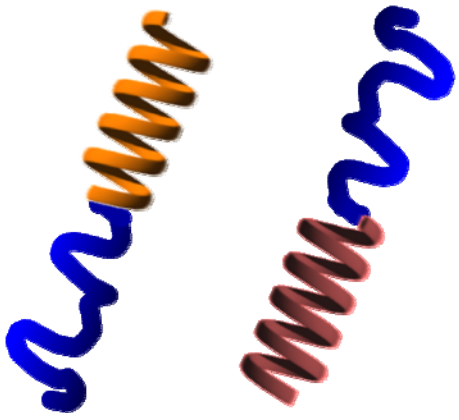

Introduction

Helical peptides are easily designed to take either helicity, right-handed or left-handed, by using L- or D-residues in the sequence. When the right-handed helix is mixed with the left-handed helix, they are expected to form a stereo-complex probably due to the convexo-concave fitness between their surfaces. By using stereo-complex formation of these helical peptides, the author demonstrates here vesicle formation from two types of peptide nanotubes by membrane fusion.

Several morphologies in the shapes of micelle, rod-shaped micelle, sheet, tube and vesicle have been prepared in solution by the current self-assembling techniques.[1–4] The author has reported on molecular assemblies of amphiphilic peptide molecules especially by using hydrophobic helical peptides at the hydrophobic core of the molecular assemblies.[5–9] Helical peptides have a good ability to be packed regularly in the molecular assembly as shown by frequent observation of helix bundles in nature.[10,11] Indeed, several hydrophobic helical peptides with attachment of suitable hydrophilic groups formed vesicular assemblies with a diameter of *ca.* 100 nm in water, which are named "peptosome".[5] Further, a peptide nanotube with a diameter of *ca*. 60 nm and a length of *ca*. 200 nm was obtained from amphiphilic block polypeptide with a hydrophobic helix, $(Sar)_{27}$-*b*-$(L\text{-Leu-Aib})_6$.[12] In the latter case, the block polypeptide initially formed a curved square sheet assembly, which was transformed quantitatively into a nanotube morphology upon heating at 90 °C for 10 min. The transformation mechanism from the curved sheet to the nanotube is just to stick two opposing hydrophobic sides of the square sheet, which is unique from other reports on nanotube formation, where a twisted long sheet or helix ribbon generally fused the edges together to grow into nanotubes.[13–17] On the other hand, in our nanotubes, the size of the nanotube is determined by the initial size of the curved square sheet, which has an advantage of a very narrow size distribution of the produced nanotubes. The reason for the sheet curving is

considered to be due to the regular packing of the right-handed helices in the hydrophobic core, similarly to the recent studies on molecular assemblies with chiral molecules.[18–31]

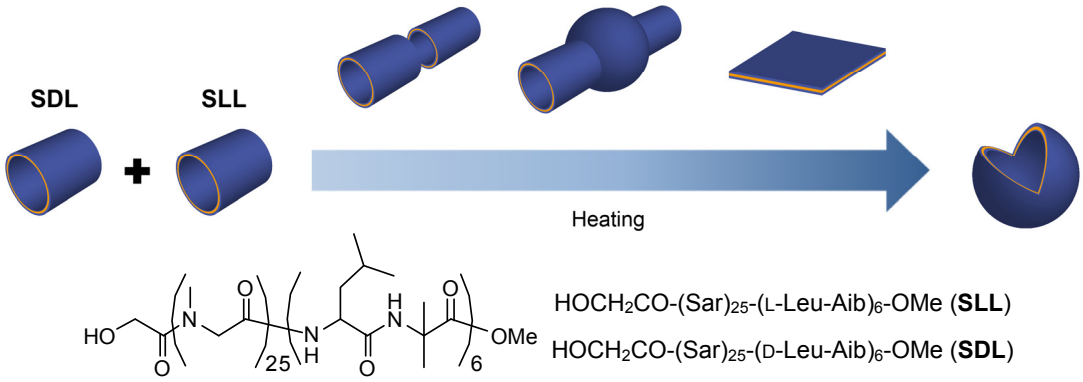

Experimental Section

Materials. Boc-L-leucine (Boc-Leu), aminoisobutylic acid (Aib) and Z-sarcosine (Z-Sar) were purchased from Watanabe Chemical Industries, Ltd. (Japan). Water was purified by a Milli-Q system (Nihon Millipore Ltd, Japan) and had a specific resistivity of *ca.* 18 MΩ cm^{-1}. All other reagents were purchased from commercial sources and used as received.

Preparation of Molecular Assemblies. Polypeptide (12 mg) was dissolved in ethanol (120 μL). Then an aliquot (30 μL) of the peptide solution was injected into a buffer (1 mL, 10 mM Tris-HCl, pH 7.4) with stirring at 4 °C. After 30 min, the dispersion was purified by Sephacryl S-100 column (1.5 × 30 cm, GE healthcare Bio-Sciences) using 10 mM Tris-HCl buffer (pH 7.4) as an eluent to remove ethanol. Molecular assemblies of different compositions were prepared similarly.

Circular Dichroism (CD). CD measurements were carried out on a JASCO J600 spectropolarimeter with an optical cell of 0.1 cm optical path length at room temperature. The

sample concentration in 10 mM Tris-HCl buffer (pH 7.4) was 0.375 mM (per amino acid residue).

Transmission Electron Microscopy (TEM) and Electron Diffraction (ED) Analysis. TEM images were taken using a JEOL JEM-2000EXII at an accelerating voltage of 100 kV. For the observation, a drop of dispersion was mounted on a carbon-coated Cu grid and stained negatively with 2 % uranyl acetate, followed by suction of the excess fluid with a filter paper.

Frozen-Hydrated/Cryogenic-TEM (Cryo-TEM). The dispersions in a buffer were frozen quickly in liquid ethane, which was cooled with liquid nitrogen. The samples were examined at 100 kV accelerating voltage at the liquid nitrogen temperature.

Fourier Transform Infrared Spectroscopy/Attenuated Total Reflection (FT-IR/ATR). Infrared transmission spectroscopy of the assembly dispersion was performed on a Fourier transform infrared spectrometer (Nicolet 6700 FT-IR, Thermo Fisher Scientific, MA) at room temperature with a solution cell. The sample concentration in ultrapure water was *ca*. 0.33 mM.

S25L12 and S25D12 (SLL and SDL). The Aib-containing dodecapeptides were synthesized by the conventional liquid phase method. Boc group of the dodecapeptide (600 mg, 0.454 mmol) was removed by treatment with trifluoroacetic acid (TFA, 6 mL) and anisole (0.6 mL). The TFA salt was washed with isopropylether and dried in vacuo for 2 h. The salt was dissolved in chloroform and washed with 4 wt% $NaHCO_3$ and saturated NaCl aqueous solutions. The organic layer was dried over anhydrous $MgSO_4$ and the solvent was removed and dried in vacuo to afford H-(Leu-Aib)$_6$-OMe (546 mg). To a solution of Sar NCA (634 mg, 5.51 mmol) in *N,N*-dimethylformamide (DMF) (12 mL), a solution of H-(Leu-Aib)$_6$-OMe in DMF/$CHCl_3$ (9:1 v/v, 273 mg / 10 mL) was added. After complete consumption of the Sar NCA was confirmed, glycolic acid (85 mg, 1.12 mmol, 5.0 eq.), 2-(1-H-7-azabenzotriazol-1-yl)-1,1,3,3-tetramethyl uronium hexafluorophosphate methanaminium

(HATU, 426 mg, 1.12 mmol, 5.0 eq.) and diisopropyl ethyl amine (DIEA, 293 mL, 1.68 mmol, 7.5 eq.) were added at 0 °C to react with the *N*-terminal, and the solution was stirred at 0 °C for 10 min and at room temperature for 10 h. Then another portions of glycolic acid (34 mg, 0.45 mmol, 2.0 eq.), HATU (170 mg, 0.45 mmol, 2.0 eq.), and DIEA (118 mL, 0.67 mmol, 3.0 eq.) were added to the solution. After stirring for 12 h, the solution was condensed, and the residue was purified by a Sephadex LH20 column with methanol as an eluent to afford polypeptided **SLL** or **SDL** (504 mg). The degree of polymerization of the poly(Sar) block was determined to be 25 from the relative areas of Sar*N*-CH_3 signal against the OCH_3 signal in the ^{1}H NMR spectra.

^{1}H NMR (400 MHz, MeOH-*d*) δ (ppm) 8.2–7.7 (m, 11H, amide), 7.4–7.3 (br, 1H, amide), 4.6–3.8 (br, 56H, LeuC$^{\alpha}H$, SarCH_2), 3.66 (s, 3H, OCH_3), 3.3–2.8 (m, 75H, Sar N-CH_3), 1.9–1.3 (m, 36H, LeuCH_2, LeuC$^{\gamma}H$, AibCH_3), 1.1–0.8 (m, 36H, Leu(CH_3)$_2$).

MALDI-TOF MS analysis also supported the degree of polymerization to be 25 (Figure 1).

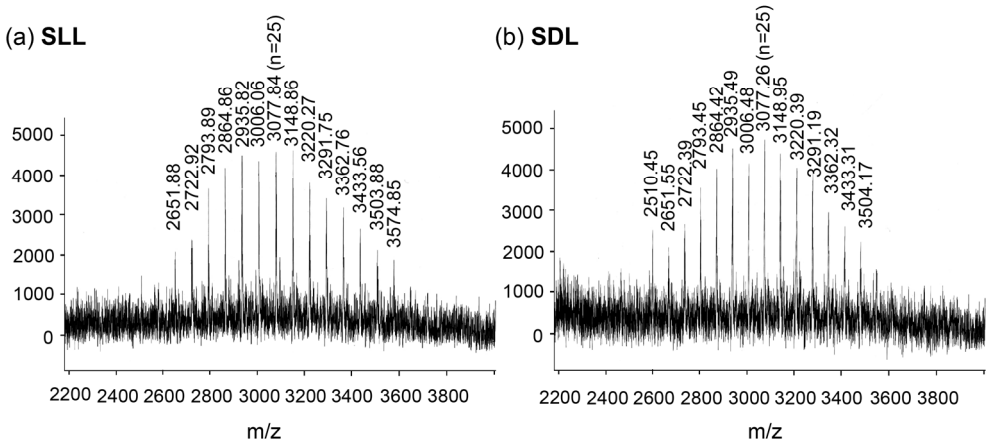

Figure 1. MALDI-TOF MS spectra of (a) **SLL** and (b) **SDL.** Poly(sarcosine) of 25 mers were attached to the *N*-terminal of hydrophobic blocks of **SLL** and **SDL**. ([M+Na]$^+$ calcd: 3077)

Results and Discussion

Peptide design and synthesis. Poly(sarcosine) is used here as a hydrophilic segment, because it is as hydrophilic as poly(ethylene glycol), and sarcosine is biodegradable by endogenous sarcosine dehydrogenase. The author has applied the amphiphilic peptide micelles made of $(Sar)_n$-*b*-$(Glu\text{-}OMe)_m$[6] or $(Sar)_n$-*b*-$(lactic\ acid)_m$[7] for *in vivo* tumor imaging by using a near-infrared fluorescence labeling probe. These poly(sarcosine) conjugates are shown to be highly biocompatible. The $(Sar)_{25}$ block was attached to the *N*-terminal of the hydrophobic helical block, (L- or D-Leu-Aib)$_6$, *via* polymerization of sarcosine *N*-carboxy anhydride (NCA) to obtain **SLL** or **SDL** (Scheme 1 and 2).

Scheme 1. Synthetic scheme of the hydrophobic polypeptide segment.

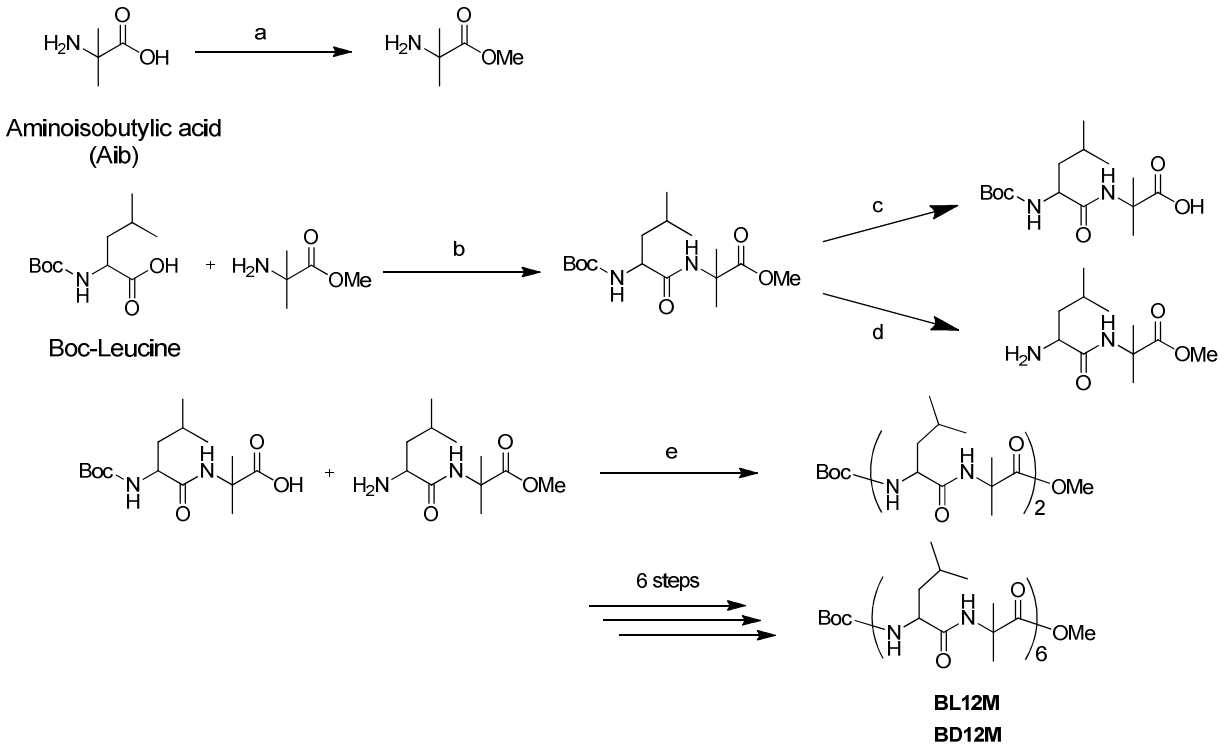

(a) $SOCl_2$/MeOH, 99 %; (b) DCC, HOBt/DMF, 93 %; (c) NaOH/MeOH, 100 %, (d) 4N HCl-dipxane, 97 %, (e) DCC, HOBt/DMF, 89 %.

Scheme 2. Synthetic scheme of the amphiphilic polypeptide segment.

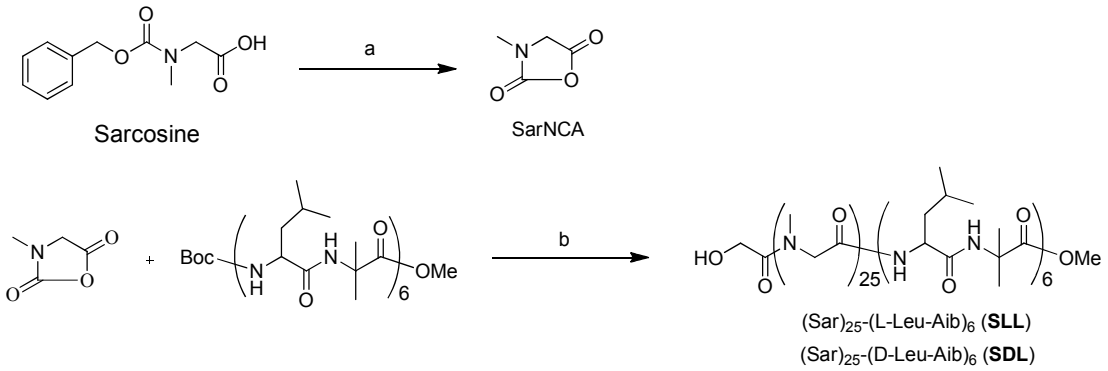

(a) $SOCl_2$, 14 %; (b) HATU, DIEA/DMF, $CHCl_3$ 95 %.

Molecular assembly prepared from SLL and SDL. Morphologies of molecular assemblies were studied by transmission electron microscope (TEM) with negative staining or cryogenic freezing. As previously reported, **SLL** as injected in buffer took a homogeneous nano curved-sheet morphology.[12] The same nano curved-sheet assembly was also obtained from **SDL** (Figure 2a). These nano curved-sheet assemblies were transformed into nanotubes by heating the molecular assembly solution at 90 °C for 10 min (Figure 2b). Circular dichroism (CD) measurements showed that **SLL** and **SDL** in the molecular assemblies took right-handed and left-handed α-helix, respectively. Further, the Cotton effect at 222 nm was slightly stronger than that at 208 nm, indicating that the helices form a tightly packed bundle structure (Figure 3).

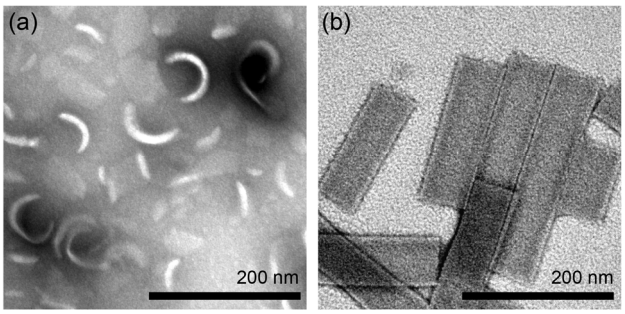

Figure 2. TEM images (negative staining with uranyl acetate) of the assembly suspension from **SDL** before (a) and after heating at 90 °C (b). The assemblies were prepared in 10 mM Tris-HCl Buffer (pH 7.4) (3 mg/mL) by the ethanol injection method.

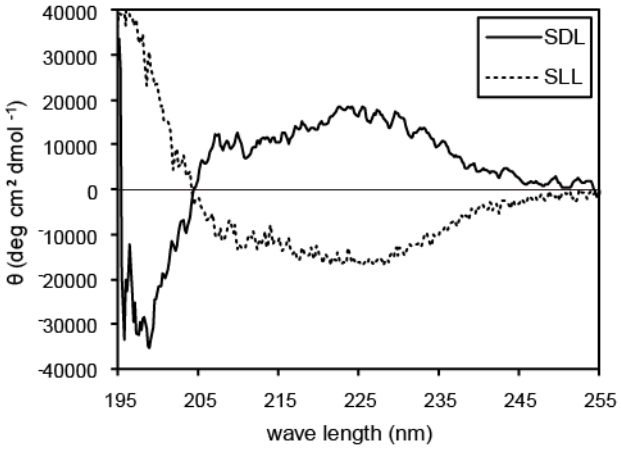

Figure 3. CD spectra of **SLL** and **SDL** in buffer. The amphiphilic polypeptides were injected into 10 mM Tris-HCl buffer (pH 7.4) (0.18 mg/mL) and then were heated at 90 °C for 10 min. These spectra suggest that the hydrophobic blocks of **SLL** and **SDL** formed right-handed and left-handed helices, and the helices were tightly packed as bundle in buffer.

The important point of the nano curved-sheet and nanotube is that they are metastable, where upon heating transformation from the nanosheet to the nanotube occurs quantitatively, and upon further heating elongation of the nanotube to double and triple was observed.[12] Even though the hydrophobic edges of the nanosheet and the nanotube are stabilized by a shielding effect of poly(sarcosine) chains nearby, the edges can be fused with other hydrophobic surfaces upon heating.

Nanotube fusion. Nanotubes were prepared separately from **SLL** and **SDL**, and two types of the nanotubes were mixed at an equimolar ratio. The mixture was heated at 90 °C for 50 min, and the time course of the morphology change was analyzed by TEM (Figure 4a–d). Before heat treatment, nanotubes with a diameter of *ca.* 70 nm and length of *ca.* 200 nm were homogeneously formed (Figure 4a). Upon heating for 10 min, planar square sheets with *ca.* 1 μm side appeared in the TEM image (Figure 4b). Then, the sheets were gradually transformed into vesicles (Figure 4c and 4d). Transformation of the sheet into the vesicle was completed within 50 min at 90 °C. With **SLL** or **SDL** alone, no such change was observed but just

elongation of the nanotubes partially. It is thus speculated that the **SLL** nanotube and the **SDL** nanotube should fuse together to transform the nanotube morphology into the planar square sheet. Indeed, the observation of a planar sheet could be reasonably explained by mixing of enantiomeric polypeptides **SLL** and **SDL** with stereo-complex formation accordingly to generate the achiral planar sheet. Whereas, **SLL** or **SDL** alone formed the curved sheet due to the one-handed helix association with a regular tilt angle between the helices. To investigate the morphology transformation mechanism in detail, the same fusion system was examined at lower temperature.

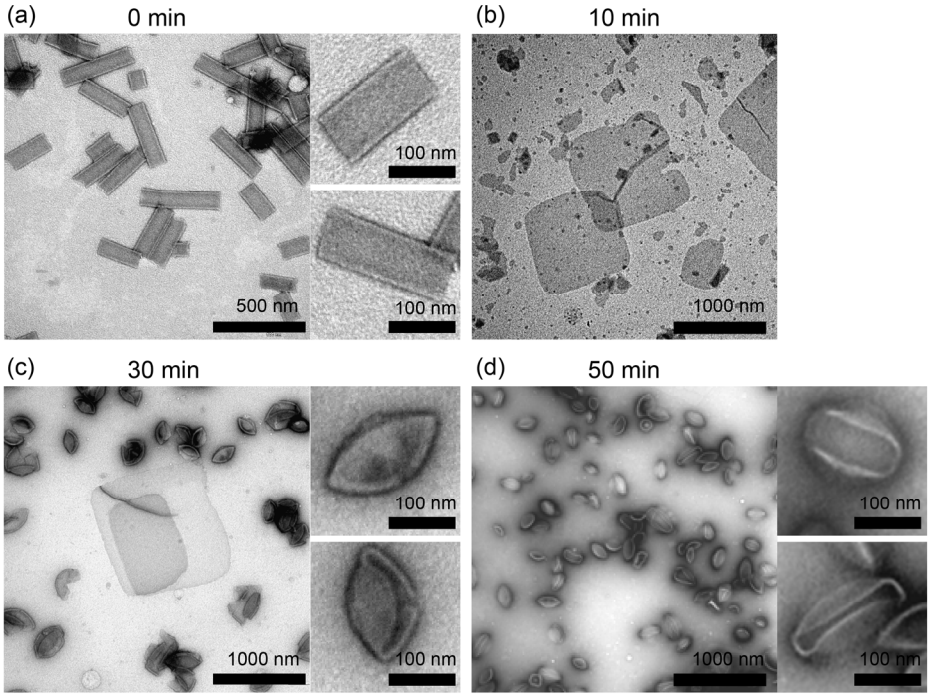

Figure 4. TEM images of the mixture of assembly suspension from **SLL** and **SDL** upon heating at 90 °C. The each assemblies were prepared in 10 mM Tris-HCl Buffer (pH 7.4) (3 mg/mL) by the ethanol injection method.

Upon heating at 50 °C, the peptide nanotube fusion process proceeded slowly compared with that at 90 °C. TEM observations revealed that upon heating at 50 °C for the initial 1–2 h, longer nanotube assemblies connecting two or more tubes were observed (Figure 5c). Hydrophobic edges at the open mouths of the nanotubes therefore triggered the

association of the nanotubes. Interestingly, some bunchy connecting regions of two nanotubes were observed (Figure 5c). This observation strongly indicates that the mixing of **SLL** and **SDL** takes place to generate a vesicle-like morphology at this connecting region. After heating for 7 h at 50 °C, the fused nanotubes were broken up and transformed into a planar square sheet with *ca.* 1.5 μm side (Figure 5d). These results indicate that the polypeptide nanotubes are connected randomly at the initial stage (association). When two types of the peptide nanotubes are connected, the right- and the left-handed helices diffuse through the connecting moieties to cause membrane fusion, because the stereo-complex is thermodynamically stable.[13] However, the diffusion of helical peptides in the membrane should be slow due to the tight packing of helices, which should be the reason for the long

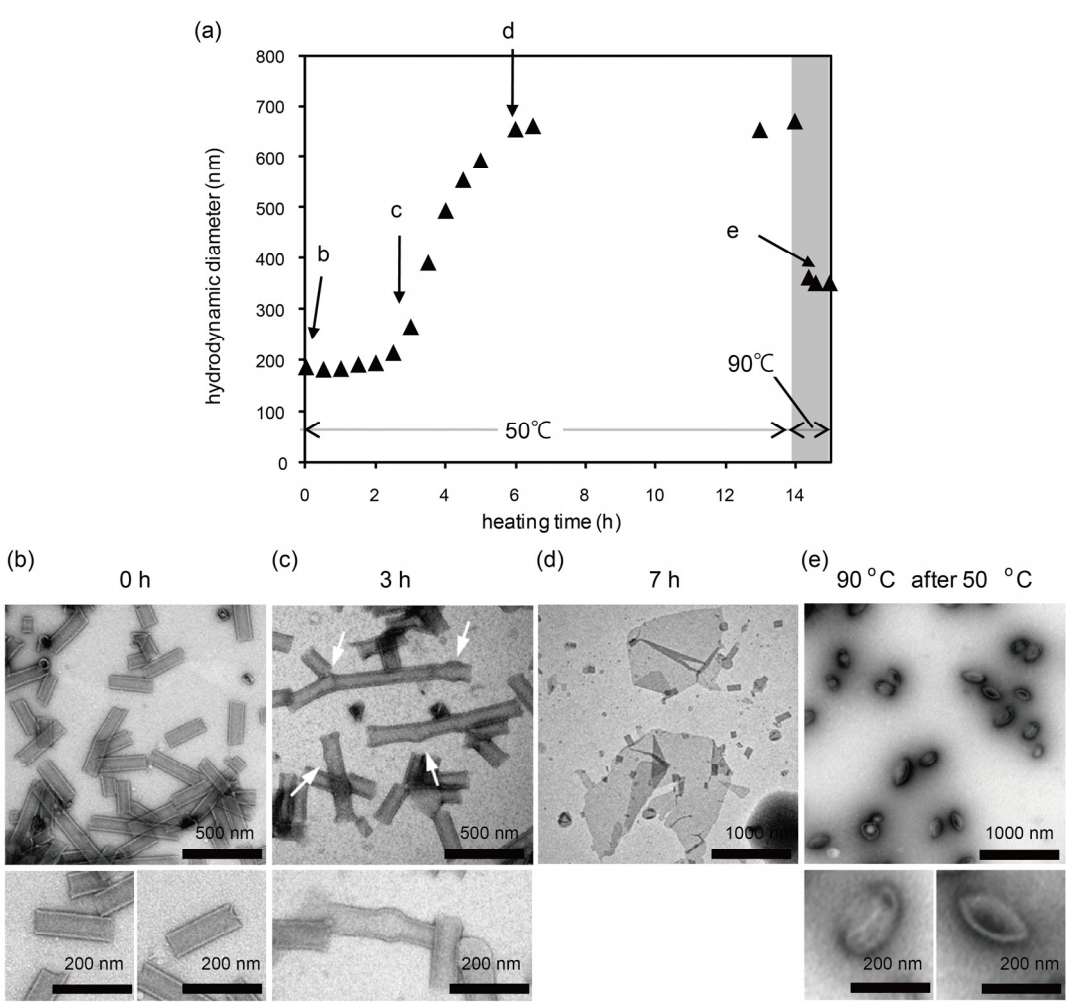

Figure 5. DLS data (a) and TEM images (b–d) of the mixture suspension upon heating at 50 °C. (e) TEM images of same sample upon heating at 90 °C for 1 h after heating at 50 °C for 14 h.

heating period for complete transformation from the nanotube to the sheet. The mixing proceeded with time, and finally the tubular structure broke up to take the planar square sheet. It took more than 7 h to form the planar sheet (Figure 5d). Upon heating at 90 °C, transformation into a vesicle was attained. The morphology changes were followed by dynamic light scattering (DLS) similar to changes in hydrodynamic diameters which are calculated from the translational diffusion coefficient by using the Stokes-Einstein equation (Figure 5a). Importantly no vesicular assembly transformation from the planar sheet was observed at 50 °C, suggesting that the transformation from the planar sheet into the vesicle requires higher energy. On the basis of analysis of many TEM images, the author thinks that the planar sheet is flexible to bend. Upon heating at 90 °C the sheet is torn off to small sheets, which then immediately close themselves to vesicle.

In the case of the nanotube suspension from **SLL** alone, the elongation was observed after heating at 50 °C for 14 h and then at 90 °C for 1 h. The diameter of nanotube was 70 nm, which was the same as that before heating. On the other hand, the length of nanotube became 200–900 nm (Figure 6).

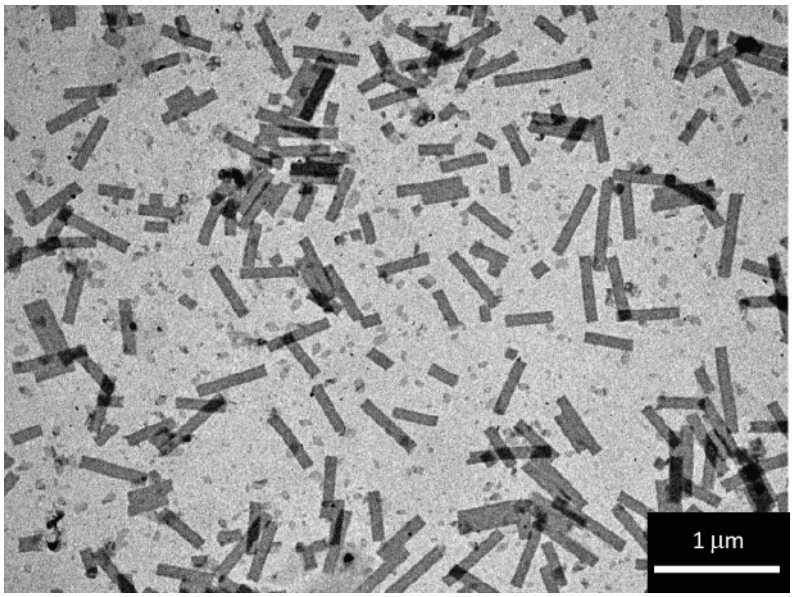

Figure 6. TEM images (negative staining with uranyl acetate) of nanotube suspension prepared from **SLL** upon heat treatment at 50 °C for 14 h and then at 90 °C for 1 h. The scale bar is 1 µm.

Vesicle induced by stereo-complex formation. The author confirmed the vesicle formation due to the stereo-complex formation by using another preparative method. An equimolar mixture of **SLL** and **SDL** in ethanol was injected into a buffer solution. The morphology of the self-assembly was a planar-sheet (Figure 7a), which was different from the curved sheet prepared from the single component. The planar sheets shown in Figure 4b, 5d, and 7a resemble each other in shape and size, supporting that these planar sheets are made of a mixture of **SLL** and **SDL**. Further, upon heating at 90 °C for 1h, vesicles were quantitatively formed (Figure 7b and 7c, cryo-TEM). The size distribution of the vesicles was very narrow around 200 nm diameter. Since this size was smaller than the expected size by closing the planar sheet with 1.5 μm side, the planar sheet should be torn off to generate the most stable size of the vesicle. This should be the reason for the narrow distribution of the vesicle diameter.

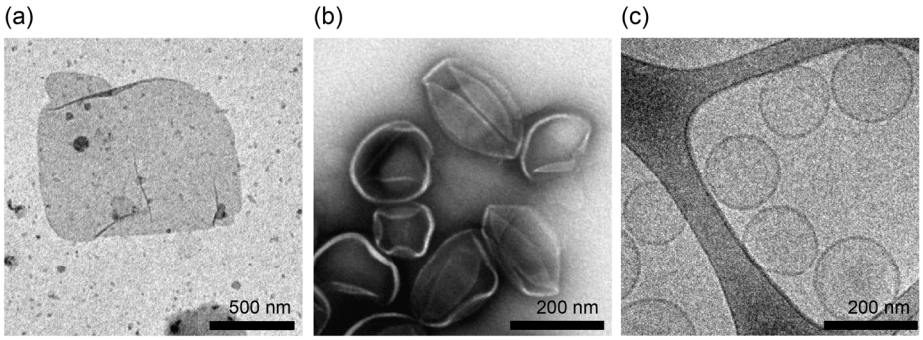

Figure 7. TEM images (negative staining with uranyl acetate; (a) and (b), cryogenic TEM; (c)) of molecular assemblies from mixtures of helical polypeptides **SLL** and **SDL**; 50/50. The assemblies were prepared in 10 mM Tris-HCl Buffer (pH 7.4) (3 mg/mL) by the ethanol injection method. Before heat treatment; (a), and after heat treatment; (b) and (c).

The author has shown two different preparation methods for the same vesicle morphology, which confirms his interpretation of vesicle formation due to the mixing of the right- and the left-handed helices in the molecular assembly, which is thermodynamically induced by the stereo-complex formation. Indeed, the electron diffraction (ED) patterns from the planar sheet of the mixture of **SLL** and **SDL** were different from those of the nanotube,

indicating a tight molecular packing of **SLL** and **SDL** in the planar sheet and therefore vesicle due to the stereo-complex formation (Figure 8). Further, the electron diffraction pattern obtained from the planar sheet assembly suggests the face-centred rectangular lattice (a = 2.65, b = 3.00, α = 90º) of **SLL** and **SDL**. On the other hand, that from the nanotube assembly showed the square lattice of **SDL**. These results also support that the molecular packing pattern of mixture assembly is different from that of single component assembly.

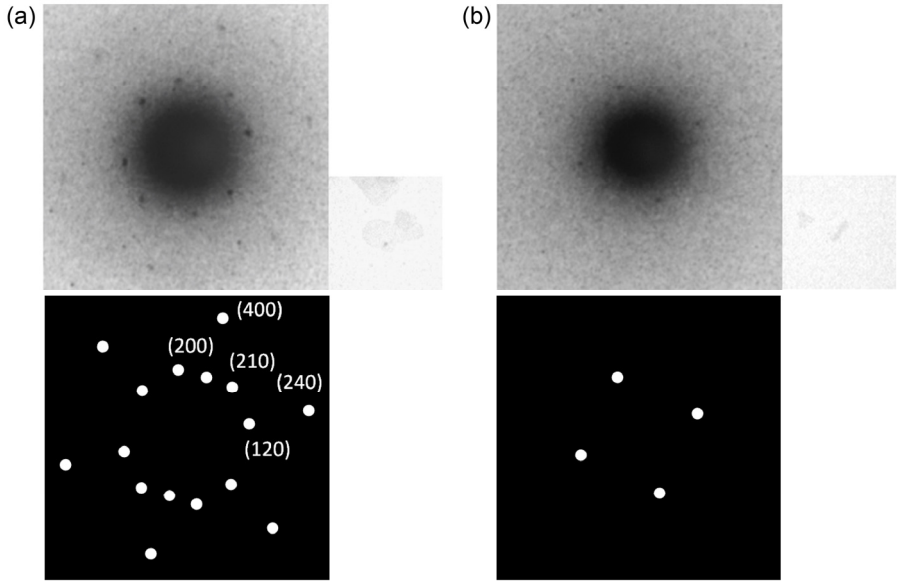

Figure 8. TEM images and electron diffraction patterns of (a) the planar sheet assembly from an equimolar mixture of **SLL** and **SDL** and (b) the nanotube assembly from a single component of **SDL** in 10 mM Tris-HCl buffer (pH 7.4).

In addition to ED analysis, the difference of molecular packing between assembly from stereo-complex component and single component was checked by the Fourier transform infrared spectroscopy/attenuated total reflection (FT-IR/ATR) analysis (Figure 9). On the assembly from single component of **SLL** and mixture of **SLL** and **SDL**, the positive peaks at 2850 cm^{-1} show the C-H asymmetrical stretching vibration modes. On the other hand, the peaks of the C-H symmetrical stretching vibration modes of each assemblies were observed at 2920 and 2927 cm^{-1}, respectively. One possible interpretation for the high-frequency shift of C-H symmetrical stretching vibration band was the decreasing of the mobility of side chain of

amino acids in the stereo-complex state. These results indicate that the intermolecular entanglement of mixture assembly is tighter than that of single component assembly.

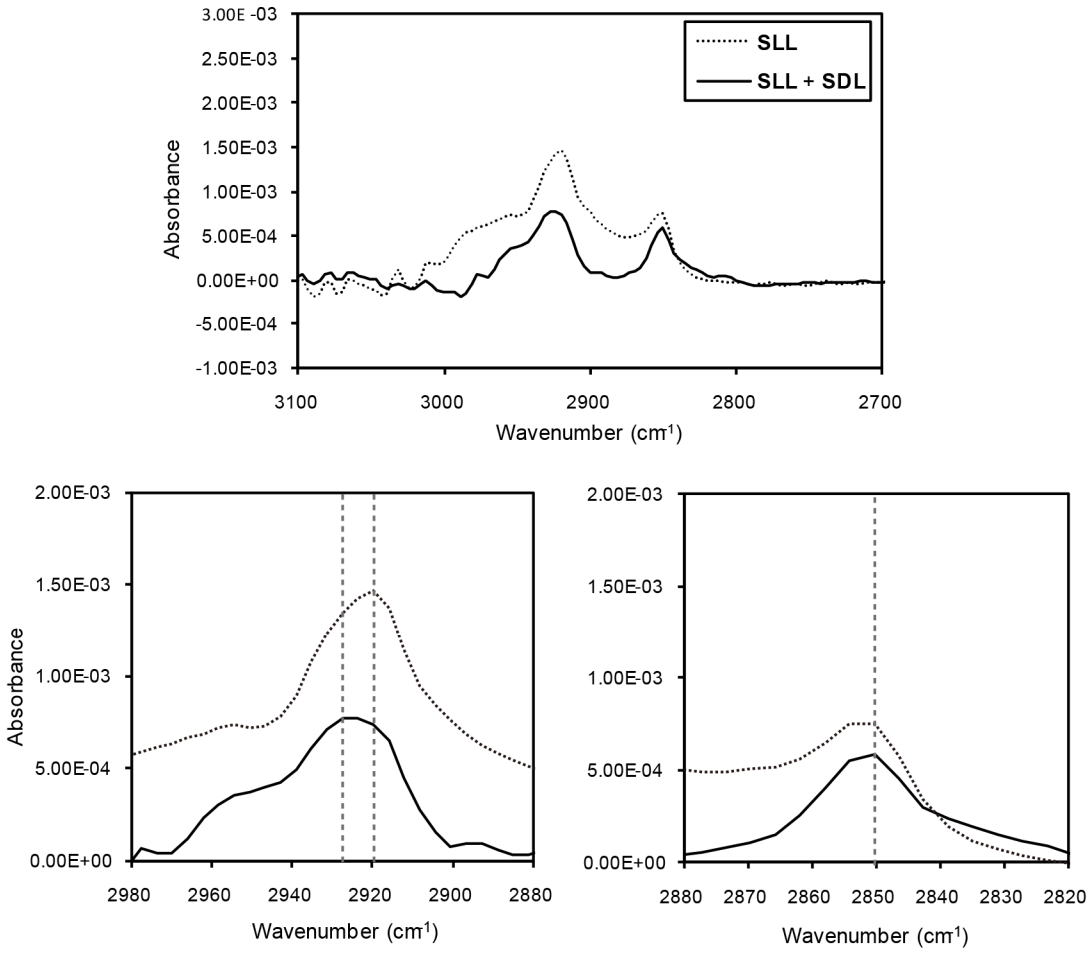

Figure 9. IR spectra in the C-H stretching region of amino acid of assembly from a mixture of **SLL** and **SDL** (solid line) and a single component of **SLL** (dash line).

References

(1) Discher, D. E.; Eisenberg, A. *Science* **2002**, *297*, 967–973.

(2) Jonkheijm, P.; van der Schoot, P.; Schenning, A. P. H. J.; Meijer, E. W. *Science* **2006**, *313*, 80–83.

(3) Engelkamp, H.; Middelbeek, S.; Nolte, R. J. M. *Science* **1999**, *284*, 785–788.

(4) Percec, V.; Dulcey, A. E.; Balagurusamy, V. S. K.; Miura, Y.; Smidrkal, J.; Peterca, M.; Nummelin, S.; Edlund, U.; Hudson, S. D.; Heiney, P. A.; Duan, H.; Magonov, S. N.; Vinogradov, S. A. *Nature* **2004**, *430*, 764–768.

(5) Kimura, S.; Kim, D.; Sugiyama, J.; Imanishi, Y. *Langmuir* **1999**, *15*, 4461–4463.

(6) Tanisaka, H.; Kizaka-Kondoh, S.; Makino, A.; Tanaka, S.; Hiraoka, M.; Kimura, S. *Bioconjugate Chemistry* **2008**, *19*, 109–117.

(7) Makino, A.; Kizaka-Kondoh, S.; Yamahara, R.; Hara, I.; Kanzaki, T.; Ozeki, E.; Hiraoka, M.; Kimura, S. *Biomaterials* **2009**, *30*, 5156–5160.

(8) Fujita, K.; Kimura, S.; Imanishi, Y. *Langmuir* **1999**, *15*, 4377–4379.

(9) Kimura, S.; Muraji, Y.; Sugiyama, J.; Fujita, K.; Imanishi, Y. *Journal of Colloid and Interface Science* **2000**, *222*, 265–267.

(10) Milburn, M. V.; Prive, G. G.; Milligan, D. L.; Scott, W. G.; Yeh, J.; Jancarik, J.; Koshland, D. E.; Kim, S. H. *Science* **1991**, *254*, 1342–1347.

(11) Parker, M. W.; Pattus, F.; Tucker, A. D.; Tsernoglou, D. *Nature* **1989**, *337*, 93–96.

(12) Kanzaki, T.; Horikawa, Y.; Makino, A.; Sugiyama, J.; Kimura, S. *Macromolecular Bioscience* **2008**, *8*, 1026–1033.

(13) Kunitake, T. *Angewandte Chemie International Edition* **1992**, *31*, 709–726.

(14) Fuhrhop, J. H.; Schnieder, P.; Boekema, E.; Helfrich, W. *Journal of the American Chemical Society* **1988**, *110*, 2861–2867.

(15) Yang, W.; Lee, E.; Lee, M. *Journal of the American Chemical Society* **2006**, *128*, 3484–3485.

(16) Yui, H.; Minamikawa, H.; Danev, R.; Nagayama, K.; Kamiya, S.; Shimizu, T. *Langmuir* **2008**, *24*, 709–713.

(17) Pouget, E.; Fay, N.; Dujardin, E.; Jamin, N.; Berthault, P.; Perrin, L.; Pandit, A.; Rose, T.; Valéry, C.; Thomas, D.; Paternostre, M.; Artzner, F. *Journal of the American Chemical Society* **2010**, *132*, 4230–4241.

(18) Zhong-can, O. *Physical Review A* **1991**, *43*, 6826–6836.

(19) Schnur, J. M. *Science* **1993**, *262*, 1669–1676.

(20) Selinger, J. V.; MacKintosh, F. C.; Schnur, J. M. *Physical Review E* **1996**, *53*, 3804–3818.

(21) Spector, M. S.; Selinger, J. V.; Singh, A.; Rodriguez, J. M.; Price, R. R.; Schnur, J. M. *Langmuir* **1998**, *14*, 3493–3500.

(22) Oda, R.; Huc, I.; Schmutz, M.; Candau, S. J.; MacKintosh, F. C. *Nature* **1999**, *399*, 566–569.

(23) Cornelissen, J. J. L. M.; Rowan, A. E.; Nolte, R. J. M.; Sommerdijk, N. A. J. M. *Chemical Reviews* **2001**, *101*, 4039–4070.

(24) Selinger, J. V.; Spector, M. S.; Schnur, J. M. *The Journal of Physical Chemistry B* **2001**, *105*, 7157–7169.

(25) Hill, J. P.; Jin, W.; Kosaka, A.; Fukushima, T.; Ichihara, H.; Shimomura, T.; Ito, K.; Hashizume, T.; Ishii, N.; Aida, T. *Science* **2004**, *304*, 1481–1483.

(26) Jin, W.; Fukushima, T.; Niki, M.; Kosaka, A.; Ishii, N.; Aida, T. *Proceedings of the National Academy of Sciences of the United States of America* **2005**, *102*, 10801–10806.

(27) Shimizu, T.; Masuda, M.; Minamikawa, H. *Chemical Reviews* **2005**, *105*, 1401–1444.

(28) Yamamoto, Y.; Fukushima, T.; Suna, Y.; Ishii, N.; Saeki, A.; Seki, S.; Tagawa, S.; Taniguchi, M.; Kawai, T.; Aida, T. *Science* **2006**, *314*, 1761–1764.

(29) Ryu, J.; Kim, H.; Huang, Z.; Lee, E.; Lee, M. *Angewandte Chemie International Edition* **2006**, *45*, 5304–5307.

(30) Brizard, A.; Aime, C.; Labrot, T.; Huc, I.; Berthier, D.; Artzner, F.; Desbat, B.; Oda, R. *Journal of the American Chemical Society* **2007**, *129*, 3754–3762.

(31) Kim, J.; Lee, E.; Kim, M.; Sim, E.; Lee, M. *Journal of the American Chemical Society* **2009**, *131*, 17768–17770.

Chapter 2

Temperature Triggered Fusion of Vesicles Composed of Right-Handed and Left-Handed Amphiphilic Helical Peptides

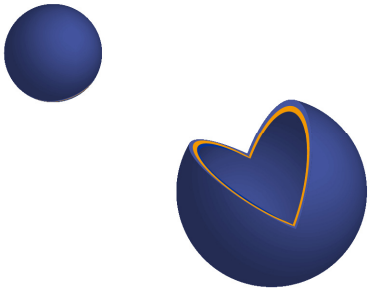

Introduction

Specific fusion of biological membranes is a central issue for many cellular processes.[1] Studies on the membrane fusion are important not only for elucidation of bioprocesses but also for applications to biomaterials including drug delivery systems. For example, liposome has been used for a model of cell membrane, and the fusion mechanism of liposomes is clarified.[2–5] However, application of liposome is not so feasible because of its weak physical property. On the other hand, vesicles are also preparable from amphiphilic polymers, which have an advantage of their robustness.[6–8] Polymer vesicles are however considered to be inactive in membrane fusion, because the membrane fluidity is significantly suppressed due to entanglement of polymer chains. We demonstrate here successful fusion of polypeptide vesicles, which are composed of $(Sar)_n$-*b*-(L- or D-Leu-Aib)$_n$. The amphiphilic block polypeptides comprise a hydrophobic helical block, which allows membrane fluidity of regularly packed helices, leading to membrane fusion.

We have reported on molecular assemblies of amphiphilic peptide molecules especially with using hydrophobic helical blocks at the hydrophobic core of the molecular assemblies.[6–10] Helical peptides have a good ability to be packed regularly in the molecular assembly as shown by frequent observation of helix bundles in nature.[11,12] Indeed, the peptide nanotube with diameter of *ca.* 70 nm and length of *ca.* 200 nm was obtained from amphiphilic block polypeptide with hydrophobic helix, $(Sar)_{25}$-*b*-(L-Leu-Aib)$_6$ (**SLL**) or $(Sar)_{25}$-*b*-(D-Leu-Aib)$_6$ (**SDL**).[13] Further, we succeeded in preparation of a vesicular assembly with using an enantiomeric mixture of amphiphilic polypeptides, **SLL** and **SDL**, which have the right- and left-handed hydrophobic helices, respectively in Chapter 1. When the right-handed helix is mixed with the left-handed helix, they form a stereo-complex probably due to the convexo-concave fitness between their surfaces.[14,15] This vesicle from an equimolar mixture of **SLL** and **SDL** (**DL** vesicle) has the size of 180 nm diameter with a narrow distribution.

Experimental Section

Materials. Boc-L-leucine (Boc-Leu), aminoisobutylic acid (Aib) and Z-sarcosine (Z-Sar) were purchased from Watanabe Chemical Industries, Ltd. (Japan). 1,2-dipalmitoyl-*sn*-glycero-3-phosphoethanolamine-*N*-(7-nitro-2-1,3-benzoxadiazol-4-yl) (NBD-PE) and 1,2-dipalmitoyl-*sn*-glycero-3-phosphoethanolamine-*N*-(lissamine rhodamine B sulfonyl) (Rho-PE) were purchased from Avanti Polar Lipids, Inc (U.S.A.). Fluorescein isothiocyanate-dextran (FITC-dextran) was purchased from Sigma-Aldrich. Water was purified by a Milli-Q system (Nihon Millipore Ltd, Japan) and had a specific resistivity of *ca.* 18 MΩ cm^{-1}. All other reagents were purchased from commercial sources and used as received.

Preparation of Molecular Assemblies. Each polypeptide (12 mg) was dissolved in ethanol (120 μL). Then an aliquot (a mixture of **SLL** (5 μL) and **SDL** (5 μL), or **S28L16** (10 μL)) of the peptide solution was injected into a buffer (1 mL, 10 mM Tris-HCl, pH 7.4) with stirring at 4 °C. Molecular assemblies of different compositions were prepared similarly.

Transmission Electron Microscopy (TEM). TEM images were taken using a JEOL JEM-2000EXII at an accelerating voltage of 100 kV. For the observation, a drop of dispersion was mounted on a carbon-coated Cu grid and stained negatively with 2 % uranyl acetate, followed by suction of the excess fluid with a filter paper.

Frozen-Hydrated/Cryogenic-TEM (Cryo-TEM). The dispersions in a buffer were frozen quickly in liquid ethane, which was cooled with liquid nitrogen. The samples were examined at 100 kV accelerating voltage at the liquid nitrogen temperature.

Dynamic Light Scattering (DLS). The DLS measurements were taken using Photal DLS-8000 at 25 °C with a transmission cell.

Fluorescent Analysis. The fluorescent spectra of assembly dispersion were obtained using JASCO FP-6600 spectro fluorometer at 25 °C with a transmission cell.

Synthesis of S14L16, S28L16 and S35L16. The amphiphilic polypeptides were synthesized by the same method in previous report.[1–3] The hexadecapeptides, $(Leu\text{-}Aib)_8$, were synthesized by the conventional liquid phase method. With using Sar NCA, the hydrophilic Sar chains attached to the N-terminal of by NCS polymerization. The degree of polymerization of the poly(Sar) block was determined to be 14, 28 and 35 from the relative areas of Sar*N*-CH_3 signal against the OCH_3 signal in the ^1H NMR spectra.

Results and Discussion

Peptide vesicle prepared from single component of S28L16 (L16 vesicle). A single component of $(Sar)_{28}$-*b*-(L-Leu-Aib)$_8$ (**S28L16**) formed a small planar sheet with *ca*. 200 nm, including a minor fraction of vesicle (a few percent, yield) in buffer at room temperature (Figure 1a). This planar sheet was transformed completely into a vesicular shape by heating at 90 °C for 1 h. Transmission electron microscopy (TEM) observation showed that this vesicle, **L16** vesicle, has the size of *ca.* 90 nm diameter (Figure 1b and 5e blue), which was agreeable

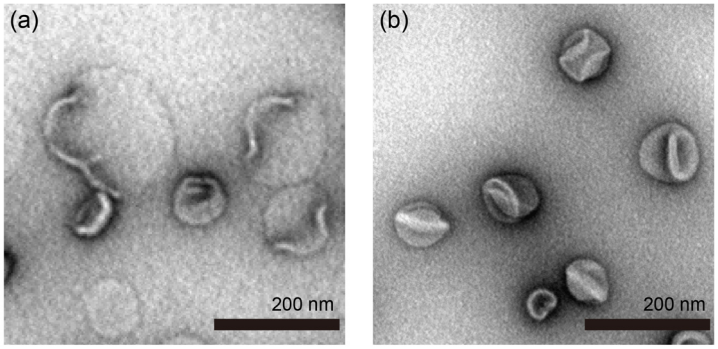

Figure 1. TEM images (negative staining with uranyl acetate) of molecular assemblies prepared from **L16** (a); before and (b); after heating at 90 °C. The assemblies were prepared in 10 mM Tris-HCl buffer (pH 7.4) (1 mg/mL) by the ethanol injection method.

with that determined by dynamic light scattering (DLS) measurements (Figure 4c filled circle). **L16** retained the morphology at least for two months on the basis of TEM observation.

Vesicle fusion. We assayed membrane fusion of these polypeptide vesicles by fluorescence resonance energy transfer (FRET) technique and TEM observations, and DLS measurements. Two kinds of **DL** vesicles were prepared; one with 0.25 % (mol/mol) 1,2-dipalmitoyl-*sn*-glycero-3-phosphoethanolamine-*N*-(7-nitro-2-1,3-benzoxadiazol-4-yl) (NBD-PE) (ex: 460 nm, em: 535 nm) and 0.25 % (mol/mol) 1,2-dipalmitoyl-*sn*-glycero-3-phosphoethanolamine-*N*-(lissamine rhodamine B sulfonyl) (Rho-PE) (ex: 560 nm, em: 583 nm), and the other without these fluorophores. When these two kinds of vesicles were mixed at room temperature, the fluorescence intensity from rhodamine at 583 nm was stronger than that from NBD at 535 nm due to FRET from NBD to Rho as both fluorophores were condensed in the same vesicle (Figure 2a). Upon heating at 90 °C, the fluorescence intensity of NBD increased with incubation time and fluorescence intensity from Rho decreased. Eventually NBD fluorescence became stronger than Rho fluorescence. The change of fluorescence pattern suggests occurrence of membrane fusion, by which the fluorophores are diluted in the fused membrane to reduce FRET. The vesicle fusion was completed within 7.5 min after heating at 90 °C, but no fusion was observed even after 2 h when heating temperature was at 80 °C (Figure 2b). There seems to be a critical temperature for membrane fusion of **DL** vesicles.

Membrane fusion of **L16** vesicles was examined by using similar methods. Two kinds of **L16** vesicles were prepared; one with 0.25 % (mol/mol) NBD-PE and 0.25 % (mol/mol) Rho-PE, and the other without these fluorophores. When these two kinds of vesicles were mixed and heated at 90 °C, no fluorescence spectral change was observed even after 2 h heating in this case (Figure 2c), suggesting that **L16** vesicles did not fuse together even at high temperature.

Morphology changes of **DL** vesicles and **L16** vesicles upon heating at 90 °C were examined by DLS and TEM observations. The hydrodynamic diameter of **DL** vesicles was *ca.*

180 nm diameter before heating and *ca*. 200 nm after heating. **L16** vesicles kept *ca*. 90 nm diameter before and after heating. TEM images of **DL** vesicles and **L16** vesicles after heating showed that the morphologies and their sizes were preserved before and after heating (Figure 2d and 2e), supporting the results of DLS measurements. In the case of fusion of **DL** vesicles, the fused vesicles should therefore fission to vesicles of the original size of *ca*. 180 nm.

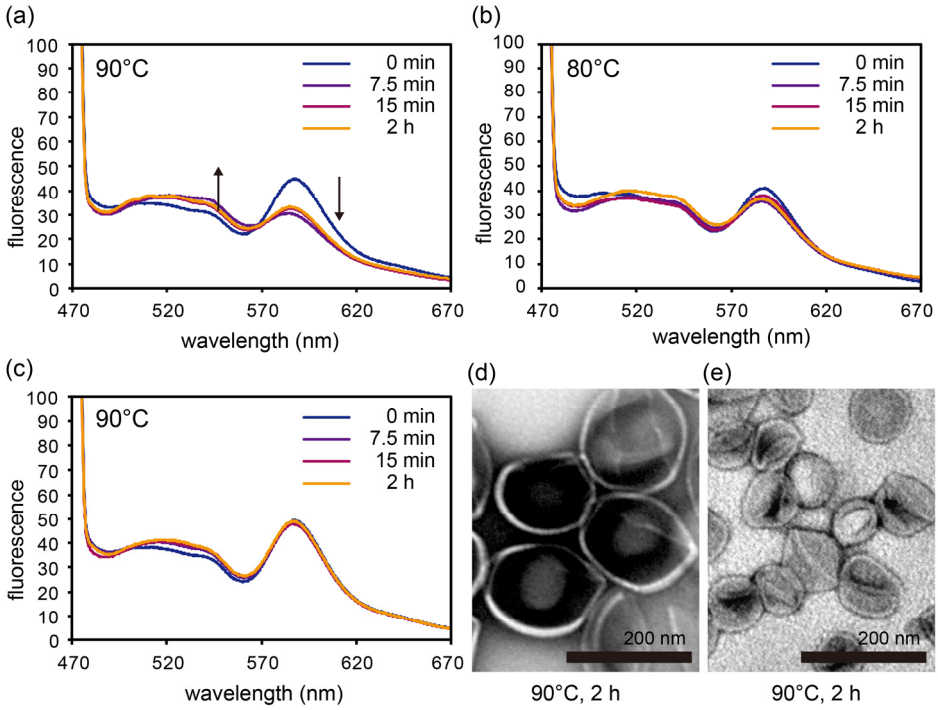

Figure 2. Emission spectra from a mixture of **DL** vesicles and **DL** vesicles containing of 0.25 % NBD-PE and 0.25 % Rho-PE upon heating (a); at 90 °C and (b); at 80 °C, and (c); from a mixture of **L16** vesicles and **L16** vesicles containing 0.25 % NBD-PE and 0.25 % Rho-PE upon heating at 90 °C. TEM images (negative staining with uranyl acetate) of (d); **DL** vesicles and (e); **L16** vesicles after heating at 90 °C. The assembly suspensions were prepared in 10 mM Tris-HCl buffer (pH 7.4) (1 mg/mL) by the ethanol injection method.

Stability of L16 vesicle. To understand the reason for inability of **L16** vesicles about membrane fusion, two other block polypeptides having different lengths of the hydrophilic block but with the same hydrophobic block were synthesized and examined on self-assembling in buffer. $(Sar)_{14}$-*b*-$(L\text{-Leu-Aib})_8$ (**S14L16**), which length of the hydrophilic block

is shorter than that of **S28L16**, formed planar sheets by the ethanol injection method. Upon heating at 90 °C for 1 h, about 10 % of **S14L16** sheets transformed into vesicles but the rest retained the shape like a planar sheet (Figure 3a). It is therefore considered that the short poly(Sar) chain cannot conceal the hydrophobic domain of the helix assembly taking a vesicular structure, where the planar sheet should bend intensively to a high curvature. On the other hand, $(Sar)_{35}$-*b*-(L-Leu-Aib)$_8$ (**S35L16**), which length of the hydrophilic block is longer than that of **S28L16**, formed very small sheets of *ca*. 30 nm square before and after heating at 90 °C for 1 h, suggesting that the long poly(Sar) chains stabilize the small sheets and prevent the sheets from growing into a large sheet for transformation into a vesicular structure (Figure 3b). Taken together, the chain length of poly(Sar) of **S28L16** is suited just for taking a vesicular structure, and thus **L16** vesicles are so stable that the vesicle fusion does not occur..

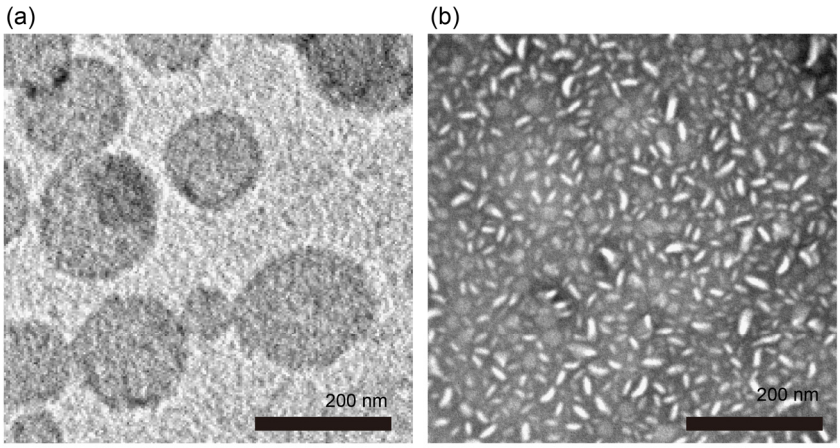

Figure 3. TEM images (negative staining with uranyl acetate) of molecular assembly prepared from (a); **S14L16** and (b); **S35L16** after heating at 90 °C.

Thermodynamic character of DL vesicle and L16 vesicle. Transformation of morphology from planar sheets into vesicles was studied in detail with varying the incubation temperature. In the case of a mixture of **SLL** and **SDL**, the hydrodynamic diameters of the molecular assembly did not change up to 80 °C for 1 h heating, and a sudden change from 600 nm (planar sheet) to *ca*. 180 nm (vesicle) upon heating at 90 °C was observed (Figure 4a). This temperature coincides with the critical temperature for fusion of **DL** vesicles determined

by the FRET method. On the other hand, in the case of **S28L16**, the hydrodynamic diameters of the molecular assemblies increased gradually from *ca*. 45 nm (small planar sheet) to *ca*. 90 nm (vesicle) with rising the temperature (Figure 4b and 4c). These observations suggest that **DL** vesicles have a phase transition temperature at 90 °C, which may reflect the sol-gel transition observed with liposome, but **S28L16** vesicles do not have.

To characterize peptide membranes further, vesicles were analysed by differential scanning calorimetry (DSC). DSC measurement of **DL** vesicles showed an endothermic peak at 89 °C (Figure 4d). The membrane may be fluidic above 89 °C to allow vesicle fusion. However, there should be another factor for vesicle fusion, when we consider **L16** vesicles. **L16** membranes should be fluidic in the temperature region examined here, because transformation of morphologies from small planar sheets into vesicles requires diffusion of peptide molecules in the membrane to realize molecular rearrangement suitable for vesicles. Membrane fluidity is not therefore enough for vesicle fusion but prerequisite. We speculated the high bending energy stored in **DL** vesicles contribute to vesicle fusion. A mixture of **SLL** and **SDL** yielded large planar sheets by the ethanol injection method, which makes a contrast to curved sheets prepared from **SLL** or **SDL**. In the mixed membranes of **SLL** and **SDL**, the helical chirality in total is cancelled out by stereo-complex formation to generate large planar sheets. On the other hand, the membranes of **SLL** or **SDL** have chirality depending on the right-handed or the left-handed helix to induce curvature of the membrane. It is therefore considered that the mixed membranes of **SLL** and **SDL** should be rigid and possess high bending energy upon taking a vesicular structure. On the other hand, the membranes of **L16** vesicles do not have such a high bending energy, which is agreeable with spontaneous formation of small vesicles of *ca*. 90 nm diameter even at room temperature, whereas **DL** vesicles take diameter of *ca*. 180 nm upon heating at 90 °C.

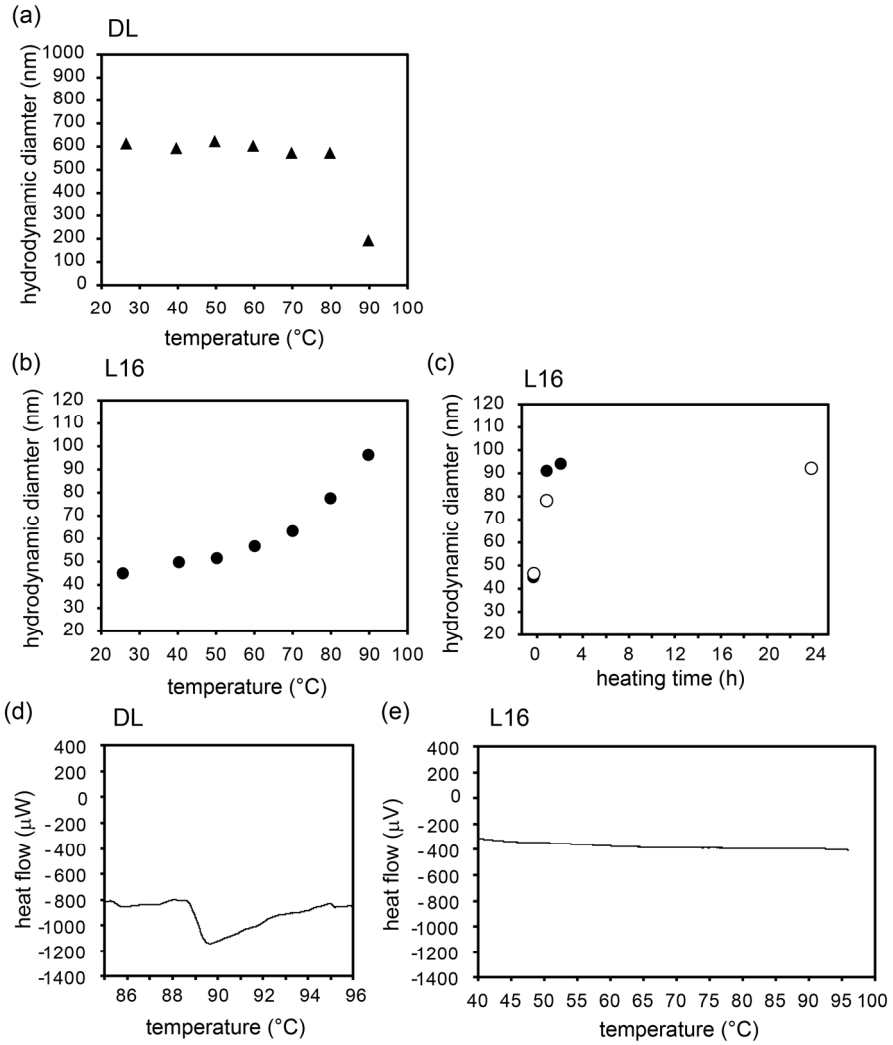

Figure 4. DLS data of transformation from planar sheets to vesicles after heating at 50, 60, 70, 80 or 90 °C for 1 h in the case of a mixture of **SLL** and **SDL**, (a); and **L16**. (b). The hydrodynamic diameters of molecular assemblies from **L16** (c) are plotted with varying the heating period at 90 °C (filled circle) and at 80 °C (open circle). DSC data of a mixture membrane of **SLL** and **SDL**, (d) and **L16** membrane (e).

Vesicle fusion between DL vesicle and L16 vesicle. Fusion of **DL** vesicles and **L16** vesicles was examined. **L16** vesicles containing 0.25 % NBD-PE and 0.25 % Rho-PE were prepared and mixed with **DL** vesicles without these fluorophores. Upon heating at 90 °C, fluorescence intensity of NBD at 535 nm increased and that of Rho at 583 nm decreased,

suggesting that these two kinds of vesicles fused together to dilute fluorophores in the membrane, resulting in reduction of FRET (Figure 5a).

On the other hand, upon heating at 80 °C even for 2 h, no fusion was suggested from the fluorescence spectra (Figure 5b). The critical temperature of 90 °C for fusion of **DL** vesicles and **L16** vesicles coincides with that for fusion of **DL** vesicles, indicating that physical change in **DL** membranes at 90 °C triggers the fusion. DLS measurement of the molecular assemblies after heating at 90 °C revealed the hydrodynamic diameter of *ca*. 140 nm, which is a value between **DL** vesicles of *ca*. 180 nm and **L16** vesicles of *ca*. 90 nm. Further, TEM image confirmed that the fused morphology was vesicle with diameter of *ca*. 140 nm (Figure 5c and 5e). The fused vesicles were stable at 25 °C at least for two weeks on the basis of DLS measurements. Taken together, **DL** vesicles and **L16** vesicles fused together upon heating at 90 °C, and the fused vesicles should fission to vesicles of the intermediate size of *ca*. 140 nm.

The fused vesicles of *ca*. 140 nm should be therefore composed of **SLL**, **SDL**, and **S28L16**. To support this interpretation, a mixture of **SLL**, **SDL**, and **S28L16** (1/1/2 w/w/w) was injected in buffer and heated at 90 °C for 1 h. TEM image of the molecular assemblies clearly showed formation of vesicles of *ca*. 140 nm diameter (Figure 5d), which are exactly the same as those prepared by fusion of **DL** vesicles and **L16** vesicles. It is therefore concluded that **DL** vesicles and **L16** vesicles fuse together at 90 °C, and the fused membrane should be composed of a homogeneous mixture of **SLL**, **SDL**, and **L16** by diffusion of the peptide molecules in the membrane. With this composition, vesicles of *ca*. 140 nm diameter should be the most stable morphology after heating at 90 °C.

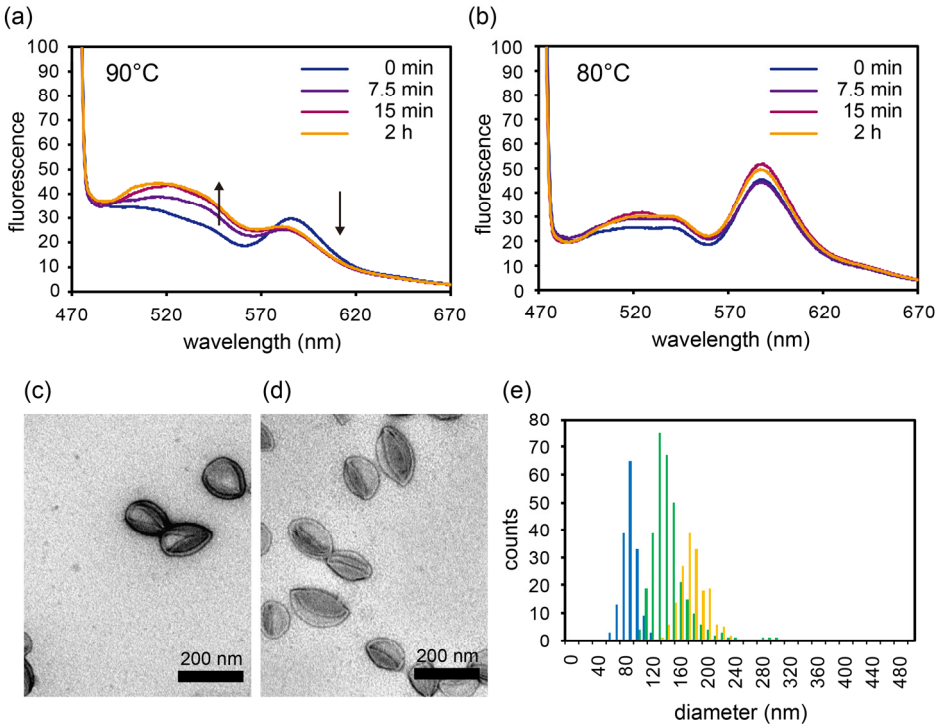

Figure 5. Emission spectra from a mixture of **DL** vesicles and **L16** vesicles containing of 0.25 % NBD-PE and 0.25 % Rho-PE upon heating (a); at 90 °C and (b); 80 °C. TEM images of (c); a mixture of two kinds of vesicles after heating at 90 °C for 1 h and (d); molecular assemblies prepared from a mixture of **SLL**, **SDL** and **L16** (1/1/2 w/w/w) after heating at 90 °C for 1 h. (e); The histogram of diameters of **L16** vesicles (blue), **DL** vesicles (yellow), and a mixture of **DL** vesicles and **L16** vesicles after heating at 90 °C for

Mechanism of vesicle fusion. To elucidate the fusion mechanism of **DL** vesicles, a release behavior of the fluorescent agent encapsulated in **DL** vesicles was studied during the vesicle fusion. Fluorescein-labeled dextran (FITC-dextran) (Mw: 4000) (ex: 480 nm, em: 520 nm) was used as an encapsulating reagent. **DL** vesicles loading FITC-dextran were prepared by the ethanol injection method using a FITC-dextran solution (2 mg/mL). The solution was heated at 90 °C for 1 h, followed by elution through a Sephacryl S-100 column (1.5 × 30 cm, GE healthcare Bio-Sciences) using 10 mM Tris-HCl buffer (pH 7.4) as an eluent (Figure 6a). The peak at fraction number 5–9 represents **DL** vesicles encapsulating FITC-dextran. The fraction number 11–20 corresponds to free FITC-dextran. The 8 th fraction was eluted again

through the same column (Figure 6b), showing nearly no leakage from **DL** vesicles during the column operation. This result showed that **DL** vesicle loaded FITC-dextran without physical adsorption. The 8 th fraction was heated again at 90 °C for 30 min, which induces vesicle fusion as described before. Then, the fraction was eluted through the same column. The elution profile clearly showed nearly no leakage during the vesicle fusion (Figure 6c). Taken together, it is concluded that **DL** vesicles fuse each other to connect two vesicular membranes, followed by fission into two vesicles of 200 nm diameters, without leaking the encapsulated reagents (Figure 7). The membranes of **DL** vesicles are therefore speculated to be very flexible for distortions during the vesicle fusion.

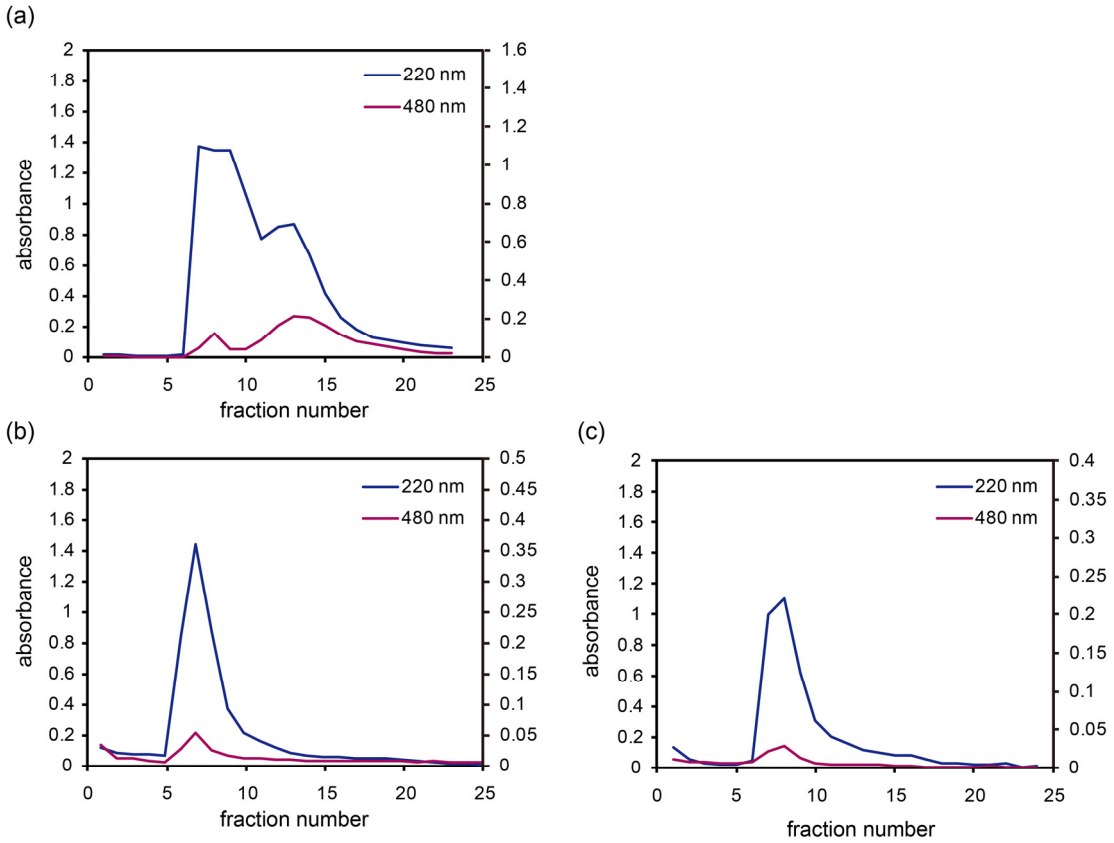

Figure 6. Elusion profile of FITC-dextran loading **DL** vesicles through Sephacryl S-100 column (a); after purification and subsequently (b); before and (c); after heat treatment at 90 °C for 30 min.

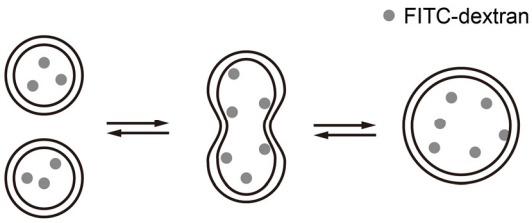

Figure 7. Schematic illustration of mechanism between FITC-dextran loading **DL** vesicles.

References

(1) Blumenthal, R.; Dimitrov, D. S. *Handbook of Physiology: Section 14: Cell Physiology*; Oxford University Press: New York, 1997, 563–603.

(2) Discher, D. E.; Eisenberg, A. *Science* **2002**, *297*, 967–973.

(3) Jonkheijm, P.; van der Schoot, P.; Schenning, A. P. H. J.; Meijer, E. W. *Science* **2006**, *313*, 80–83.

(4) Engelkamp, H.; Middelbeek, S.; Nolte, R. J. M. *Science* **1999**, *284*, 785–788.

(5) Percec, V.; Dulcey, A. E.; Balagurusamy, V. S. K.; Miura, Y.; Smidrkal, J.; Peterca, M.; Nummelin, S.; Edlund, U.; Hudson, S. D.; Heiney, P. A.; Duan, H.; Magonov, S. N.; Vinogradov, S. A. *Nature* **2004**, *430*, 764–768.

(6) Tanisaka, H.; Kizaka-Kondoh, S.; Makino, A.; Tanaka, S.; Hiraoka, M.; Kimura, S. *Bioconjugate Chemistry* **2008**, *19*, 109–117.

(7) Makino, A.; Kizaka-Kondoh, S.; Yamahara, R.; Hara, I.; Kanzaki, T.; Ozeki, E.; Hiraoka, M.; Kimura, S. *Biomaterials* **2009**, *30*, 5156–5160.

(8) Fujita, K.; Kimura, S.; Imanishi, Y. *Langmuir* **1999**, *15*, 4377–4379.

(9) Kimura, S.; Kim, D.; Sugiyama, J.; Imanishi, Y. *Langmuir* **1999**, *15*, 4461–4463.

(10) Kimura, S.; Muraji, Y.; Sugiyama, J.; Fujita, K.; Imanishi, Y. *Journal of Colloid and Interface Science* **2000**, *222*, 265–267.

(11) Milburn, M. V.; Prive, G. G.; Milligan, D. L.; Scott, W. G.; Yeh, J.; Jancarik, J.; Koshland, D. E.; Kim, S. H. *Science* **1991**, *254*, 1342–1347.

(12) Parker, M. W.; Pattus, F.; Tucker, A. D.; Tsernoglou, D. *Nature* **1989**, *337*, 93–96.

(13) Kanzaki, T.; Horikawa, Y.; Makino, A.; Sugiyama, J.; Kimura, S. *Macromolecular Bioscience* **2008**, *8*, 1026–1033.

(14) Ikada, Y.; Jamshidi, K.; Tsuji, H.; Hyon, S. H. *Macromolecules* **1987**, *20*, 904–906.

(15) Brizzolara, D.; Cantow, H.; Diederichs, K.; Keller, E.; Domb, A. J. *Macromolecules* **1996**, *29*, 191–197.

Chapter 3

Rational Design of Peptide Nanotubes for Varying Diameters and Lengths

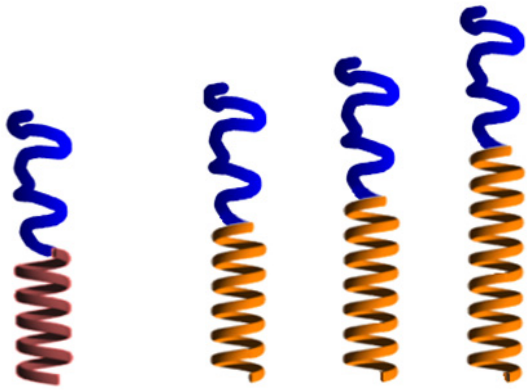

Introduction

Precise control of morphology is an important challenge in the field of molecular self-assembly.[1–4] Nano-ordered tubular assemblies, nanotubes, are of interest due to their numerous possible applications. For example, hollow tubular structures provide closed reaction chambers when adjusting the space to guest molecules as demonstrated by protein-folding chaperonins[5,6] and protein-degradation enzymes.[7] Peptide amphiphiles have been used for preparation of molecular assemblies in a wide range of morphologies such as micelles,[8] cylinder micelles,[9] fibers,[10] nanotubes,[11,12] and vesicles.[13] The group of authors has reported that amphiphilic peptides, especially composed of hydrophobic helical peptides, form vesicles (named peptosomes) and nanotubes uniquely on their narrow size distribution.[14–19] Indeed helical peptides have the ability to pack in regular mode in molecular assemblies as shown by frequent occurrence of helix bundles in proteins.[20,21]

$(Sar)_{27}$-*b*-$(L\text{-Leu-Aib})_6$, an amphiphilic helical peptide, was found to form peptide nanotubes with a diameter of about 70 nm and a length of about 200 nm.[14] The self-assembling process is constituted of two steps. Initially, the amphiphilic helical peptide forms a curved square sheet assembly upon dispersion in buffer at room temperature. Heating the dispersion at 90 °C for 10 min triggers the morphological conversion from the curved sheet to nanotube. The length of the nanotube is further increased by additional heating for 24 h to reach about 1 μm; however, it is difficult to obtain very long nanotubes. For the preparation of the longer peptide nanotubes, nanotubes with more robust membranes are required.

In the present study the effect of stereo-complexes on helix association in molecular assemblies was examined. A typical example of stereo-complex formation was reported between the right-handed and the left-handed helices of poly-$(\text{lactic acid})_n$. The stereo-mixture was found to possess improved properties in terms of mechanical strength and heat resistance than each enantiomer.[22,23] Correspondingly, a mixture of right-handed and left-handed helical

peptides is expected to form a stereo-complex as a result of the convex-concave complementarities of their surfaces. In this report, we demonstrate that indeed robust and long nanotubes are obtained as a result of the stereo-complex formation between right- and left-handed helices differing in their helix lengths.

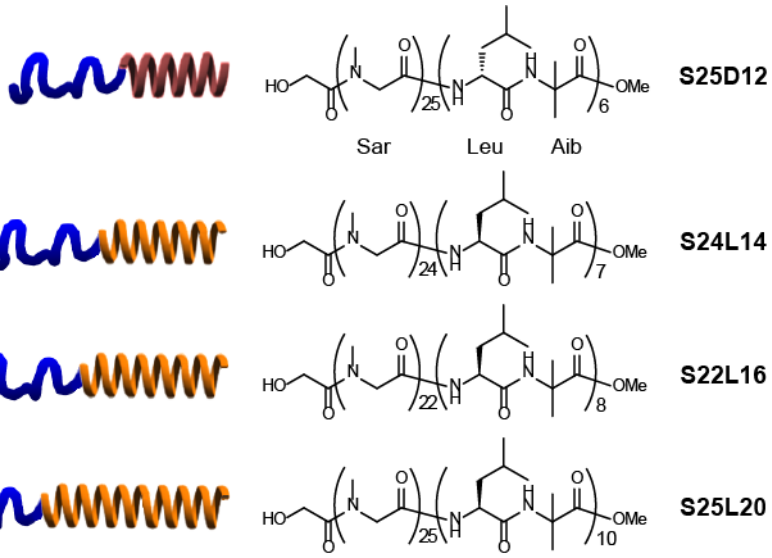

Molecular structure of the amphiphilic polypeptides. The $(Sar)_m$ constitutes the unstructured hydrophilic block and $(Leu\text{-}Aib)_n$ the hydrophobic α-helical block.

Experimental Section

Materials. Boc-L-leucine (Boc-Leu), aminoisobutylic acid (Aib) and Z-sarcosine (Z-Sar) were purchased from Watanabe Chemical Industries, Ltd. (Japan). Water was purified by a Milli-Q system (Nihon Millipore Ltd, Japan) and had a specific resistivity of *ca.* 18 MΩ cm^{-1}. All other reagents were purchased from commercial sources and used as received.

Preparation of Molecular Assemblies. Equimolar mixtures of two polypeptides (1 μmol each) were dissolved in ethanol (40 μl) and injected into a buffer (1 ml, 10 mM Tris-HCl, pH7.4) under stirring at 4 °C. After 30 min, the dispersions were heated at 90 °C for a specified period.

Circular Dichroism (CD). CD measurements were carried out on a JASCO J600 spectropolarimeter with an optical cell of 0.1 cm optical path length at room temperature. The sample concentration in 10 mM Tris-HCl buffer (pH 7.4) was 0.375 mM (per amino acid residue).

Transmission Electron Microscopy (TEM). TEM images were taken using a JEOL JEM-2000EXII at an accelerating voltage of 100 kV. For the observation, a drop of dispersion was mounted on a carbon-coated Cu grid and stained negatively with 2 % uranyl acetate, followed by suction of the excess fluid with a filter paper.

Synthesis of S24L14, S22L16 and S25L20. The synthesis schemes of these peptides are same as that of **S25L12** in Chapter 1. The Aib-containing dodecapeptide was synthesized by the conventional liquid phase method. Boc group of the dodecapeptide (400 mg, 0.263 mmol) was removed by treatment with trifluoroacetic acid (TFA, 4 mL) and anisole (0.4 mL). The TFA salt was washed with isopropylether and dried in vacuo for 2 h. The salt was dissolved in chloroform and washed with 4 wt% $NaHCO_3$ and saturated NaCl aqueous solutions. The organic layer was dried over anhydrous $MgSO_4$ and the solvent was removed and dried in vacuo to afford H-(Leu-Aib)$_7$-OMe (287 mg). To a solution of Sar NCA (465 mg, 4.04 mmol) in *N,N*-dimethylformamide (DMF) (8 mL), a solution of H-(Leu-Aib)$_6$-OMe in DMF/$CHCl_3$ (9:1 v/v, 283 mg/10 mL) was added. After complete consumption of the Sar NCA was confirmed, glycolic acid (77 mg, 1.01 mmol, 5.0 eq.), 2-(1-H-7-azabenzotriazol-1-yl)-1,1,3,3-tetramethyl uronium hexafluorophosphate methanaminium (HATU, 384 mg, 1.01 mmol, 5.0 eq.), and diisopropyl ethyl amine (DIEA, 264 mL, 1.52 mmol, 7.5 eq.) were added at 0 °C to react with the *N*-terminal, and the solution was stirred at 0 °C for 10 min and at room temperature for 10 h. Then another portions of glycolic acid (31 mg, 0.40 mmol, 2.0 eq.), HATU (151 mg, 0.40 mmol, 2.0 eq.), and DIEA (106 mL, 0.6 mmol, 3.0 eq.) were added to the solution. After stirring for 12 h, the solution was condensed, and the residue was purified by a Sephadex LH20 column with methanol as an eluent to afford polypeptide **S24L14**. The degree of polymerization of the poly(Sar) block was determined to be 24 from the relative areas of Sar*N*-CH_3 signal against the OCH_3 signal in the ^{1}H NMR spectra.

^{1}H NMR (400 MHz, MeOH-*d*) δ (ppm) 8.2–7.7 (m, 11H, amide), 7.4–7.3 (br, 1H, amide), 4.6–3.8 (br, 56H, LeuC$^{\alpha}H$, SarCH_2), 3.66 (s, 3H, OCH_3), 3.3–2.8 (m, 72H, Sar N-CH_3), 1.9–1.3 (m, 36H, LeuCH_2, LeuC$^{\gamma}H$, AibCH_3), 1.1–0.8 (m, 36H, Leu(CH_3)$_2$).
MALDI-TOF MS analysis also supported the degree of polymerization to be 24.

S22L16 and **S25L20** were synthesized by the same method as **S24L14**. MALDI-TOF MS analysis supported the degree of polymerization to be 22 and 25.

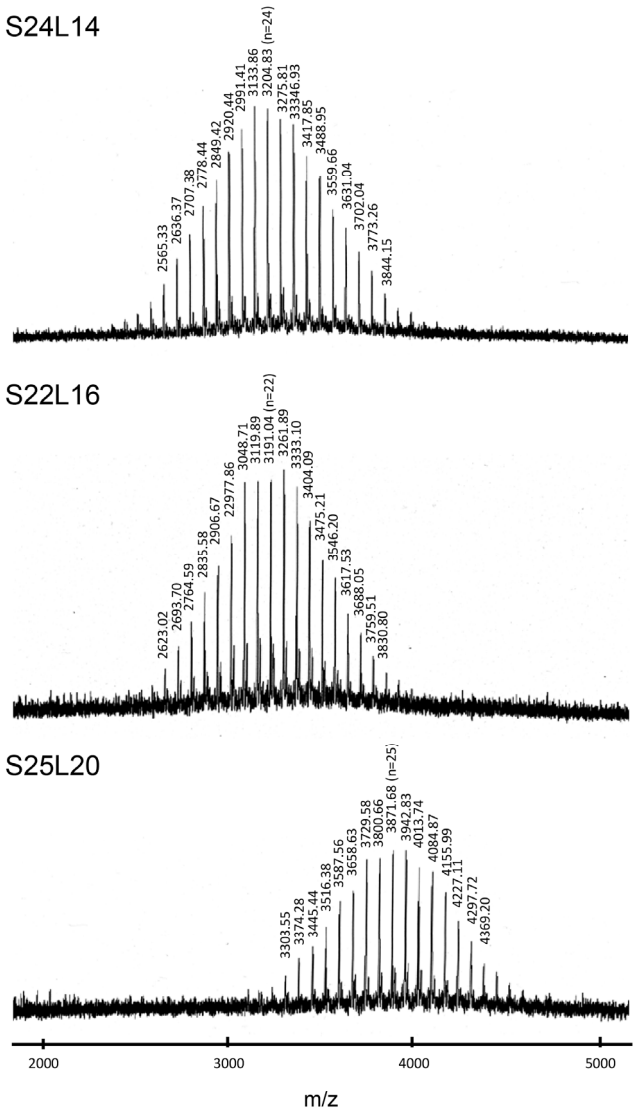

Figure 1. MALDI-TOF MS spectra of **S24L14**, **S22L16**, and **S25L20.** Poly(sarcosine) of 24 mers, 22 mers, and 25 mers were attached to the *N*-terminal of hydrophobic blocks. ([M+Na]$^+$ calcd: 3204, 3191, and 3871)

Results and Discussions

Peptide design. The hydrophilic block of $(Sar)_n$ was attached to the *N*-termini of the hydrophobic helical blocks of $(D\text{-Leu-Aib})_6$ and $(L\text{-Leu-Aib})_m$ (m = 7, 8 and 10) via polymerization of sarcosine NCA to obtain **S25D12, S24L14, S22L16,** and **S25L20** (Figure 1), respectively. Similar sizes of the Sar block were adopted to avoid the complexity of molecular parameters inducing morphology change. Circular dichroism (CD) spectra of each peptide in buffer after heat treatment at 90 °C for 24 hours indicated, as expected, the presence of a left-handed α-helix for **S25D12** and right-handed α-helices for **S24L14**, **S22L16**, and **S25L20** (Figure 4).

Molecular assembly from a mixture of enantiomeric peptides. The morphologies of the molecular assemblies of mixtures of two components after heat treatment at 90 °C for 24 hours were analyzed by transmission electron microscopy (TEM) with negative staining. One component of the peptide mixture was the **S25D12** with its left-handed α-helix. As second component **S24L14, S22L16,** and **S25L20** were added with their right-handed α-helices of different lengths. In the case of the equimolar mixture of **S25D12** and **S24L14** (**DL14**) nanotubes of 200 nm diameter and 400 nm length and elliptical planar sheets of 200–300 nm were obtained (Figure 2a and 6). On the other hand, the mixture of **S25D12** and **S22L16** (**DL16**) yields long nanotubes of 70 nm diameter and 2–30 μm length and planar sheets of 50–200 nm (Figure 2b and 6), whereby single- and multi-walled long nanotubes of **DL16** were detected (Figure 2d and 2e**)**. A mixture of **S25D12** with the longest right-handed α-helix **S25L20** (**DL20**) led to the formation of short nanotubes with 70 nm diameter and 100–600 nm length as well as twisted ribbons of 300 nm (Figure 2c and 6). No multi-walled nanotubes were found in the cases of **DL14** and **DL20**.

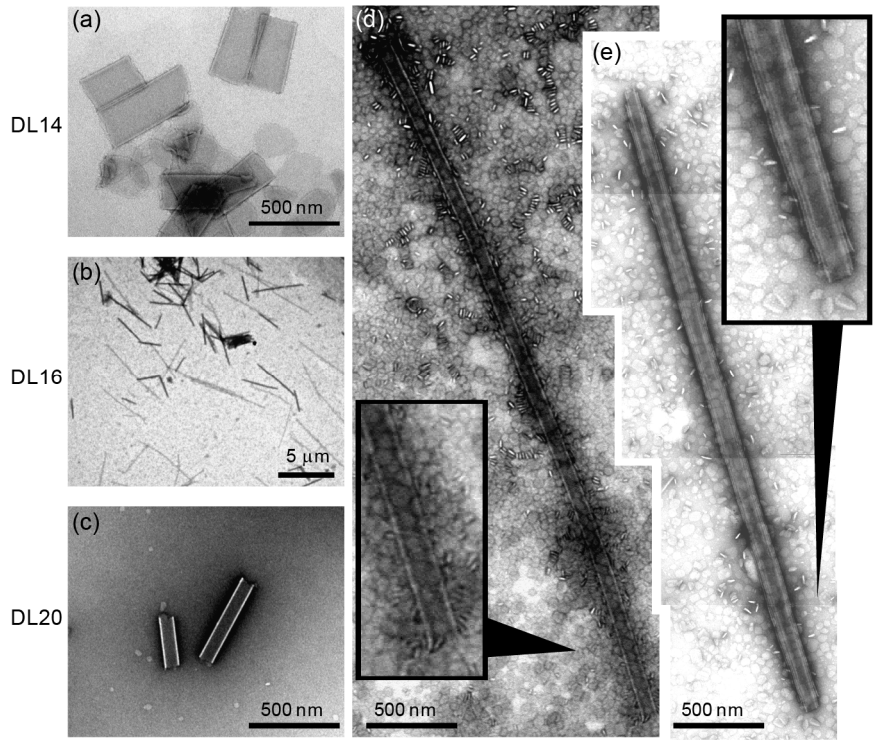

Figure 2. TEM images (negative staining with uranyl acetate, (a–e)) of molecular assemblies from equimolar mixtures of helical polypeptides **S25D12** and **S24L14**, (a); **S25D12** and **S22L16**, (b), (d), (e); **S25D12** and **S25L20**, (c)). The assemblies were prepared in 10 mM Tris-HCl buffer (pH 7.4) (2 μmol/mL) by the ethanol injection method and heat treatment. (d) and (e) show the magnified view of (b).

CD analysis. In the first instance the question was examined whether the nanotubes observed in these mixtures were indeed consisting of the two components. For this purpose the assembly dispersions of **DL14**, **DL16** and **DL20** were purified by a Sephacryl S-100 column to obtain fractions including the dominant nanotubes. CD spectra of these fractions showed negative Cotton effects with intensities that were smaller than those of the molecular assemblies prepared from the corresponding single components **S24L14**, **S22L16** and **S25L20** (Figure 3). The reduced intensities can be attributed to the coexistence of **S25D12** in the nanotubes. Indeed, the residual intensities increased in the order of **DL14** < **DL16** < **DL20**, which corresponds to the order of the helix-length difference of **S24L14** < **S22L16** < **S25L20** from **S25D12**. The molar ratios of the left- and the right-handed helix in the nanotubes as estimated from the intensities of the Cotton effects were 1/0.97 for **S25D12**/**S24L14**, 1/0.95

for **S25D12**/**S22L16** and 1/0.93 for **S25D12**/**S25L20**, confirming that the nanotubes are composed of equimolar mixtures of the peptides. Furthermore, the increased ratio of the intensity at 222 nm compared to that at 208 nm indicated a helix bundle structure, which results from the strong association of neighbouring helices.[24]

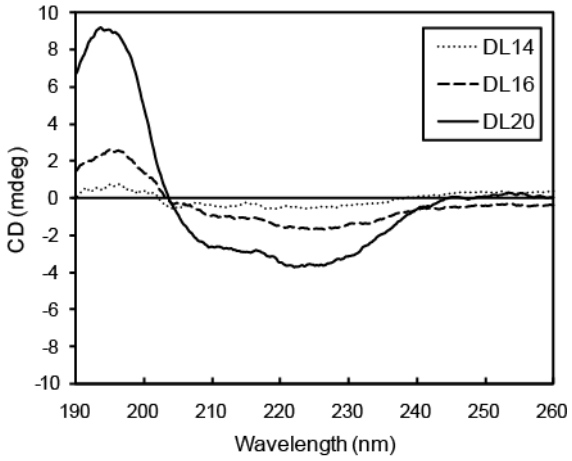

Figure 3. CD spectra of assemblies from **DL14** (dot line), **DL16** (dash line) and **DL20** (solid line) in Tris buffer after heating at 90 °C for 24 h and purification through a Sephacryl S-100 column. The increased ratio of the intensity at 222 nm compared to that at 208 nm indicates a helix bundle structure**.**

Conformation of the hydrophobic segment of **S24L14**, **S22L16**, **S25L20** and **S25D12** in a buffer was analyzed by CD spectroscopy (Figure 4), to show α-helical structure with bundle formation. The intensities at 208 nm of **DL14**, **DL16**, and **DL20** in a buffer were −0.57803, −1.36097 and −2.9804 mdeg, respectively. Compared with those of **S24L14**, **S22L16** and **S25L20** in a buffer, −5.22089, −6.5002, and −8.05515 mdeg, respectively, the molecular assemblies of **DL14**, **DL16**, and **DL20** are estimated to be composed of mixtures of two helices with excess presence of the right-handed helices by 1.6 mer, 3.4 mer and 7.4 mer, respectively. This estimation is agreeable with equimolar mixtures of the two helices in feed.

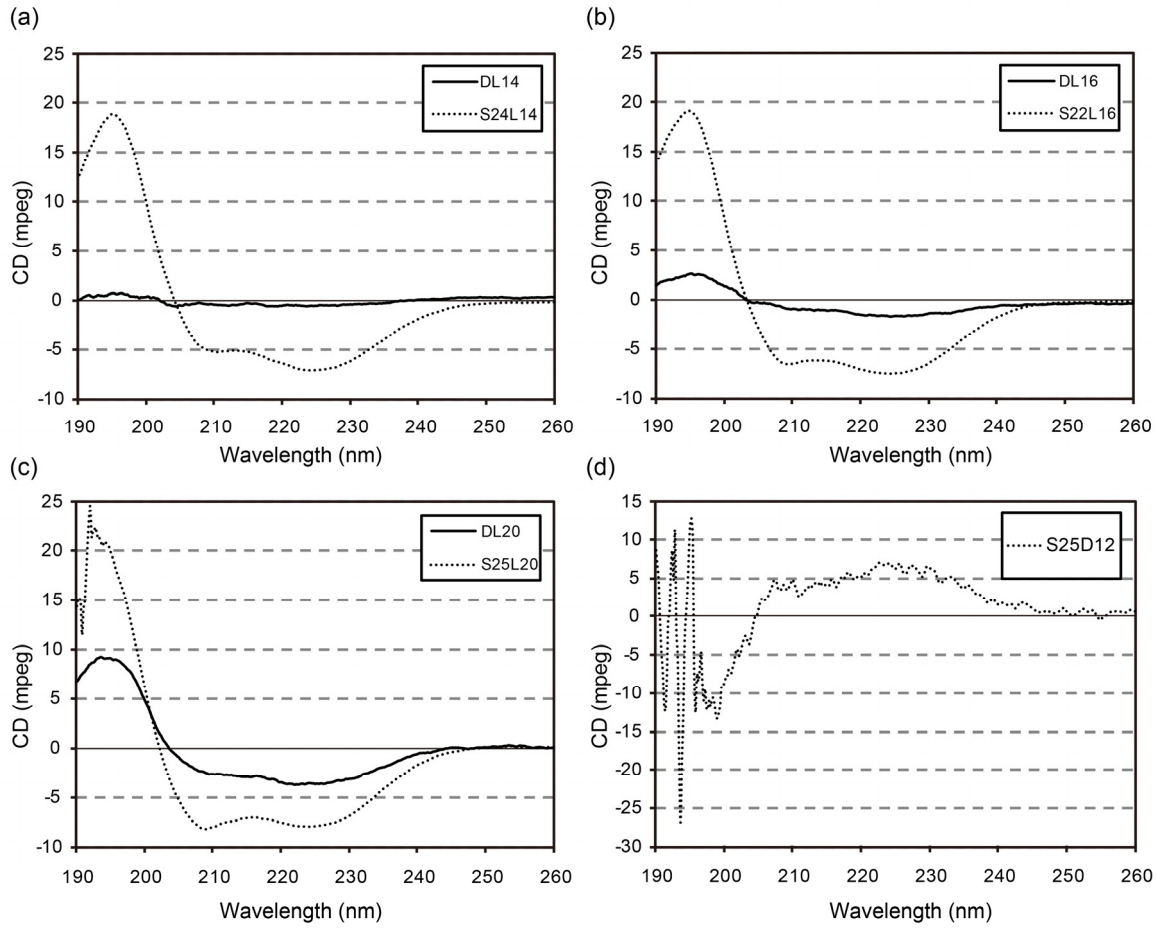

Figure 4. CD spectra of **S24L14**; (a), **S22L16**; (b), **S25L20**; (c) and **S25D12** in a buffer (d). The amphiphilic polypeptides were injected into a 10 mM Tris-HCl buffer (pH 7.4) (0.18 mg/mL), and then were heated at 90 °C for a specified period. CD spectra were measured after purification through a Sephacryl S-100 column (elusion solvent: buffer). These spectra suggest that the hydrophobic blocks of **S24L14**, **S22L16** and **S25L20** formed right-handed and that of **S25D12** formed left-handed in the molecular assemblies without mutual influence on the helicity.

Molecular assembly of a single component of peptides. TEM observations of the molecular assemblies prepared from the single components of **S25D12**, **S24L14**, **S22L16** and **S25L20**, supported the coexistence of the two peptides in the nanotubes of **DL14**, **DL16** and **DL20**. In fact, TEM images showed that **S25D12** and **S24L14** formed in the buffer nanotubes of 70 nm diameter and 200 nm length, while **S22L16** yielded vesicles of 100 nm diameter and

S25L20, small planar sheets (Figure 5), which are different from the nanotubes obtained from **DL14**, **DL16**, and **DL20**.

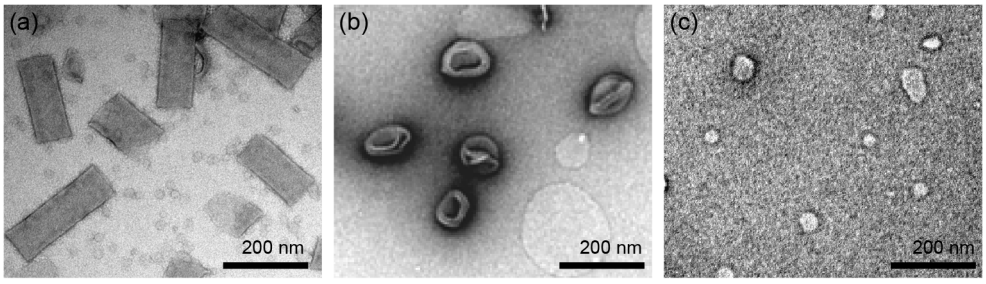

Figure 5. TEM images (negative staining with uranyl acetate; (a–c)) of molecular assemblies from single component of helical polypeptides **S24L14**; (a), **S22L16**; (b) and **S25L20**; (c)). The molecular assemblies were prepared in a 10 mM Tris-HCl buffer (pH 7.4) (1 μmol/mL) by the ethanol injection method after heat treatment at 90 °C for 1 h. The scale bars are 200 nm.

Properties of nanotubes. The membrane thicknesses of the assemblies prepared from **DL14**, **DL16** and **DL20** were of about 10 nm. In the membranes, the helices are supposed to be aligned in an interdigitated manner with anti-parallel orientation to gain the favorable dipole-dipole stabilization between peptide helices. Since the hydrophobic helical peptide has 2–3 nm chain length, the sarcosine chain length should be 7–8 nm in the assembly, suggesting a moderately extended conformation of the poly(Sar) chain in the membrane. The ^{1}H-NMR spectra of **S25D12**, **S24L14**, **S22L16** and **S25L20** in methanol showed two kinds of N-CH_3 signals due to the coexistence of the *cis* and *trans* configurations of sarcosine amides (data not shown), indicating that the poly(Sar) chains are flexible.[25,26]

The diameter of the nanotubes in the case of **DL14** was the largest among the present combinations of two kinds of peptides. **S25D12** alone formed a curved sheet before heat treatment in the preparation of the molecular assembly, because the left-handed helices should be molecularly packed in a consecutive twisted manner with a defined tilt angle between the helices as demonstrated by cholesteric liquid crystals of helical compounds. Upon mixing the

left- and the right-handed helix, the twisting property should be lost in the molecular assembly, resulting in a smaller curvature of the nanotube of **DL14** than that of **S25D12**. However, there is a mismatch of the helix lengths by two residues between **S25D12** and **S24L14**, which leads to the curvature of the molecular assembly because of the excess helicity in the hydrophobic core. This is the reason why **DL14** yields thick nanotubes of moderate curvature.

On the other hand, in the cases of **DL16** and **DL20** the mismatch lengths are 4 residues (6 Å) and 8 residues (12 Å), respectively, which should cause a large curvature of the nanotubes. However, **DL16** yielded the long nanotubes of about 10 μm in contrast to the short nanotubes of **DL20**. To better understand the differences in the morphologies on the molecular basis, the process of formation of these molecular assemblies were analyzed by TEM measurements before and after heat treatment.

Mechanism of morphology formation. In the case of **DL14**, planar elliptical sheets of 20 nm minor axis and 100 nm major axis were formed before heat treatment (Figure 6a). Upon heat treatment at 90 °C for 24 h, the planar sheets grew up to the large elliptical sheets of 200 nm minor axis and 400 nm major axis (Figure 6b). In these TEM images many structures under transformation from planar sheets into nanotubes were also observed (Figure 6g–l). The nanotube formation is thus explained as follows. The large elliptical sheets are rolled up, and the opposite hydrophobic edges stick together to form nanotubes followed by rearrangement at the open mouth of the nanotubes from ragged ends to blunt ends. The resulting nanotube length is relatively uniform (Figure 7), because the nanotube is formed directly from a planar sheet, size of which is determined by the growth conditions of 90 °C for 24 h. No further nanotube elongation has taken place.

In the case of **DL16**, planar rectangular sheets with sides of 30 nm and 50 nm were observed before heat treatment (Figure 6c). Upon heat treatment at 90 °C for 24 h, the planar sheets also grew up to the moderate size of rectangular sheets with sides of 150 nm and 200 nm; however, no large sheets were formed (Figure 6d). In the same TEM images, nanotubes

of 70 nm diameter and 200 nm length as well as the long nanotubes were identified (Figure 6m and 6n). The long nanotubes are thus formed by continuous attachment of the sheets to the open mouth of the nanotube, which are then rolled up to form the elongated nanotubes with ragged ends (Figure 6o and 8). The wide distribution in nanotube lengths can also be accounted for by this mechanism (Figure 7).

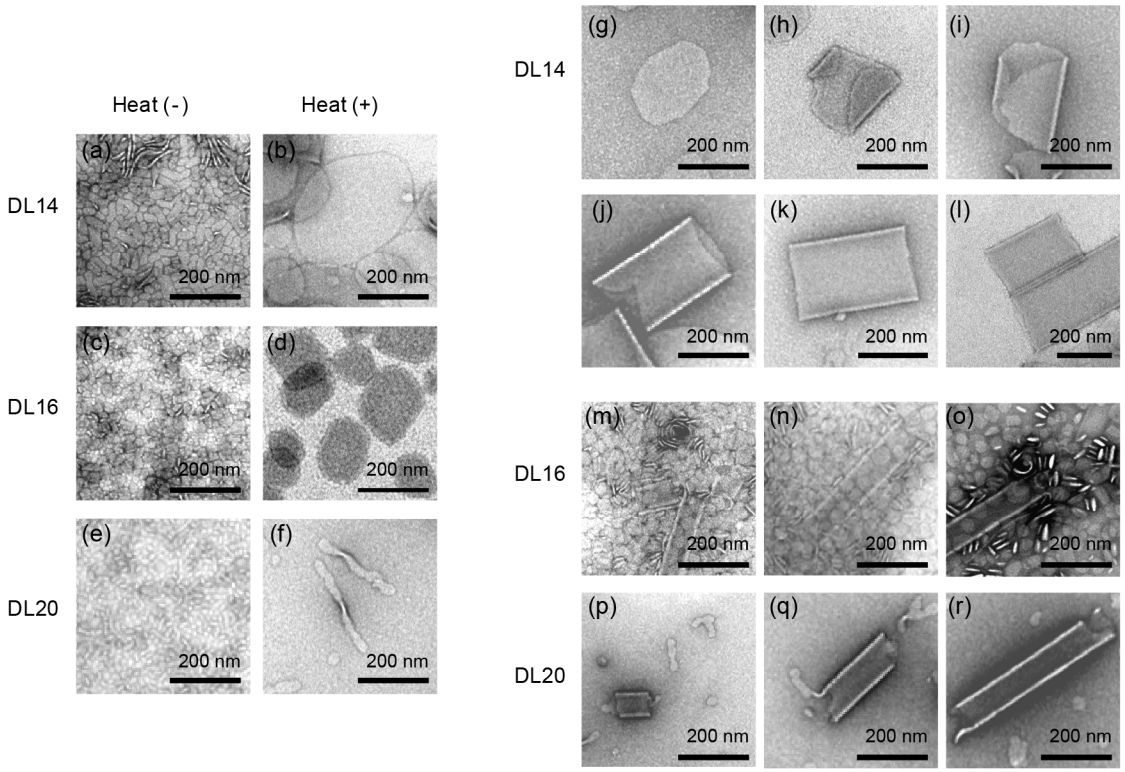

Figure 6. TEM images of each sheet structure of **DL14**, (a) and (b); **DL16**, (c) and (d); and **DL20**, (e) and (f). The formation mechanism from sheet or micelle to nanotubes of **DL14**, (g–l); **DL16**, (m–o); **DL20**, (p–r); respectively. The assemblies were prepared in 10 mM Tris-HCl buffer (pH 7.4) (2 μmol/mL) by the ethanol injection method. Before heat treatment, (a), (c), (e); and after heat treatment at 90 °C for 24 h, (b), (d), (f) and (g–r).

The aspect ratio of the longest nanotube was 430, which has 70 nm diameter and 30 μm length (Figure 9). The nanotubes took straight morphology, reflecting their stiff property. Furthermore, upon heat treatment at 90 °C, the elongation of **DL16** nanotube was also observed by microscopy (Figure 10).

In the case of **DL20**, micelles of about 20 nm and nanotubes of 70 nm diameter and 100 nm length coexisted before heating (Figure 6e). Upon heat treatment at 90 °C for 24 h, the twist ribbons and the nanotubes of 70 nm diameter and 100–600 nm length were formed (Figure 6f). As the open mouth of **DL20** nanotubes looks ragged similarly to that of **DL16** nanotubes, the transformation mechanism of **DL20** is the same as that of **DL16** (Figure 6p–r). However, the large mismatch of the helix lengths in the case of **DL20** favors formation of stable twist ribbons, which hinders the elongation of nanotubes.

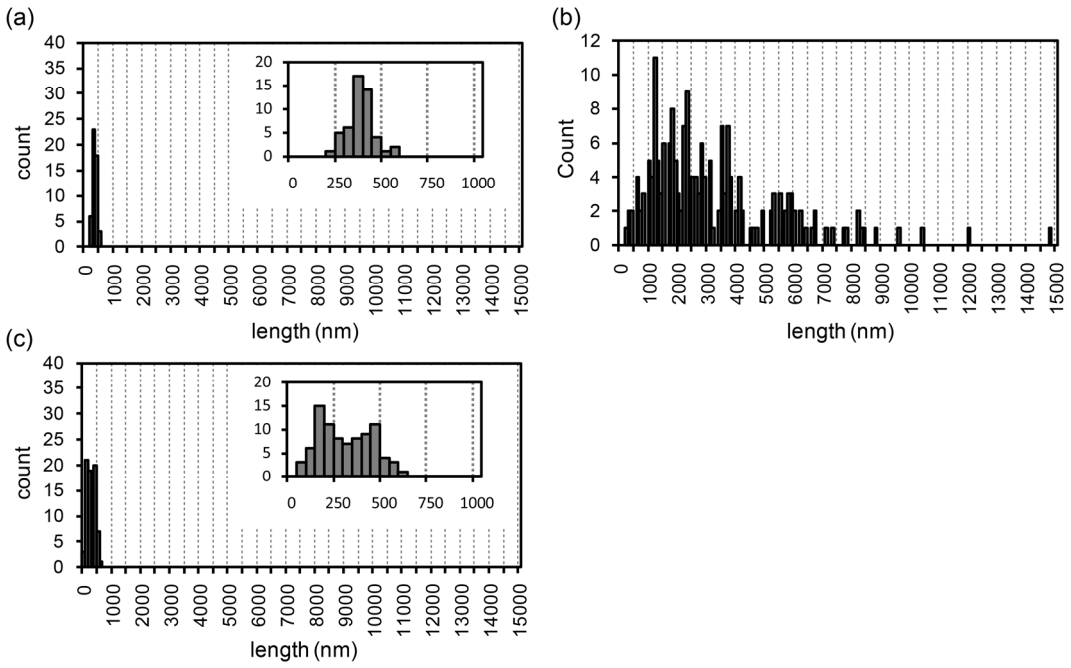

Figure 7. Histogram of the nanotube lengths of **DL14**; (a), **DL16**; (b), and **DL20**; (c) in a Tris-HCl buffer after heating at 90 °C for 24 h.

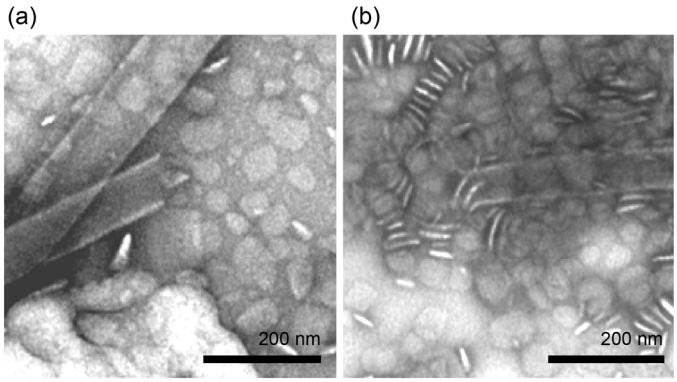

Figure 8. TEM images (negative staining with uranyl acetate) of the open mouth of long nanotubes prepared from **DL16**. The molecular assemblies were prepared in a 10 mM Tris-HCl buffer (pH 7.4) (2 μmol/mL) by the ethanol injection method after heat treatment at 90 °C for 1 h. The scale bars are 200 nm.

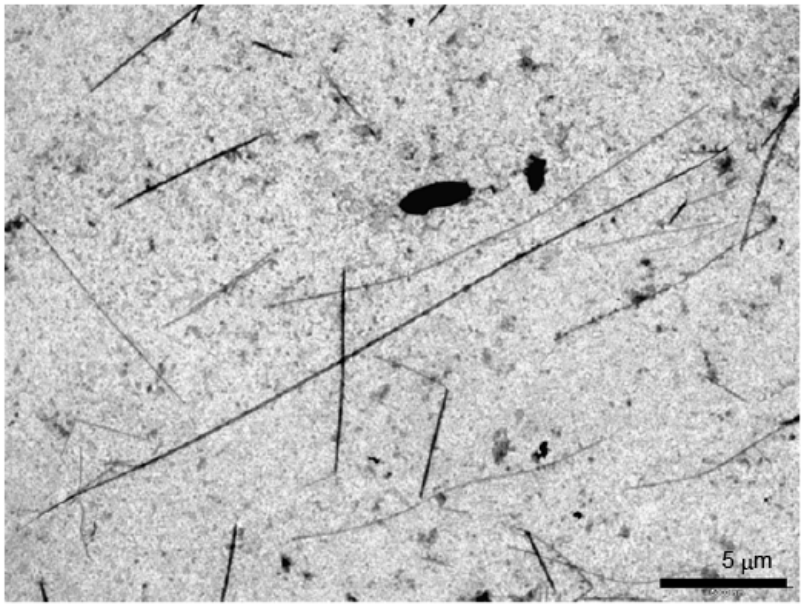

Figure 9. TEM images (negative staining with uranyl acetate) of molecular assemblies from **DL16**. The assemblies were prepared in 10 mM Tris-HCl buffer (pH 7.4) (2 μmol/mL) by the ethanol injection method after heat treatment at 90 °C for 24 h. The arrow shows the longest peptide tube. The scale bar is 5 μm.

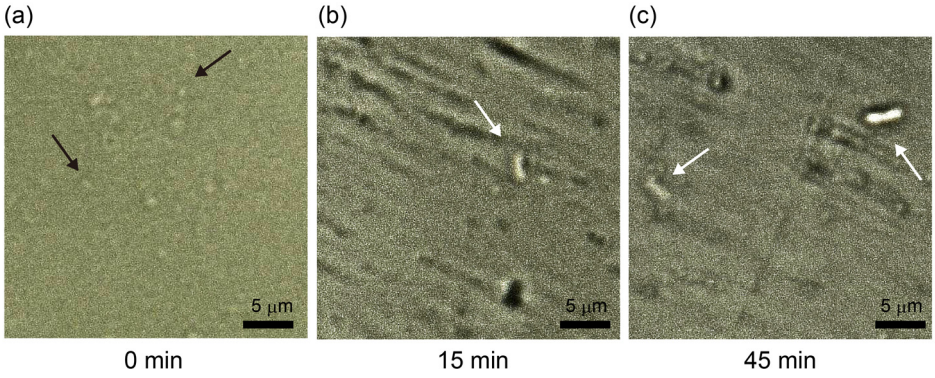

Figure 10. Histogram of the nanotube lengths of **DL14**; (a), **DL16**; (b), and **DL20**; (c) in a Tris-HCl buffer after heating at 90 °C for 24 h.

References

(1) Discher, D. E.; Eisenberg, A. *Science* **2002**, *297*, 967–973.

(2) Engelkamp, H.; Middelbeek, S.; Nolte, R. J. M. *Science* **1999**, *284*, 785–788.

(3) Jonkheijm, P.; van der Schoot, P.; Schenning, A. P. H. J.; Meijer, E. W. *Science* **2006**, *313*, 80–83.

(4) Percec, V.; Dulcey, A. E.; Balagurusamy, V. S. K.; Miura, Y.; Smidrkal, J.; Peterca, M.; Nummelin, S.; Edlund, U.; Hudson, S. D.; Heiney, P. A.; Duan, H.; Magonov, S. N.; Vinogradov, S. A. *Nature* **2004**, *430*, 764–768.

(5) Sigler, P. B.; Xu, Z.; Rye, H. S.; Burston, S. G.; Fenton, W. A.; Horwich, A. L. *Annual Review of Biochemistry* **1998**, *67*, 581–608.

(6) Horwich, A. L.; Weber-Ban, E. U.; Finley, D. *Proceedings of the National Academy of Sciences of the United States of America* **1999**, *96*, 11033–11040.

(7) Voges, D.; Zwickl, P.; Baumeister, W. *Annual Review of Biochemistry* **1999**, *68*, 1015–1068.

(8) Kim, W.; Thévenot, J.; Ibarboure, E.; Lecommandoux, S.; Chaikof, E. *Angewandte Chemie International Edition* **2010**, *49*, 4257–4260.

(9) Zhang, S. *Nat Biotech* **2003**, *21*, 1171–1178.

(10) Cui, H.; Muraoka, T.; Cheetham, A. G.; Stupp, S. I. *Nano Letters* **2009**, *9*, 945–951.

(11) Scanlon, S.; Aggeli, A. *Nano Today 3*, 22–30.

(12) Gao, X.; Matsui, H. *Advanced Materials* **2005**, *17*, 2037–2050.

(13) Holowka, E. P.; Sun, V. Z.; Kamei, D. T.; Deming, T. J. *Nat Mater* **2007**, *6*, 52–57.

(14) Kanzaki, T.; Horikawa, Y.; Makino, A.; Sugiyama, J.; Kimura, S. *Macromolecular Bioscience* **2008**, *8*, 1026–1033.

(15) Tanisaka, H.; Kizaka-Kondoh, S.; Makino, A.; Tanaka, S.; Hiraoka, M.; Kimura, S. *Bioconjugate Chemistry* **2008**, *19*, 109–117.

(16) Makino, A.; Kizaka-Kondoh, S.; Yamahara, R.; Hara, I.; Kanzaki, T.; Ozeki, E.; Hiraoka, M.; Kimura, S. *Biomaterials* **2009**, *30*, 5156–5160.

(17) Fujita, K.; Kimura, S.; Imanishi, Y. *Langmuir* **1999**, *15*, 4377–4379.

(18) Kimura, S.; Kim, D.; Sugiyama, J.; Imanishi, Y. *Langmuir* **1999**, *15*, 4461–4463.

(19) Kimura, S.; Muraji, Y.; Sugiyama, J.; Fujita, K.; Imanishi, Y. *Journal of Colloid and Interface Science* **2000**, *222*, 265–267.

(20) Milburn, M. V.; Prive, G. G.; Milligan, D. L.; Scott, W. G.; Yeh, J.; Jancarik, J.; Koshland, D. E.; Kim, S. H. *Science* **1991**, *254*, 1342–1347.

(21) Parker, M. W.; Pattus, F.; Tucker, A. D.; Tsernoglou, D. *Nature* **1989**, *337*, 93–96.

(22) Fukushima, K.; Kimura, Y. *Polymer International* **2006**, *55*, 626–642.

(23) Fukushima, K.; Chang, Y.; Kimura, Y. *Macromolecular Bioscience* **2007**, *7*, 829–835.

(24) Gibson, N. J.; Cassim, J. Y. *Biochemistry* **1989**, *28*, 2134–2139.

(25) Toniolo, C.; Bonora, G. M.; Schilling, F. C.; Bovey, F. A. *Macromolecules* **1980**, *13*, 1381–1385.

(26) Kimura, S.; Imanishi, Y. *International Journal of Biological Macromolecules* **1981**, *3*, 183–187.

Chapter 4

Patchwork Self-Assembling with Using Chiral Amphiphilic Helical Peptides Generates Nano-Size Round-Bottom Flask

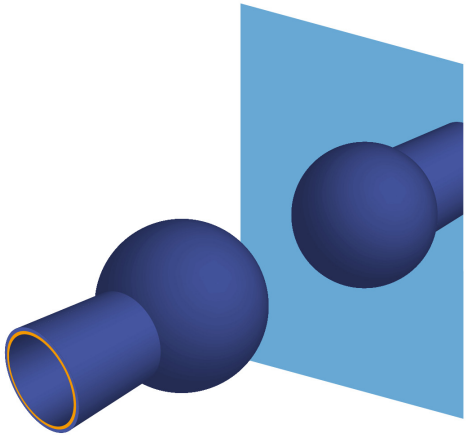

Introduction

In cells, the author can find out various complex morphologies of submicron sized molecular assemblies. On the other hand, simple morphologies in the shape of micelle, rod-shaped micelle, sheet, tube and vesicle have been prepared in solution by using the current self-assembling techniques.[1–4] In most cases, hydrophilic and hydrophobic moieties of amphiphilic compounds are carefully adjusted to adopt one specific type of these morphologies. On the other hand, the author reports here a novel morphology of a round-bottom flask molecular assembly, which has a nanotube connecting to a vesicle with one sheet of membrane but phase-separated.

The group of authors has reported on molecular assemblies of amphiphilic peptide molecules especially with using hydrophobic helical segments at the hydrophobic core of the molecular assemblies.[5–9] Helical peptides have a good ability to be packed regularly in the molecular assembly as shown by frequent observation of helix bundles in nature.[10,11] Indeed, the peptide nanotube with diameter of *ca*. 60 nm and length of *ca*. 200 nm was obtained from amphiphilic block polypeptide with hydrophobic helix, $(Sar)_{25}$-*b*-(L- or D-Leu-Aib)$_6$ in Chapter 1.[12] In this case, the block polypeptide initially formed a curved square sheet assembly, which was transformed into nanotube morphology upon heating at 90 °C for 10 min. The mechanism for the nanotube formation is based on the regular packing of the one-handed helices in the hydrophobic core as reported by the recent many studies on molecular assemblies with chiral molecules.[13–24] Further, the author succeeded in preparation of a vesicular assembly with using an enantiomeric mixture of amphiphilic polypeptides, $(Sar)_{25}$-*b*-(L-Leu-Aib)$_6$ and $(Sar)_{25}$-*b*-(D-Leu-Aib)$_6$, which has the right- and left-handed hydrophobic helices, respectively in Chapter 1. When the right-handed helix is mixed with the left-handed helix, they form a stereo-complex probably due to the convexo-concave fitness between their surfaces.[25,26] The stability of the membrane from a stereo-complex is thus higher than that from a single component in Chapter 1 and 3.

Poly(sarcosine) is used here as a hydrophilic segment, because it is as hydrophilic as poly(ethylene glycol), and sarcosine is biodegradable by endogenous sarcosine dehydrogenase. The author has applied the amphiphilic peptide micelles made of $(Sar)_n$-*b*-$(Glu\text{-}OMe)_m$[5] or $(Sar)_n$-*b*-$(lactide)_m$[6] for *in vivo* tumor imaging with using near-infrared fluorescence labelling probe. These poly(sarcosine) conjugates are shown to be highly biocompatible.

In the previous report, an equimolar mixture of **SLL** and **SDL** (Figure 1) generated a vesicular assembly. The author changes here the composition of the mixture to study on the effect of the composition on morphology.

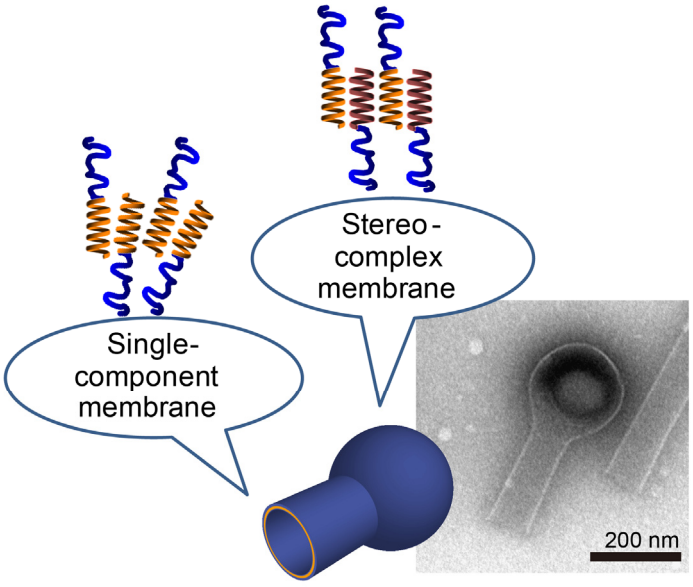

Experimental Section

Materials. Boc-L-leucine (Boc-Leu), aminoisobutylic acid (Aib) and Z-sarcosine (Z-Sar) were purchased from Watanabe Chemical Industries, Ltd. (Japan). Gold nano particle (10 nm) was purchased from British Biocell International (U.K.). Water was purified by a Milli-Q

system (Nihon Millipore Ltd, Japan) and had a specific resistivity of *ca.* 18 MΩ cm^{-1}. All other reagents were purchased from commercial sources and used as received.

Preparation of Molecular Assemblies. Polypeptide (12 mg) was dissolved in ethanol (120 μL). Then an aliquot (30 μL) of the peptide solution was injected into a buffer (1 mL, 10 mM Tris-HCl, pH 7.4) with stirring at 0 °C. After 30 min, the dispersion was purified by Sephacryl S-100 column (1.5 × 30 cm, GE healthcare Bio-Sciences) using 10 mM Tris-HCl buffer (pH 7.4) as an eluent to remove ethanol. Molecular assemblies of different compositions were prepared similarly.

Circular Dichroism (CD). CD measurements were carried out on a JASCO J600 spectropolarimeter with an optical cell of 0.1 cm optical path length at room temperature. The sample concentration in 10 mM Tris-HCl buffer (pH 7.4) was 0.375 mM (per amino acid residue).

Transmission Electron Microscopy (TEM). TEM images were taken using a JEOL JEM-2000EXII at an accelerating voltage of 100 kV. For the observation, a drop of dispersion was mounted on a carbon-coated Cu grid and stained negatively with 2 % uranyl acetate, followed by suction of the excess fluid with a filter paper.

Synthesis of sSLL. sSLL was prepared by the same method as **SLL** but the capping reagent was lipoic acid instead of glycolic acid. After complete consumption of Sar NCA was confirmed, lipoic acid (50 mg, 5.0 eq.), HATU (90 mg, 5.0 eq.) and triethylamine (64 μL, 7.5 eq.) were added to the solution. After stirring for 12 h, another lipoic acid (25 mg, 2.5 eq.), HATU (45 mg, 2.5 eq.) and triethylamine (32 μL, 3.8 eq.) were added to the solution. After stirring for 12 h, the solution was condensed, and the residue was purified by a Sephadex LH20 column with methanol as an eluent to afford **sSLL.**

^{1}H NMR(400 MHz, MeOH-*d*) δ (ppm) 8.2–7.7 (m, 11H, amide), 7.4–7.3 (br, 1H, amide), 4.6–3.8 (br, 56H, LeuC$^{\alpha}H$, SarCH_2), 3.66 (s, 3H, OCH_3), 3.55 (quin, 1H, SSC*H*), 3.3–2.8 (m, 79H, Sar N-CH_3, SSCH_2, CH_2CH_2CO), 2.5–2.4 (br, 2H, $SSCH_2CH_2$), 2.0–1.7 (br, 8H,

C*H*$_2$CH$_2$CH$_2$CH$_2$CO, CH$_2$ C*H*$_2$CH$_2$CH$_2$CO, CH$_2$CH$_2$C*H*$_2$CH$_2$CO, CH$_2$CH$_2$CH$_2$C*H*$_2$CO), 1.7–1.3 (m, 36H, LeuC*H*$_2$, LeuC$^{\gamma}$*H*, AibC*H*$_3$), 1.1–0.8 (m, 36H, Leu(C*H*$_3$)$_2$).

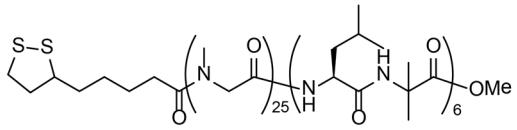

sSLL

Results and Discussion

Morphology of molecular assembly. Morphology of the molecular assembly prepared from a mixture of **SLL** and **SDL** (20/80 or 80/20 w/w) was studied by transmission electron microscope (TEM) with negative staining. The mixture as injected in buffer produced a mixture of nano curved-sheets and large planar-sheets (Figure 1a and 1b). Upon heating at 90 °C, these sheets were transformed into homogenous nano round-bottom flasks (Figure 1c and 1d). The sizes of the spherical part and the neck part were around 180 nm in diameter and *ca*. 60 nm in diameter and 200 nm in length, respectively. These sizes are compatible with those of the nanotubes and vesicles prepared from **SLL** or **SDL** and a mixture of **SLL** and **SDL** (50/50 w/w), respectively,[12] suggesting that the nano round-bottom flask morphology is a chimera assembly of the nanotube and the vesicle.

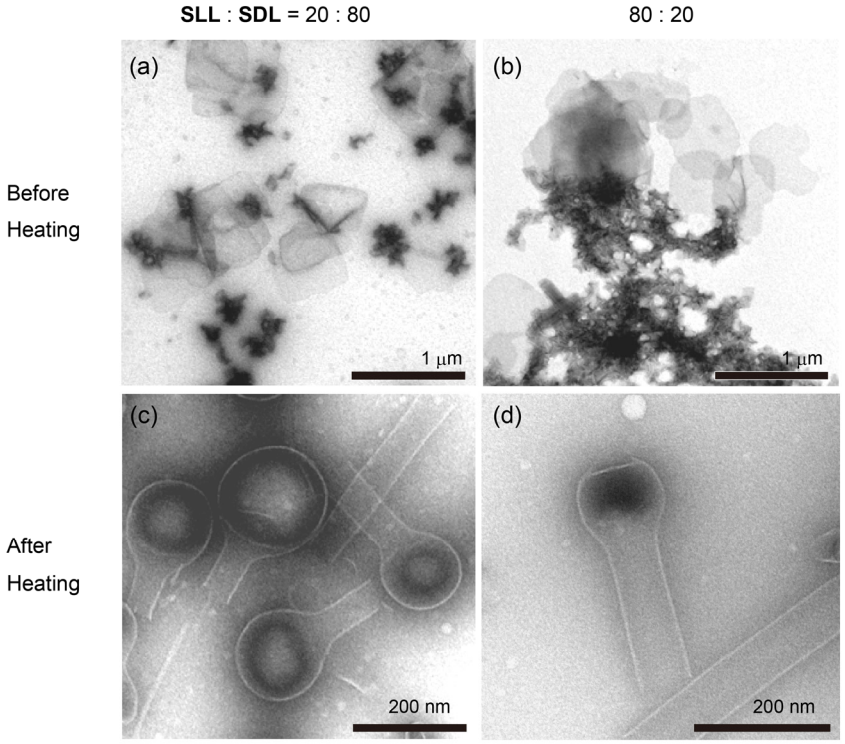

Figure 1. TEM images (negative staining with uranyl acetate; (a–d)) of molecular assemblies from mixtures of helical polypeptides **SLL** and **SDL**; 20/80; (a) and (c); 80/20; (b) and (d)). The assemblies were prepared in 10 mM Tris-HCl Buffer (pH 7.4) (3 mg/mL) by the ethanol injection method. Before heat treatment; (a) and (b), and after heat treatment; (c) and (d).

CD analysis. The author investigated CD spectral features of the assembled mixture of the enantiomeric polypeptides **SLL** and **SDL**. Both polypeptides were mixed in ethanol at molar ratios of **SLL** and **SDL** from pure **SLL** (enantiomeric excess; −100), 80/20 (−60), 60/40 (−20), 50/50 (0), 40/60 (20), 20/80 (60), and pure **SDL** (100), and the mixtures were injected into a Tris-HCl buffer. The obtained suspensions were heated at 90 °C for 1 h and then allowed to stand at 25 °C. The CD spectra of the suspensions changed the CD intensities in a linear relation with the enantiomeric excess (Figure 2). The linear relationship clearly showed that both peptides in the assemblies should keep their respective helicity in solution.

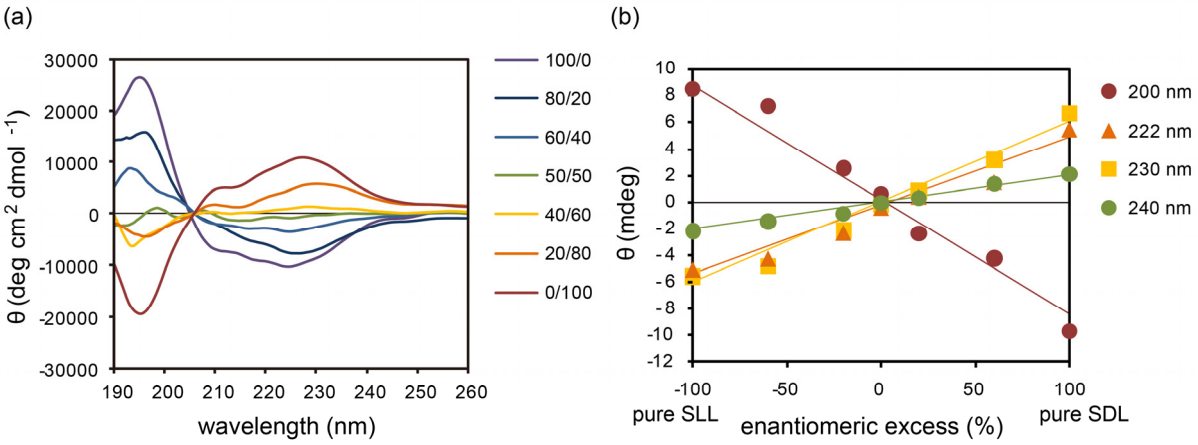

Figure 2. CD spectra (a) and intensity change of CD signals at 200, 222, 230, and 240 nm (b) with changing the mixing ratio of **SLL** and **SDL** in the molecular assemblies. The molecular assemblies were formed from varying mole ratios of amphiphilic polypeptides, **SLL** and **SDL,** in 10 mM Tris-HCl Buffer (0.18 mg/mL). Enantiomer excess (%) = |**SDL** − **SLL**| / (**SDL** + **SLL**) × 100.

Location of SLL in molecular assembly. The compositions of **SLL** and **SDL** in the spherical part and the neck part of the nano round-bottom flask were evaluated in order to examine the presumption that the nano round-bottom flask is a fused assembly of the vesicles and the nanotubes. **SLL** distribution in the molecular assemblies was analyzed by using **sSLL**, which has lipoic acid at the *N*-terminal of the hydrophilic poly(sarcosine) block of **SLL.** Since the structural difference between **SLL** and **sSLL** is only in the molecular terminal, the location of **sSLL**, which is visualized by binding of gold nano particles (GNP) by the TEM images, is regarded as the distribution of **SLL** in the molecular assembly. Molecular assemblies composed of mixtures of **SDL** and **SLL** + **sSLL** with varying ratios, 0/100, 20/80, 50/50, 80/20, and 100/0 (w/w) (the content of **sSLL** is 10 % of **SLL** + **sSLL**), were prepared and heated at 90 °C for 1 h. To the dispersions, GNPs (diameter of 10 nm) were added at 25 °C, and an aliquot was placed on a Cu grid for TEM measurement. TEM images were taken after washing excess amount of GNP with buffer (10 mM Tris-HCl, pH 7.4) (Figure 3).

As shown in Figure 3a, the **SLL** nanotube containing **sSLL** was bound by GNPs homogeneously on the surface, whereas the nanotube of **SDL** was not stained by GNPs

(Figure 3e), indicating the binding of GNP specific to **sSLL** and no physisorption under the present conditions (Figure 3a and 3e). The round-bottom flask prepared with **SLL**/**SDL** ratio at 80/20 (Figure 3b) and the vesicle with **SLL**/**SDL** ratio at 50/50 (Figure 3c) were bound by GNPs on the whole surface, indicating homogenous distribution of **SLL** at any places of the assemblies. On the other hand, the nano round-bottom flask prepared with **SLL**/**SDL** ratio at 20/80 (Figure 3d) was stained by GNPs only on the spherical surface but not on the neck part. These observations of GNP staining clearly show that the spherical part of the nano round-bottom flask is made of an equimolar mixture of **SLL** and **SDL**, and the neck part is formed from a single component of **SLL** or **SDL** depending on the excess peptide in the mixture. This observation is explained by the phase separation in the nano round-bottom flask due to the stereo-complex formation between the right-handed and left-handed helices. The stereo-complex is so stable that an equimolar mixture of **SLL** and **SDL** is phase-separated to form the vesicular part of the nano round-bottom flask, and the rest of the peptide is used for the nanotube part.

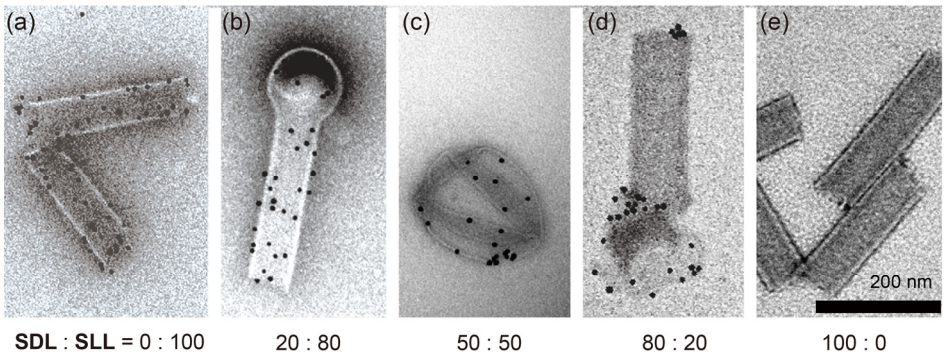

Figure 3. Distribution of GNPs on the surface of the molecular assemblies from mixtures of various **SLL**/**SDL** ratios; 100/0; (a), 80/20; (b), 50/50; (c), 20/80; (d), 0/100; (e). An aliquot of GNP (10 nm) suspension was added to the molecular assemblies on the TEM grid. In these cases, **SLL** contained **sSLL** of 10 wt%. The scale bar is 200 nm.

Transformation from planar sheet into vesicle. The transformation process from the nano planar-sheet into the vesicle was traced by time lapse analysis with TEM. An equimolar

mixture of **SLL** + 10 % **sSLL** and **SDL** in the presence of GNPs was heated at 90 °C. Initially, GNPs were uniformly dispersed on the planar-sheet surface (Figure 4a), indicating uniform distribution of **SLL** and **SDL** in the assembly. Upon heating for 30 min, the GNPs gathered on the edge region of the planar sheet, and the planar sheet was rounded off (Figure 4b–d). Finally, the GNP bound by **sSLL**s were excluded as a result of the vesicle formation. It is thus speculated that the heating should work as anneal to eliminate defects in the molecular assembly as well as to reduce the hydrophobic edges which are unstable by being exposed to water.

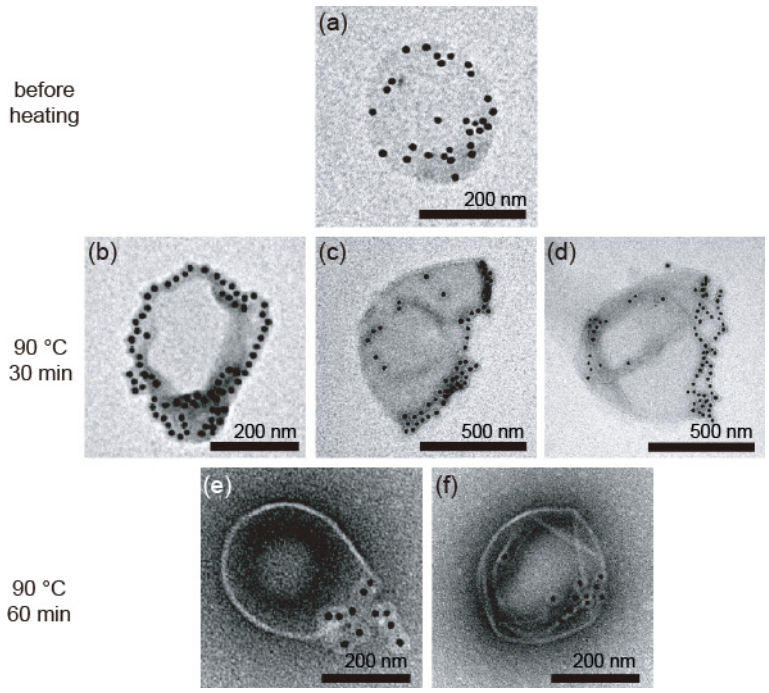

Figure 4. Formation mechanism of the vesicle assembly from a mixture of **SLL** and **SDL** 50/50. In this case, **SLL** contained 10 wt% of **sSLL**. Time lapse TEM images with keeping temperature at 90 °C. The scale bar shows (a), (b), (e), (f), 100 nm and (c), (d), 200 nm.

These results suggest that the nanotube acts as an auxiliary for the transformation from the planar-sheet into sphere morphology due to the hydrophobic edges. The edges of the planar-sheet may attach favourably to the edges of the nanotube because the fused structure is energetically stable by reduction of the hydrophobic edges. Accordingly, the planer-sheet

wrapped up to reduce the edge length, and finally, the planer-sheet transformed into sphere morphology at the terminal of the nanotube like the round-bottom flask. Indeed, upon heat treatment at 90 °C for 1h of the mixture of the nanotube from single component and the vesicle from stereo-complex, the round-bottom flask type morphology could not be observed. This result also supports our presumption.

Optimization of preparation. Instead of starting from the mixture of **SLL** and **SDL** (80/20), the **SLL** nanotube and the planar sheet of **SLL** and **SDL** (50/50), where the concentration ratio of **SLL** and **SDL** in total is 80/20, were mixed and heated. With this two-step method, the yield of the nano round-bottom flask increases as high as 38 % (the number of the round-bottom flask / (the number of the round-bottom flask + the number of the nanotube) = 168/443 in six TEM images), which coincides with the calculated value for quantitative production without the vesicle transformation (Figure 5).

The calculation method is followed: the occupied surface area of a molecule, **SLL**, is same to that of **SDL** in assembly. So, the percentage of constituent molecules, **SLL** or **SDL**, of morphology can be calculated by the surface area of it. Now, **SLL**/**SDL** = 75/25 in this system, because the nanotube of **SLL** (50 wt%) and the planar sheet composed of an equimolar mixture of **SLL** and **SDL** (25 and 25 wt%), were prepared, and then, both molecular assemblies were mixed. The surface area of the spherical part (diameter = 180 nm) of round-bottom flask type conformation is 101736 nm^2. This part is composed of a mixture of **SLL** (25 wt%) and **SDL** (25 wt%). On the other hand, the surface area of the neck part (diameter 60 nm and length 200 nm) of it is 37680 nm^2, suggesting that this part is composed of **SLL** (19 wt%), by (25 + 25) × (37680/101736). Therefore, It is considered that the rest **SLL** (31 wt%) formed the free nanotube in this system, indicating that the ratio of the round-bottom flask conformation (the round-bottom flask / (the round-bottom flask + the free nanotube)) is 19 / (19 + 31).

The nano round-bottom flask can be thus obtained by two different methods, suggesting that the nano round-bottom flask should be thermodynamically stable. The author can preserve the dispersion of the nano round-bottom flask for more than two months at room temperature without any morphological change. It is concluded that the phase separation into the spherical domain of the equimolar mixture of **SLL** and **SDL** and the nanotube domain of **SLL** or **SDL** single-component in the nano round-bottom flask is caused thermodynamically and not kinetically.

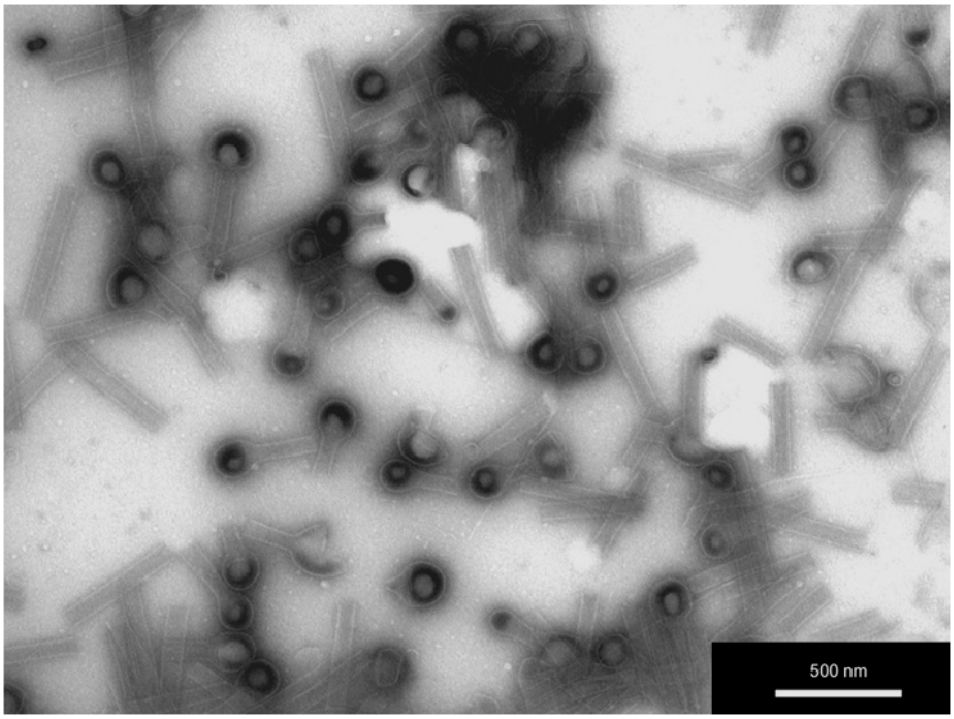

Figure 5. TEM images (negative staining with uranyl acetate) of molecular assemblies after heating (90 °C, 1 h) a mixture of the nanotube prepared from **SLL** and the planer sheet prepared from an equimolar mixture of **SLL** and **SDL**. The nanotube and the planer sheet assemblies were prepared in 10 mM Tris-HCl buffer (pH 7.4) (3 mg/mL) by the ethanol injection method with and without heat treatment, respectively.

References

(1) Discher, D. E.; Eisenberg, A. *Science* **2002**, *297*, 967–973.

(2) Jonkheijm, P.; van der Schoot, P.; Schenning, A. P. H. J.; Meijer, E. W. *Science* **2006**, *313*, 80–83.

(3) Engelkamp, H.; Middelbeek, S.; Nolte, R. J. M. *Science* **1999**, *284*, 785–788.

(4) Percec, V.; Dulcey, A. E.; Balagurusamy, V. S. K.; Miura, Y.; Smidrkal, J.; Peterca, M.; Nummelin, S.; Edlund, U.; Hudson, S. D.; Heiney, P. A.; Duan, H.; Magonov, S. N.; Vinogradov, S. A. *Nature* **2004**, *430*, 764–768.

(5) Tanisaka, H.; Kizaka-Kondoh, S.; Makino, A.; Tanaka, S.; Hiraoka, M.; Kimura, S. *Bioconjugate Chemistry* **2008**, *19*, 109–117.

(6) Makino, A.; Kizaka-Kondoh, S.; Yamahara, R.; Hara, I.; Kanzaki, T.; Ozeki, E.; Hiraoka, M.; Kimura, S. *Biomaterials* **2009**, *30*, 5156–5160.

(7) Fujita, K.; Kimura, S.; Imanishi, Y. *Langmuir* **1999**, *15*, 4377–4379.

(8) Kimura, S.; Kim, D.; Sugiyama, J.; Imanishi, Y. *Langmuir* **1999**, *15*, 4461–4463.

(9) Kimura, S.; Muraji, Y.; Sugiyama, J.; Fujita, K.; Imanishi, Y. *Journal of Colloid and Interface Science* **2000**, *222*, 265–267.

(10) Milburn, M. V.; Prive, G. G.; Milligan, D. L.; Scott, W. G.; Yeh, J.; Jancarik, J.; Koshland, D. E.; Kim, S. H. *Science* **1991**, *254*, 1342–1347.

(11) Parker, M. W.; Pattus, F.; Tucker, A. D.; Tsernoglou, D. *Nature* **1989**, *337*, 93–96.

(12) Kanzaki, T.; Horikawa, Y.; Makino, A.; Sugiyama, J.; Kimura, S. *Macromolecular Bioscience* **2008**, *8*, 1026–1033.

(13) Zhong-can, O. *Physical Review A* **1991**, *43*, 6826–6836.

(14) Schnur, J. M. *Science* **1993**, *262*, 1669–1676.

(15) Selinger, J. V.; MacKintosh, F. C.; Schnur, J. M. *Physical Review E* **1996**, *53*, 3804–3818.

(16) Oda, R.; Huc, I.; Schmutz, M.; Candau, S. J.; MacKintosh, F. C. *Nature* **1999**, *399*, 566–569.

(17) Cornelissen, J. J. L. M.; Rowan, A. E.; Nolte, R. J. M.; Sommerdijk, N. A. J. M. *Chemical Reviews* **2001**, *101*, 4039–4070.

(18) Selinger, J. V.; Spector, M. S.; Schnur, J. M. *The Journal of Physical Chemistry B* **2001**, *105*, 7157–7169.

(19) Hill, J. P.; Jin, W.; Kosaka, A.; Fukushima, T.; Ichihara, H.; Shimomura, T.; Ito, K.; Hashizume, T.; Ishii, N.; Aida, T. *Science* **2004**, *304*, 1481–1483.

(20) Jin, W.; Fukushima, T.; Niki, M.; Kosaka, A.; Ishii, N.; Aida, T. *Proceedings of the National Academy of Sciences of the United States of America* **2005**, *102*, 10801–10806.

(21) Shimizu, T.; Masuda, M.; Minamikawa, H. *Chemical Reviews* **2005**, *105*, 1401–1444.

(22) Yamamoto, Y.; Fukushima, T.; Suna, Y.; Ishii, N.; Saeki, A.; Seki, S.; Tagawa, S.; Taniguchi, M.; Kawai, T.; Aida, T. *Science* **2006**, *314*, 1761–1764.

(23) Ryu, J.; Kim, H.; Huang, Z.; Lee, E.; Lee, M. *Angewandte Chemie International Edition* **2006**, *45*, 5304–5307.

(24) Brizard, A.; Aime, C.; Labrot, T.; Huc, I.; Berthier, D.; Artzner, F.; Desbat, B.; Oda, R. *Journal of the American Chemical Society* **2007**, *129*, 3754–3762.

(25) Ikada, Y.; Jamshidi, K.; Tsuji, H.; Hyon, S. H. *Macromolecules* **1987**, *20*, 904–906.

(26) Brizzolara, D.; Cantow, H.; Diederichs, K.; Keller, E.; Domb, A. J. *Macromolecules* **1996**, *29*, 191–197.

Chapter 5

Morphology Collage with Using Phase-Separation of Peptide Membranes; “Patchwork Self-Assembling”

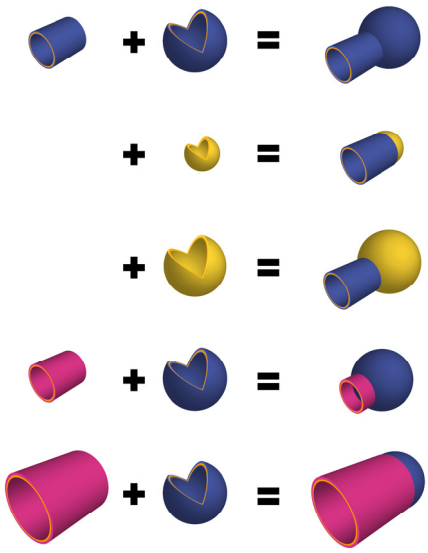

Introduction

Self-assembling of amphiphilic molecules is prevailing in living systems, and the selection of morphology of the molecular assemblies is explained generally on the basis of the molecular amphiphilicity. For example, molecular assemblies in water are found to take either morphology of micelle, wormlike micelle, or lamellar including nanotube and vesicles.[1–4] In most cases, the critical packing parameters of amphiphiles successfully predict the selection of morphology in water.[5] On the other hand, the author showed that a novel morphology of nano round-bottom flask was prepared by a pair of chiral amphiphilic peptides, right-handed helix and left-handed helix, with forming stereo-complex between them and phase separation in membrane in Chapter 4. The morphology is regarded as a joint of nanotube and vesicle, and the author named the assembling as patchwork assembly. Here, the author extends this patchwork assembly to other morphologies. These unique assemblies of different shapes and sizes should be useful for various fields, for example, to know the effects of shape and size of nanoparticles on cellular internalization and intracellular trafficking.[6]

The author has reported on molecular assemblies of amphiphilic peptide molecules especially with using hydrophobic helical segments at the hydrophobic core of the molecular assemblies.[7–11] Helical peptides have a good ability to be packed regularly in the molecular assembly as shown by frequent observation of helix bundles in nature.[12,13] Indeed, the peptide nanotube with diameter of *ca*. 70 nm and length of *ca*. 200 nm was obtained from amphiphilic block polypeptides with a hydrophobic helical block, $(Sar)_{25}$-*b*-(L-Leu-Aib)$_6$ (**SLL**) or $(Sar)_{25}$-*b*-(D-Leu-Aib)$_6$ (**SDL**), as a result of tight and regular packing of helices at the hydrophobic core of the membrane.[14] Further, the author succeeded in preparation of a vesicular assembly with using an equimolar mixture of **SLL** and **SDL** in Chapter 1. When the right-handed helix is mixed with the left-handed helix, they are considered to form a stable stereo-complex, which drives molecular assembling to take vesicular structure.[15,16]

The nanotube and the vesicle were then connected to generate a nano round-bottom flask just by mixing the nanotube of **SLL** or **SDL** and a planar sheet of an equimolar mixture of **SLL** and **SDL** followed by heat treatment. This assembly consists of the spherical membrane of stereo-complex of **SLL** and **SDL** and the tubulous membrane of **SLL** or **SDL** in Chapter 1. The round-bottom flask formation is driven by the decrease of the hydrophobic edges and the phase separation into a single component domain and a **SLL** and **SDL** stereo-complex domain in membrane.

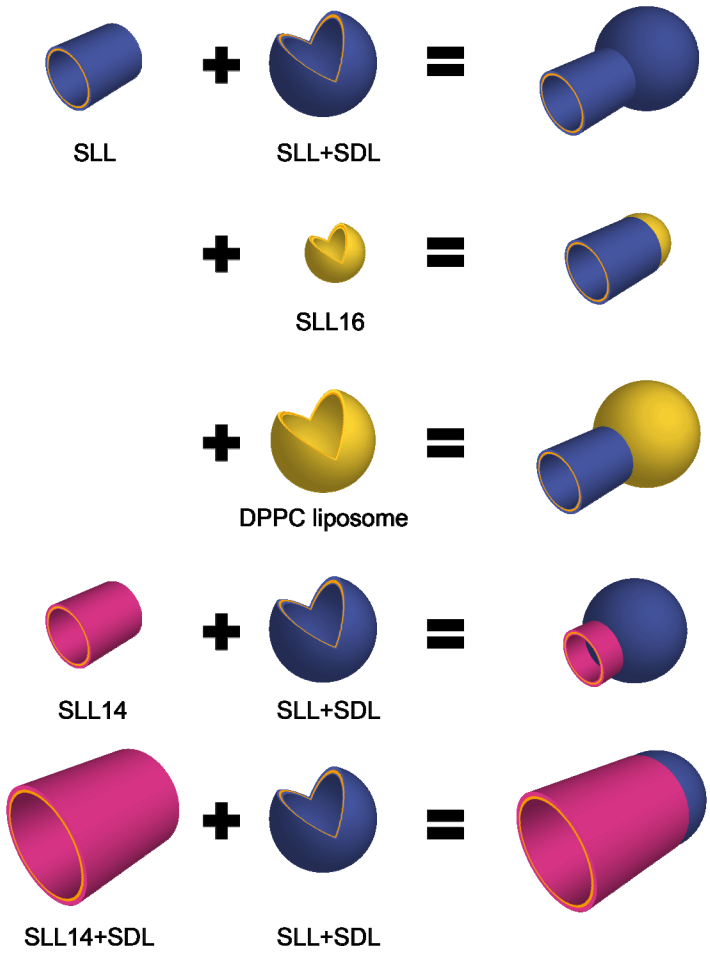

Figure 1. Schematic illustration of "patchwork self-assembly".

Experimental Section

Materials. Boc-L-leucine (Boc-Leu), aminoisobutylic acid (Aib) and Z-sarcosine (Z-Sar) were purchased from Watanabe Chemical Industries, Ltd. (Japan). Dipalmitoylphosphatidylcholine (DPPC) and cholesterol were purchased from Avanti Polar Lipids. Inc. (U.S.A.). Water was purified by a Milli-Q system (Nihon Millipore Ltd, Japan) and had a specific resistivity of *ca.* 18 MΩ cm^{-1}. All other reagents were purchased from commercial sources and used as received.

Preparation of Molecular Assemblies. Polypeptide (12 mg) was dissolved in ethanol (120 μL). Then an aliquot (30 μL) of the peptide solution was injected into a buffer (1 mL, 10 mM Tris-HCl, pH 7.4) with stirring at 4 °C. After 30 min, the dispersion was purified by Sephacryl S-100 column (1.5 × 30 cm, GE healthcare Bio-Sciences) using 10 mM Tris-HCl buffer (pH 7.4) as an eluent to remove ethanol. Molecular assemblies of different compositions were prepared similarly.

Transmission Electron Microscopy (TEM). TEM images were taken using a JEOL JEM-2000EXII at an accelerating voltage of 100 kV. For the observation, a drop of dispersion was mounted on a carbon-coated Cu grid and stained negatively with 2 % uranyl acetate, followed by suction of the excess fluid with a filter paper.

Frozen-Hydrated/Cryogenic-TEM (Cryo-TEM). The dispersions in a buffer were frozen quickly in liquid ethane, which was cooled with liquid nitrogen. The samples were examined at 100 kV accelerating voltage at the liquid nitrogen temperature.

Results and Discussion

Sphere part of a single component peptide membrane. The author found out that $(Sar)_{22}$-*b*-(L-Leu-Aib)$_8$ (**SLL16**) also self-assembles into vesicle. In buffer, **SLL16** formed a planar sheet at room temperature, and transformed morphology into a vesicular shape with *ca*. 80 nm diameter upon heating at 90 °C for 1 h in Chapter 3 (Figure 2a). The vesicle diameter fits to the diameter of **SLL** nanotube, which is considered suitable for making a new morphology of a round-bottom test tube (2nd row of Figure 1). Accordingly, **SLL16** planar sheets were incubated with **SLL** nanotubes, and the dispersion was heated at 90 °C for 1 h. As shown in Figure 2b, a test tube with a round bottom was observed by TEM. The sizes of the neck part and the round bottom part correspond to those of nanotube and vesicle, suggesting that the test tube morphology should be formed with a membrane where **SLL** and **SLL16** are phase-separated to build up the corresponding parts of tube and vesicle in the test tube morphology. The nano test tube morphology is thus a chimera assembly of a vesicle and a nanotube. The membrane thickness of the spherical part is 10 nm, which is the same as that of the vesicle prepared from **SLL16**. The yields of the test tube and the nanocapsule, where the both mouths of nanotube are sealed with round-bottom shaped membrane, under the condition of mixing equal amount of **SLL** and **SLL16** are 45 % and 36 %, respectively, and the rest is vesicle and irregular morphology (n = 526).

The yields of nanocapsule increased drastically from 11 % to 36 % and further to 67 % with increasing the mixing ratio of **SLL16** and **SLL** from 0.5/1 to 1/1 and further to 2/1 (w/w) (Figure 2c). On the other hand, the yields of the nano test tube changed from 31 % (n = 130) to 45 % and down to 16 % (n = 421) with increasing the mixing ratio (Figure 2g). This result indicates that target morphology can be prepared as a major fraction by optimizing the mixing ratio of the nanotube and the planar sheet.

When an ethanol solution of the mixture of **SLL** and **SLL16** (1/1 w/w) was injected into a buffer followed by heating at 90 °C for 1 h, the self-assembled test tube and the nanocapsule were identified by TEM observation, which morphologies were similar to those obtained by mixing the nanotube of **SLL** and the planar sheet of **SLL16** after heating. The yields of the test tube and the nanocapsule are 41 % and 38 %, respectively (Figure 3). The shapes and sizes of the test tube and the nanocapsule are independent on the preparation methods of the two different ways, indicating that these chimera morphologies are

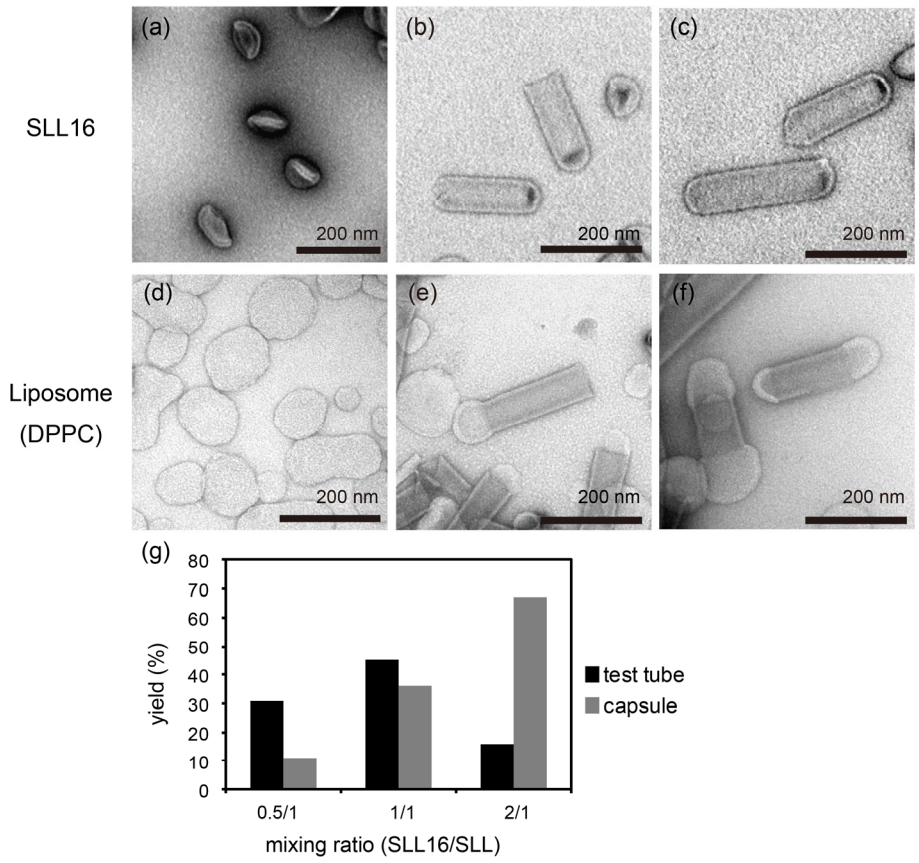

Figure 2. TEM images (negative staining with uranyl acetate; (a–f)) of molecular assemblies from mixtures of **SLL** nanotube and **SLL16** planar sheet; 0/1; (a); 1/1; (b) and 1/2; (c) and from mixtures of **SLL** nanotube and DPPC liposome; 0/1; (d); 1/1; (e) and (f). The yield of morphologies of molecular assembly prepared at each mixing ratio; (g). The assemblies were prepared in 10 mM Tris-HCl Buffer (pH 7.4) (1 mg/mL) by heating a mixture suspension of **SLL** nanotube and **SLL16** planar sheet, which prepared by the ethanol injection method, or DPPC+Cholesterol in ethanol, at 90 °C for 1 h.

thermodynamically stable. In fact, these molecular assemblies retain morphology at least for 1 month on the basis of TEM observation.

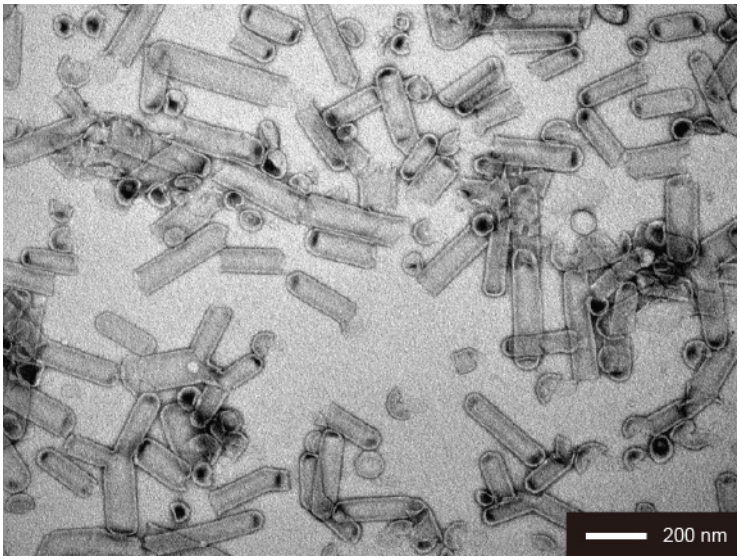

Figure 3. TEM images (negative staining with uranyl acetate) of molecular assemblies from mixtures of **SLL** and **SLL16** with ratio of 1/1 (w/w). The assemblies were prepared in 10 mM Tris-HCl Buffer (pH 7.4) (1 mg/mL) by the ethanol injection method and heat treatment with a mixture of **SLL** and **SLL16** in ethanol (40 μL).

Sphere part of liposome. One mouth of the **SLL** nanotube is thus possible to be sealed by spherical peptide membranes of two types made of either a mixture of **SLL** and **SDL** or **SLL16**. The author extends the trial of sealing the nanotube with vesicle forming membrane to the other kind of vesicle, liposome. A mixture of DPPC and cholesterol at a molar ratio of 55/45 generated liposome (Figure 2d). The mixture in ethanol was injected to the **SLL** nanotube suspension (molar ratio of DPPC/**SLL**, 1/1) in buffer and heated at 90 °C for 1 h. In the TEM images, the round-bottom flask assembly was observed (Figure 2e). The sizes of diameter and length of the neck part of the round-bottom flask are similar to those of the **SLL** nanotube. The membrane thickness of the neck part is *ca*. ~10 nm, which is the same as that of the **SLL** nanotube, supporting that the neck part is made of **SLL**. On the other hand, the round bottom part of the round-bottom flask shows a smaller morphology than liposome,

and the membrane thickness of *ca*. 15 nm is obviously larger than that of liposome (Figure 2d), suggesting that the round-bottom shaped membrane should be composed of a mixture of DPPC, cholesterol, and **SLL**.

In addition to the round-bottom flask, a dumbbell shaped assembly, where the both mouths of the nanotube are sealed with a spherical membrane, is observed (Figure 2f). The yields of the round-bottom flask and the dumbbell are 19 % and 18 % (n = 253), respectively, and the rest is irregular aggregates of liposomes and nanotubes.

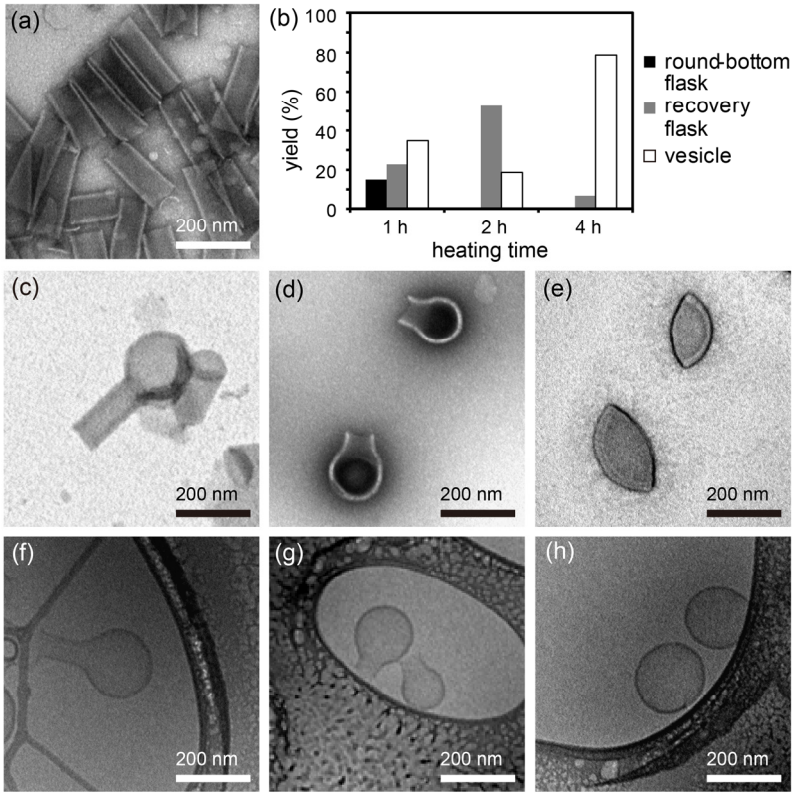

Figure 4. TEM images (negative staining with uranyl acetate; (a), and (c–e), cryo-TEM; (f–h)) of molecular assemblies from mixtures of **SLL14** nanotube and **SLL+SDL** planar sheet; 1/0; (a); 1/1; (c–h). The yield of morphologies of molecular assembly upon heating at 90 °C for 1, 2 and 4h (b). The assemblies were prepared in 10 mM Tris-HCl Buffer (pH 7.4) (1 mg/mL) by heating a mixture suspension of **SLL14** nanotube and **SLL+SDL** planar sheet prepared by the ethanol injection method, separately at 90 °C for certain hours.

Neck part of SLL14 nanotube. It is therefore shown that three different vesicular membranes can joint to the mouths of the **SLL** nanotube. Subsequently, the **SLL** nanotube part is replaced with other nanotubes with keeping the vesicle of an equimolar mixture of **SLL** and **SDL** as the counterpart of the chimera assembly (4 th and 5 th rows in Figure 1). The first example of the different nanotube was prepared from $(Sar)_{24}$-*b*-$(L\text{-Leu-Aib})_7$ (**SLL14**). **SLL14** upon injection into a buffer and heating forms a nanotube of 70 nm diameter and 200 nm length, which sizes are the same as those of the **SLL** nanotube in Chapter 3 (Figure 4a). When the **SLL14** nanotube was mixed with a planar sheet prepared form **SLL** and **SDL**, as expected, a round-bottom flask is obtained upon heating at 90 °C for 1 h, whose sizes of the neck and the round sphere are 70 nm tubular diameter, 200 nm length, and 180 nm spherical diameter, which are similar to those prepared from the **SLL** nanotube and a planar sheet of **SLL** and **SDL** (Figure 4c and 4f).

However, the yield of the round bottom flask is 15 %, which is significantly less than that of 38 % in the case of preparation from the **SLL** nanotube and the planar sheet of **SLL** and **SDL**. On the other hand, other morphologies of vesicle (30 % yield), a recovery flask (23 % yield), which has a shorter neck than a round-bottom flask, and nanotube (19 %) are observed by TEM observation. Extension of the heating period from 1 h to 2 h at 90 °C yielded no round-bottom flask, but the yield of a recovery flask increases significantly up to 53 % (Figure 4b, 4d and 4g). Further, in the case of a heating period of 4 h, the recovery flask diminished its fraction down to 7 % yield, and vesicle (79 % yield) becomes a major fraction of the existing morphologies (Figure 4b, 4e and 4h). It is thus speculated that the most thermodynamically stable morphology should be vesicle followed by recovery flask and round-bottom flask in this order. Since the transformation from one morphology into the other requires high energy (heat treatment at 90 °C), the molecular assemblies can be trapped into each morphology kinetically by choosing the heating period suitably for transformation into each morphology. Indeed, once the molecular assembly was trapped either in round-bottom flask, recovery flask, or vesicle, each shape was stable in solution at room temperature at least for two weeks.

Taken together, the patchwork assemblies result in different ways with changing the amphiphilic helical peptide of the starting nanotube from **SLL** to **SLL14**, which difference in the peptide sequence is just two residues of Leu-Aib. In the case of a mixture of **SLL** and **SDL** in the excess presence of either component, molecular assemblies are formed with phase separation into an excessive component part and a stereo-complex part in membrane. On the other hand, in the case of a mixture of **SLL**, **SDL**, and **SLL14**, these three kinds of peptides are miscible in membrane. Starting with a **SLL14** nanotube and a planar sheet of **SLL** and **SDL**, these two types of assemblies stick together to give a round-bottom flask. With heating further, the three kinds of peptides starts to mix together by diffusion of each component across the connecting region between the neck part and the round sphere part of the round-bottom flask. Via intermediate morphology of recovery flask, vesicle is prevailing eventually due to complete mixing of the three kinds of peptides.

This interpretation is supported by the following results. When a mixture of **SLL** and **SDL** (2/8 w/w) was injected into a buffer, round-bottom flask was a major morphology upon heating, suggesting occurrence of phase separation in membrane in Chapter 4. On the other hand, when a mixture of **SLL**, **SDL**, and **SLL14** (1/1/2 w/w/w) was injected into a buffer, vesicle was a major morphology upon heating, supporting the complete mixing of the three kinds of peptides.

Neck part of large nanotube from stereo-complex peptide membrane. Second type of thick nanotube was prepared from an equimolar mixture of **SDL** and **SLL14,** which forms a nanotube with 200 nm diameter and 500 nm length (Figure 5a and 5d). When a nanotube prepared from **SDL** and **SLL14** was mixed with a planar sheet prepared from **SLL** and **SDL** with ratio of 1/1 (v/v), a round-bottom test tube is generated, whose neck part has the sizes of 200 nm diameter and *ca*. 500 nm length (Figure 5b and 5e). This test tube morphology is reasonably explained by sticking the planar sheet to one mouth of the nanotube followed by transformation of the planar sheet into spherical membrane to seal the mouth of the nanotube upon heating at 90 °C for 1 h. The test tube morphology was retained even with a longer

heating period for 2h, suggesting that it is thermodynamically stable with keeping phase separation.

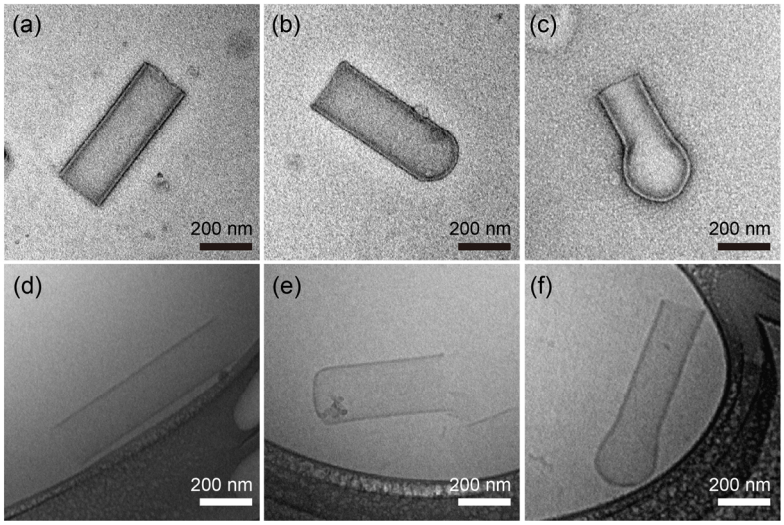

Figure 5. TEM images (negative staining with uranyl acetate; (a), (b) and (c), and cryo-TEM; (d), (e) and (f)) of molecular assemblies from mixtures of **SLL14+SDL** nanotube and **SLL+SDL** planar sheet; 1/0; (a) and (d); 1/1; (b), (c), (e) and (f). The assemblies were prepared in 10 mM Tris-HCl Buffer (pH 7.4) (1 mg/mL) by heating a mixture suspension of **SLL14+SDL** nanotube and **SLL+SDL** planar sheet prepared by the ethanol injection method, separately at 90 °C for 1 h.

Noticeably, the round bottom size of the test tube did not exceed over the diameter of the nanotube as shown in Figure 5a. In other words, the diameter of the round bottom seems to be determined by the diameter of the nanotube. On the other hand, when a mixture of **SDL** and **SLL14** nanotube and **SLL** and **SDL** planar sheet was incubated in buffer at room temperature for 30 min, round-bottom flask was observed upon subsequent heating at 90 °C for 1 h (Figure 5c, 5f and 6b). In the latter case, the planar sheets prepared from **SLL** and **SDL** at room temperature took a large area of *ca*. 1 μm square. The nanotubes prepared from **SDL** and **SLL14** should therefore stick to the large planar sheet during 30 min incubation, resulting in formation of a large spherical bottom upon heating at 90 °C. When the nanotubes prepared from **SDL** and **SLL14** was mixed and heated immediately at 90 °C, the planar sheets

should be torn off into small sheets before sticking to the mouth of the nanotube. As a result, the round bottom part did not exceed over the size of the nanotube. This presumption was supported by the result that a large planar sheet with 1 μm square, which was formed from a mixture of **SLL** and **SDL** at room temperature, was reported that a small sheet roll up and stick the hydrophobic edge to vesicle with 180 nm diameter when a planar sheet transformed into vesicle at 90 °C by 1 h (Figure 4 in Chapter 4). Indeed from TEM observations, it was expected that a small planar sheet was generated by breaking of a large sheet at 90 °C (Figure 7).

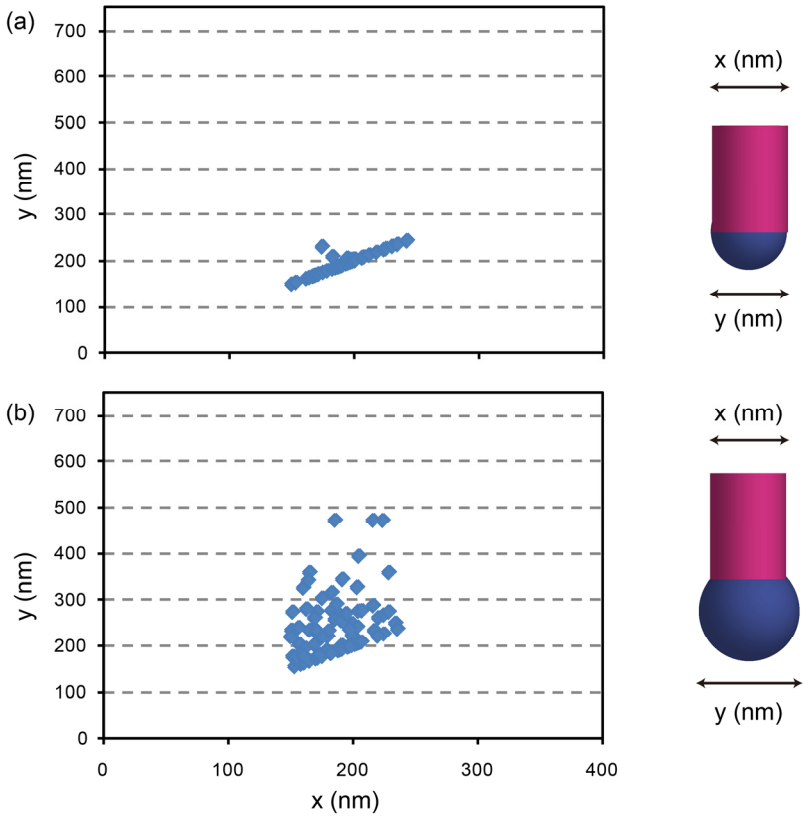

Figure 6. Distribution of the diameter of spherical part vs that of neck part of a round-bottom flask from a combination of **SLL14**+**SDL** nanotube and **SLL**+**SDL** planar sheet without; (a); and with standing for 30 min; (b); upon heat treatment at 90 °C for 1 h.

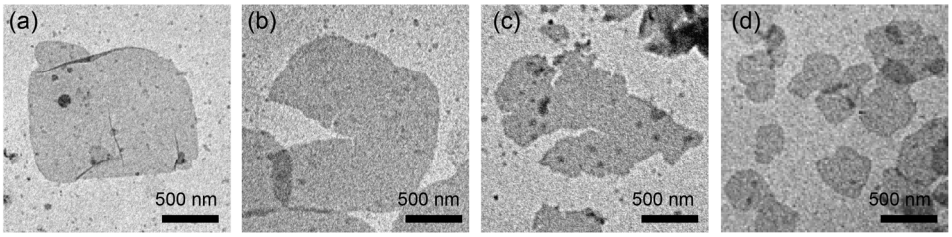

Figure 7. TEM images (negative staining with uranyl acetate) of molecular assemblies from a equimolar mixtures of **SLL** and **SDL** upon the heat treatment at 90 °C for 0 min (a) and 10 min; (b–d). The assemblies were prepared in 10 mM Tris-HCl Buffer (pH 7.4) (1 mg/mL) by the ethanol injection method from an ethanol solution of **SLL** and **SDL** (40 μL).

The character of vesicles and nanotubes, which was used to preparation of patchwork assembly in this report, was shown in table 1. In table 2, the morphologies of molecular assembly prepared by this method "patchwork self-assembling" were summarised.

Table 1. The character of vesicles and nanotubes for the preparation of patchwork assembly.

Amphiphile	Morphology		diameter (nm)	length (nm)
	Before heating	After heating		
SLL+**SDL** (1/1, w/w)[a,b]	Planar sheet	Vesicle	180	
SLL16[c]	Planar sheet	Vesicle	80	
DPPC		Vesicle		
SLL[a,d]	Curved sheet	Nanotube	70	200
SLL14[c]	Curved sheet	Nanotube	70	200
SLL14+**SDL** (1/1, w/w)[c]	Planar sheet	Nanotube	200	500

a: Chapter 1; b: Chapter 2; c: Chapter 3; and d: Chapter 4.

Table 2. The summary of the patchwork assemblies from two different membranes

Neck Part	Spherical Part	Morphology
SLL	**SLL+SDL**	Round-bottom flask
	SLL16	Test tube
		Nanocapsule
	DPPC	Round-bottom flask
		Dumbell
SLL14	**SLL+SDL**	Round-bottom flask
		Recovery flask
		Vesicle
SLL14+SDL	**SLL+SDL**	Test tube
		Round-bottom flask

References

(1) Discher, D. E.; Eisenberg, A. *Science* **2002**, *297*, 967–973.

(2) Jonkheijm, P.; van der Schoot, P.; Schenning, A. P. H. J.; Meijer, E. W. *Science* **2006**, *313*, 80–83.

(3) Engelkamp, H.; Middelbeek, S.; Nolte, R. J. M. *Science* **1999**, *284*, 785–788.

(4) Percec, V.; Dulcey, A. E.; Balagurusamy, V. S. K.; Miura, Y.; Smidrkal, J.; Peterca, M.; Nummelin, S.; Edlund, U.; Hudson, S. D.; Heiney, P. A.; Duan, H.; Magonov, S. N.; Vinogradov, S. A. *Nature* **2004**, *430*, 764–768.

(5) Israelachvili, J. N. *Intermolecular and Surface Forces, Second Edition*; Academic Press, 1992.

(6) Gratton, S. E. A.; Ropp, P. A.; Pohlhaus, P. D.; Luft, J. C.; Madden, V. J.; Napier, M. E.; DeSimone, J. M. *Proceedings of the National Academy of Sciences* **2008**, *105*, 11613–11618.

(7) Tanisaka, H.; Kizaka-Kondoh, S.; Makino, A.; Tanaka, S.; Hiraoka, M.; Kimura, S. *Bioconjugate Chemistry* **2008**, *19*, 109–117.

(8) Makino, A.; Kizaka-Kondoh, S.; Yamahara, R.; Hara, I.; Kanzaki, T.; Ozeki, E.; Hiraoka, M.; Kimura, S. *Biomaterials* **2009**, *30*, 5156–5160.

(9) Fujita, K.; Kimura, S.; Imanishi, Y. *Langmuir* **1999**, *15*, 4377–4379.

(10) Kimura, S.; Kim, D.; Sugiyama, J.; Imanishi, Y. *Langmuir* **1999**, *15*, 4461–4463.

(11) Kimura, S.; Imanishi, Y. *International Journal of Biological Macromolecules* **1981**, *3*, 183–187.

(12) Milburn, M. V.; Prive, G. G.; Milligan, D. L.; Scott, W. G.; Yeh, J.; Jancarik, J.; Koshland, D. E.; Kim, S. H. *Science* **1991**, *254*, 1342–1347.

(13) Parker, M. W.; Pattus, F.; Tucker, A. D.; Tsernoglou, D. *Nature* **1989**, *337*, 93–96.

(14) Kanzaki, T.; Horikawa, Y.; Makino, A.; Sugiyama, J.; Kimura, S. *Macromolecular Bioscience* **2008**, *8*, 1026–1033.

(15) Ikada, Y.; Jamshidi, K.; Tsuji, H.; Hyon, S. H. *Macromolecules* **1987**, *20*, 904–906.

(16) Brizzolara, D.; Cantow, H.; Diederichs, K.; Keller, E.; Domb, A. J. *Macromolecules* **1996**, *29*, 191–197.

Concluding Remarks

This section briefly summarizes the results of investigation on the preparation, characterization, and morphology analysis of molecular assemblies composed of amphiphilic polypeptides having a hydrophobic helical segment.

Chapter 1 demonstrated a new method for vesicle preparation by novel fusion between two types of nanotubes, which were composed either of the right-handed helix or the left-handed helix. The fusion was driven by the stereo-complex formation of these helical amphiphiles. Morphology transformation process from the nanotube into the vesicle was composed of four steps; i) nanotube association, ii) mixing of right- and left-handed helices, iii) break-up of the tubular structure to the planar sheet structure, and iv) closing to the vesicular structure.

Chapter 2 dealt with two examples of vesicle fusion. In either case, phase transition occurred in membranes of a mixture of **SLL** and **SDL** at 90 °C, which triggered fusion for themselves and the other type of peptide vesicles. The fused membrane allowed diffusion of constituent peptide amphiphilies, followed by fission into vesicles whose diameter was determined by the composition of the fused membrane. The driving force of vesicle fusion was considered to be a bending energy of the mixed membranes of **SLL** and **SDL** upon taking a vesicular structure. It was therefore expected that fusion ability of these peptide vesicles could be widely varied by designing the constituent peptide molecules.

Chapter 3 demonstrated the analysis of the morphologies formed by the right- and left-handed α-helical peptides with mismatched helix lengths. For example, when two peptides with mismatch length of four residues were mixed, long and straight peptide nanotube of more than 30 μm length and 70 nm diameter was formed. The elongation of the peptide nanotubes became possible here because of the strengthened membrane due to the stereo-complex formation of the right- and the left-handed helices. The curvature of

nanotubes was affected by the degree of mismatch length between the right- and the left-handed helices.

Chapter 4 presented a new method for a novel complex morphology by self-assembling. The unique self-assembling process was driven by the stereo-complex formation of the helical amphiphiles. When **SLL** and **SDL** were mixed at 20/80 or 80/20, they were phase-separated into the pure component domain and the 1/1 stereo-complex domain to yield the round-bottom flask morphology. The nano round-bottom flask morphology was considered to be a combined morphology of nanotube and vesicle, and this preparation method was named as "patchwork self-assembling".

Chapter 5 showed various possibilities to generate novel complex morphologies by self-assembling. The strategy was based on the combination of two different membranes, where one membrane constituted nanotube and the other had a vesicle-forming property. When the two kinds of membranes were mixed together, the latter membrane associated with the mouth of the nanotube to decrease the total energy of the hydrophobic edge line. However, the each component stayed at each membrane by phase separation, resulting in generation of chimera morphologies. These morphologies were thermodynamically stable, and were retained even after a long heating process. On the other hand, in the case of combination between nanotube of **SLL14** and vesicle of **SLL+SDL,** various morphologies of the round-bottom flask, the recovery flask, and the vesicle were prepared under kinetically controlled processes dependent on the heating time.

As demonstrated in the present thesis, the molecular assemblies, which are composed of amphiphilic polypeptides having a hydrophobic helical segment, show unique morphologies and properties, which are accompanied by stereo-complex formation between the right-handed and the left-handed helical peptides, membrane fusion due to the membrane fluidity, and phase separation in assembled membranes. With all these notable points for preparations of molecular assemblies, the author successfully demonstrates a new aspect of molecular assembly of more complex morphology, which is named as "Patchwork

Self-Assembling". The author therefore believes that the important findings of this thesis should be of interest not only for materials scientists and supramolecular chemists but also for many scientists in other fields of medical chemistry, organic chemistry, and biological chemistry and so on.

List of Publications

Chapter 1 Transformation of Peptide Nanotubes to Vesicle via Fusion Driven by Stereo-Complex Formation

Ueda, M.; Makino, A.; Imai, T.; Sugiyama, J.; Kimura, S.

Chemical Communications, (in press, DOI: 10.1039/C0CC04209A)

Chapter 2 Temperature Triggered Fusion of Vesicles Composed of Right-Handed and Left-Handed Amphiphilic Helical Peptides

Ueda, M.; Makino, A.; Imai, T.; Sugiyama, J.; Kimura, S.

Langmuir, (submitted)

Chapter 3 Rational Design of Peptide Nanotubes for Varying Diameters and Lengths

Ueda, M.; Makino, A.; Imai, T.; Sugiyama, J.; Kimura, S.

Journal of Peptide Science, **2011**, *17(2)*, 94–99.

Chapter 4 Patchwork Self-assembling with Using Chiral Amphiphilic Helical Peptides Generates Nano-Size Round-Bottom Flask

Ueda, M.; Makino, A.; Imai, T.; Sugiyama, J.; Kimura, S.

Soft Matter, (submitted)

Chapter 5 Morphology Collage with Using Phase-Separation of Peptide Membranes; "Patchwork Self-Assembling"

Ueda, M.; Makino, A.; Imai, T.; Sugiyama, J.; Kimura, S.

Angewandte Chemie International Edition, (submitted)

Other Publications

"New Morphologies Prepared from Stereocomplex of Amphiphic Helical Polypeptides"
Ueda, M.; Makino, A.; Imai, T.; Sugiyama, J.; Kimura, S.
Polymer Preprints, **2010**, *51(2)*, 454–455.

"Nanotube and Vesicle Formation with Using Amphiphilic Polypeptides of Right- and Left-Handed Helices"
Ueda, M.; Makino, A.; Imai, T.; Sugiyama, J.; Kimura, S.
Peptide Science, **2010**, *2009 46th* 63–64.

"Peptide Supramolecular Assembly"
Kimura, S.; Makino, A.; Ueda, M.; Kanzaki T.
Kobunshi, **2009**, *58(9)*, 657–660.

"Construction of Nanotubes Using Helix Peptide"
Kanzaki, T.; Ueda, M.; Kimura, S.
Nippon Kagakusen-i Kenkyusho Koenshu (Annual Report of the Research Institute for Chemical Fibers, Japan), **2009**, *66*, 64–70.

"A New Aspect of Molecular Assembling with Using Amphiphilic Helical Peptides"
Ueda, M.; Kimura, S.
Nippon Kagakusen-i Kenkyusho Koenshu (Annual Report of the Research Institute for Chemical Fibers, Japan) (in press)

Acknowledgement

This thesis summarizes the author's studies during 2008–2010 under the direction of Professor Shunsaku Kimura at Department of Material Chemistry, Graduate School of Engineering, Kyoto University.

The author would like to express his sincerest gratitude to Professor Shunsaku Kimura for his continuous guidance, suggestion and encouragement throughout this work. The author is deeply grateful to Dr. Akira Makino for their constant advices and valuable discussions throughout this work. The author wishes to thank Professor Junji Sugiyama and Dr. Tomoya Imai at Research Institute for Sustainable Humanosphere (RISH), Kyoto University, for permitting the use of the transmission electron microscopy, and for their technical supports and critical suggestions.

Grateful acknowledgment is also made to Dr. Tomoyuki Morita and Dr. Masashi Ohmae for critical suggestions, practical advice and fruitful discussion. The author would like to express his gratitude to Professor Toshikazu Takigawa at Department of Material Chemistry, Graduate School of Engineering, Kyoto University and Professor Kazunari Akiyoshi at Department of Polymer Chemistry, Graduate School of Engineering, Kyoto University for their instructive comments.

The author wishes to express special acknowledgment to Ms. Kaori Takemoto, Mr. Naoya Yoshioka, and Mr. Akihiro Uesaka for their great discussion and study with him as a member of the molecular assembly group in the Kimura laboratory. The author also would like to thank Ms. Itsuko Nakamura, Mr. Tetsu Takemasa, Mr. Yusuke Ishihara, and Mr. Hidenori Nakayama for their communications with him and giving grateful three years, and thank the other members of Professor Kimura's group for their encouragement and treasured memories.

Finally, He expresses his deepest appreciation to his friends and family, especially his parents, Mr. Kazukiyo Ueda and Mrs. Yoko Ueda, for their continuous understanding, helpful support, and deep affection.

Motoki Ueda
Department of Materical Chemistry
Graduate School of Engineering
Kyoto University
2011